A classical view of quantum entanglement

ETH
Eidgenössische Technische Hochschule Zürich
Swiss Federal Institute of Technology Zurich

Winter Semester 2004/2005 Prof. Dr. K. Hess

Master's Thesis at the Department of Information Technology and Electrical Engineering

A classical view of quantum entanglement

by

Manuel Aschwanden

UIUC Supervisor:	Prof. Dr. K. Hess
ETHZ Advisor:	Prof. Dr. W. Fichtner
ETHZ Co-Advisor:	Prof. Dr. A. Schenk
Issue Date:	October 4, 2004
Submission Date:	April 3, 2005

Acknowledgments

First and most of all, I would like to thank Prof. Karl Hess for giving me the opportunity to work with him on the challenging topic of quantum information. I have had the benefit of many discussions with Professor Hess on quantum mechanics, information theory and related areas in physics. I would also like to thank Professor Walter Philipp for introducing me to Kolmogorov's probability theory and Salvador Barraza-Lopes for helpful discussions and commentary.
I also wish to express my gratitude to my two supervisors, Professor Wolfgang Fichtner and Professor Andreas Schenk, at the Integrated Systems Laboratory at ETH Zurich. Without the help of Professor Fichtner and the financial support of IIS, this work would not have been possible.

Urbana, April 3, 2005

Manuel Aschwanden

Abstract

This Master's Thesis addresses the question of what is quantum entanglement. This question is of importance for engineering and information theory because of the possibility of quantum computing. Key to the answer of this question is the debate between Einstein and Bohr relating to this subject. Throughout this thesis the view of Einstein is given special and only consideration. It is appropriate to examine this view 100 years after Einstein's famous papers that have laid the foundation and given the principles for this debate. The thesis examines the key experiments by the Aspect and Zeilinger groups that purport to give a decision against Einstein and shows that existing results are far from conclusive. Some of the discussions are built on known criticisms of the Aspect and Zeilinger experiments some are new, in particularly those relating to the classical information theory of Shannon.

The Pan *et al.* realization [1] of the Greenberger-Horne-Zeilinger (GHZ) Gedankenexperiment is approached here with classical methods.

The quantum mechanical model for the GHZ Gedankenexperiment that was realized by Pan *et al.* is generally accepted and it is commonly assumed that classical objective local theories can not explain the experiment. Pan *et al.* have presented a local realistic model and have shown that it does not suffice to explain their experiments. However, in this thesis it is shown that a modified local realistic model based on instruction sets can reproduce the experimental results reported by Pan *et al.* with a statistically smaller error than the predictions of the quantum mechanical model presented by Pan *et al.*. As a consequence, these experimental results can not be used to prove quantum nonlocality.

In addition to the modified local realistic model an objective local model based on time and setting dependent equipment parameters is also presented. This model confirms a fortiori that the Pan *et al.* realization of the GHZ Gedankenexperiment can not be used to exclude all classes of objective local models. Therefore the Pan *et al.* realization of the GHZ Gedankenexperiment can not be used to prove the completeness of quantum mechanics or the existence of nonlocalities.

An objective local model based on a novel version of the detection inefficiency loophole is developed for the Aspect experiments [2, 3, 4] that experimentally realizes Bohm's variant of the EPR Gedankenexperiment. It is shown that also the Aspect-type experiments are not loophole free and that they cannot be used without doubt to prove the completeness of quantum mechanics.
In the second part of this thesis, Shannon's classical information theory is applied to the Pan *et al.* realization of the GHZ Gedankenexperiment. The entropy analysis shows that entanglement has a classical information theoretical interpretation and that the strength of entanglement can be quantified. Furthermore, a generalized entropic Bell test is defined.

Contents

Chapter 1

Introduction

In 1935 Einstein, Podolsky and Rosen (EPR) published a paper about the completeness of quantum mechanics [5]. In a Gedankenexperiment they constructed a paradox from which they concluded that quantum mechanics is not a complete description of the physical reality.
The EPR paper resulted in many discussions and papers. One of the first replies came from Niels Bohr [6].
29 years after the EPR paper, John Bell used the setup of the EPR-Bohm Gedankenexperiment to derive an inequality based on the assumption that the elements of reality can be described by hidden parameters [7, 8]. He showed that certain quantum mechanical predictions violate this inequality. Therefore he concluded that no hidden variable theory can explain the quantum mechanical predictions for the EPR experiment.
In the following years many theoretical and experimental papers were published. Most of them supported the quantum mechanical predictions. The most famous of these papers are the Clauser-Horne-Shimony-Holt generalization of the Bell theorem [9], Mermin's quantum mechanical operator based Gedankenexperiment [10] and Alain Aspects experimental realization of the EPR-Bohm Gedankenexperiment [2, 3] based on delayed choices for the measuring equipment setting.
In 1989 Greenberger, Horne and Zeilinger (GHZ) [11] have constructed a multiparticle version of the Bell theorem, based on a system containing three or more correlated spin-1/2 particles. The experimental realization of this Gedankenexperiment was achieved ten years later by Pan *et al.* [1]. Pan and his co-workers interpret their findings as the first three-particle test of local realism following the GHZ argument. In their final analysis they conclude that no objective local model can explain the experimental results and that quantum nonlocality is therefore proven.

Despite these experimental results, many physicists resist to believe in the correctness of these proofs and they doubt that quantum mechanics is a complete theory. Especially quantum nonlocality that is based on entanglement is strongly doubted by many physicist. The question whether or not quantum mechanics is a complete theory is of greatest interest because newly emerging research fields such as quantum computing and teleportation are based on non-classical phenomena such as entanglement.

In this work, several objective local models are developed to analyze the experimental realization of the EPR experiment and the GHZ experiment. All investigated models satisfy the locality condition defined by EPR: "Since at the time of measurement the two systems no longer interact, no real change can take place in the second system in consequence of anything that may be done to the first system." [5]. In addition, Claude E. Shannon's classical information theory [12, 13, 14] is used to analyze the Pan *et al.* realization of the GHZ Gedankenexperiment.

The aim of this work is to reestablish local realism and to point out that the experiments considered to prove nonlocality have significant loopholes that allow the development of objective local theories for the observed phenomena.

In the first chapter, a brief history of the completeness discussion of quantum mechanics is given. Then the Aspect experiments are analyzed. In the following chapter, the experimental realization of the GHZ Gedankenexperiment by Pan et al. is investigated. It is shown that the Pan *et al.* experiment can not be used to draw conclusions about the existence of quantum nonlocality. In addition, several objective local models for the Pan *et al.* realization of the GHZ Gedankenexperiment are introduced. In chapter 5, Shannon's classical information theory is used to derive conditions that can be used to decide whether or not an experiment can be explained with random variables that are all defined on one common probability space. At the end a conclusion of the work is given and possible future research activities are identified.

Chapter 2

History

2.1 Introduction

At the beginning of the 20^{th} century several groundbreaking physical theories emerged. As is well known, Albert Einstein is the father of the special and general relativity theory that radically changed our space-time picture. Although nowadays most people associate Einsteins name with relativity theory, he also contributed some major ideas to quantum mechanics. In 1905 he explained for example the photoelectric effect by describing a photon as particle like entity. Although Max Planck used in his derivation of the black body radiation formula quantized energies, Einstein was the first to go the full length toward particles of light.
In the following years Louis de Broglie realized that not only photons have a wave-particle duality but also other elementary particles like electrons. In 1926 Erwin Schrödinger combined the Helmholtz equation and the de Broglie description of the electron and derived his famous wave equation[1]. Heisenberg had given some what earlier a quantum theory that appeared to be different but it turned out that the two theories are fully equivalent.
The interpretation of these theories was developed by the Copenhagen school lead by Niels Bohr. The Copenhagen interpretation is based on the complementary wave particle picture and on Born's *probability* explanation of the absolute square of the wave function. Bohr maintains that nature exhibits both behaviors (particle and wave) at the same time and that the act of measurement forces the decision. One could say that everything in the past is particles and everything in the future waves. The cornerstone of the quantum description is the quantum state. A measurement

[1] In his first paper he gave a more complicated derivation.

results in one single outcome of all the possible outcomes for that quantum state. The outcomes are equal to eigenvalues of the underlying eigenvalue equation.
One major principle of the Copenhagen interpretation of quantum mechanics was stated by Heisenberg. He formulated the uncertainty principle. In simple words, the uncertainty principle states that the exact value of position and momentum of a particle can not be known at the same time. Niels Bohr first disliked this idea but accepted it at the end and interpreted it as impossible simultaneous measurability of the untouched nature (general state before reduction by measurement) [15].
After receiving recognition for this work and the new quantum mechanics, Heisenberg and Born[2] declared in 1927 at the Solvay physics conference in Brussels, Belgium, that quantum mechanics is complete and irrevocable [15]. Several leading physicists such as Schrödinger or Einstein disagreed with this Heisenberg-Born statement and they believed until the end of their lives that it is incorrect. In a joint work with Podolsky and Rosen, Einstein formulated in 1935 a Gedankenexperiment that should show that quantum mechanics is not a complete theory.

2.2 The EPR Gedankenexperiment

In 1935 A. Einstein, B. Podolsky and N. Rosen (EPR) published a famous paper [5] in which they question the completeness of quantum mechanics. They did not question the usefulness of quantum mechanics as a powerful theory but they conclude from their Gedankenexperiment that quantum mechanics is not a complete theory and that there has to be a more fundamental description of the physical reality. In the following paragraph a short summary of the 1935 paper is presented.
The original question was the following: "Can Quantum-Mechanical Description of Physical Reality Be Considered Complete?" [5] To answer this question EPR define a necessary condition for a complete theory: "every element of the physical reality must have a counterpart in the physical theory" [5]. Besides this completeness condition the term physical reality was defined: "If, without in any way disturbing a system, we can predict with certainty (i.e., with probability equal to unity) the value of a physical quantity, then there exists an element of physical reality corresponding to this physical quantity." [5]
In the following, EPR state the Heisenberg uncertainty principle: "When the momentum of a particle is known, its coordinate has no physical reality." More generally, if the operators corresponding to two physical quantities do not commute, then the

[2]Born also gave the probability description of quantum mechanics.

simultaneous knowledge of both physical quantities is not possible. From this general behavior of quantum mechanics EPR derive two mutually exclusive statements:

INC: "*The quantum mechanical description of a system given by the state function is incomplete*".

NSV: " *Observables represented by noncommuting operators cannot have simultaneous reality* (i.e., cannot have simultaneously sharp values)." [16]

In the following EPR assume that the wave function (or state) of a system contains a complete description of the physical reality. Together with the reality criterion this assumption leads to a contradiction[3] .
EPR use in their analysis a state of two particles I and II that are known at a certain time. It is assumed that particle I and II interact during the time interval $t = 0...T$. The resulting state created in this interaction is described by the wave packet Ψ. After $t = T$ the two systems do not interact. Starting from this situation EPR make two different reductions of the wave packet Ψ. This means that two different quantities are measured on system I. The two systems (I and II) are so far apart that no interaction can happen. Nevertheless, the second system (II) is left in states with two different wave functions. EPR conclude therefore that "it is possible to assign two different wave functions ... to the same reality" [5]. Subsequently they show that if two operators corresponding to two different physical quantities do not commute, the simultaneous knowledge of both quantities is not possible. From this they conclude that it is indeed possible to assign two different wave functions to the same reality. But "since either one or the other, but not both of the quantities P and Q can be predicted, they are not simultaneously real. This makes the reality of P and Q depend upon the process of measurement carried out on the first system, which does not disturb the second system in any way." [5]. Finally they conclude that the wave function can not provide a complete description of physical reality.

2.3 Bohr's Answer

In the same year Niels Bohr answered in a paper [6] with the same title as the EPR paper. Bohr used several experiments in which particles pass through slits in a diaphragm to explain the "complementarity principle" and why EPR's argument is not

[3] Fine summarizes the reasoning of EPR in a standard logical argument: "The argument develops in two parts. The first part demonstrates the validity of the disjunction $(INC) \vee (NSV)$. The second part shows the validity of the conditional $\neg(INC) \rightarrow \neg(NSV)$. The authors then conclude from this that (INC) must hold." [16]

appropriate for the Copenhagen interpretation of quantum mechanics.
The basic idea of Bohr's complementarity principle is the fact that when one entity of a complementary pair (i.e. momentum or position) is measured, the information of the other is always destroyed. This means that it is impossible to know everything about a microscopic physical system, as required by EPR.
Bohr shows in his paper that it is impossible to know at the same time the position and the momentum of a particle when doing experiments in which particles pass through slits in a diaphragm. From this he concludes that the experimental results depend on the measuring equipment and the measured physical quantities. They are an inseparable entity. For example "if a measurement proves the wave nature of radiation or matter, then it is impossible to prove the particle nature in the same measurement, and conversely." [17] In the 1935 paper Bohr concludes from his particle-slit experiments that "only the mutual exclusion of any two experimental procedures, permitting the unambiguous definition of complementary physical quantities, which provides room for new physical laws, the coexistence of which might at first sight appear irreconcilable with the basic principles of science. It is just this entirely new situation as regards the description of physical phenomena, that the notion of *complementarity* aims at characterizing." [6] The mutually exclusive measurability of position and momentum (non commuting physical quantities) is therefore the reason why the paradox derived by EPR can be solved by the complementarity principle.
At the end of his paper, Bohr states the importance of complementarity. "In fact this new feature of natural philosophy means a radical revision of our attitude as regards physical reality, which may be paralleled with the fundamental modification of all ideas regarding the absolute character of physical phenomena, brought about by the general theory of relativity." [6]
Although Bohr tried in many other attempts to convince Einstein of the complementarity principle, Einstein always refused to accept it as a principle in a physical sense. Einstein mainly refused it because of Bohr's failure to provide a clear formulation that could be experimentally tested. Besides Einstein, many other physicists did not agree with the nonlocality predicted by the EPR experiment.
In 1964 John Bell approached this problem. Originally he wanted to show that John von Neumann's nonlocality existence proof [18] was deficient. Bell wanted to find a way to relate such existence proofs to questions of locality. His research resulted in the famous Bell inequality.

2.4 The Bell inequality

In 1964 J. S. Bell [7, 8] constructed a mathematical proof that originally intended to show that a hidden variable theory can exist. Subsequently, however, he showed that a local theory contradicts the quantum mechanical predictions.
Bell derived his inequality, using the Bohm variant of the EPR Gedankenexperiment (Figure 2.1). A source sends correlated information to the two independent stations

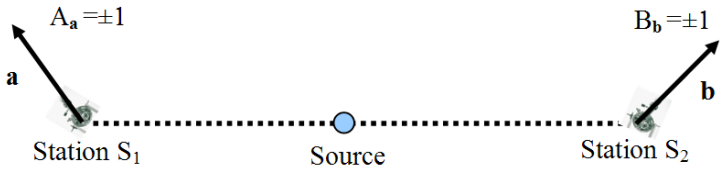

Figure 2.1: Experimental setup of the EPR-Bohm experiment. A source sends correlated information to two independent stations.

S_1 and S_2. These two stations can have different independent measuring equipment settings controlled by the setting parameter $\mathbf{s}$ in station S_1 ($A_\mathbf{s}$) or in station S_2 ($B_\mathbf{s}$).

In the derivation of his inequality, Bell uses the following three assumptions [7].

1. **Source Parameter Λ:** Suppose a hidden variable Λ exists and is defined on the probability space Ω. In addition the probability distribution $\rho(\lambda)$ of Λ is defined.

$$\Lambda = \Lambda(\omega) \quad \omega \in \Omega$$

$$P\{\Lambda \in F\} = P\{\omega : \Lambda(\omega) \in F\} = \int_F \rho(\lambda) d\lambda \qquad F \in \mathscr{L} \tag{2.1}$$

$$\int_{\mathscr{L}} \rho(\lambda) d\lambda = 1 \tag{2.2}$$

   Here $\mathscr{L}$ is the set of values Λ can assume.

2. **The random variables A and B** depend only on Λ and on the respective setting vectors[4]. They are defined on the same probability space.

$$A = A_\mathbf{a}(\Lambda) = A_\mathbf{a}(\Lambda(\omega)) \tag{2.3}$$

[4]The settings in each station are also described by a random variable S. Because the two random variables S and Λ are stochastically independent they both can be defined on a common product probability space.

$$B = B_{\mathbf{b}}(\Lambda) = B_{\mathbf{b}}(\Lambda(\omega)) \overset{perfect\ correlation}{=} -A_{\mathbf{b}}(\Lambda(\omega)) \tag{2.4}$$

3. **Equal probability condition** of possible outcomes:

$$P(A_{\mathbf{a}} = +1) = P(A_{\mathbf{a}} = -1) = \frac{1}{2} \tag{2.5}$$

Bell derived from these assumptions his celebrated inequality [7]:

$$|E(A_{\mathbf{a}}B_{\mathbf{b}}) - E(A_{\mathbf{a}}B_{\mathbf{c}})| \leq 1 + E(A_{\mathbf{b}}B_{\mathbf{c}}) \tag{2.6}$$

or modified by using (Equation 2.4)

$$|E(A_{\mathbf{a}}A_{\mathbf{b}}) - E(A_{\mathbf{a}}A_{\mathbf{c}})| \leq 1 - E(A_{\mathbf{b}}A_{\mathbf{c}}). \tag{2.7}$$

In addition, Bell shows that quantum mechanics predicts a violation of this inequality (2.6) for certain combinations of unitary measuring vector orientations (Figure 2.2).

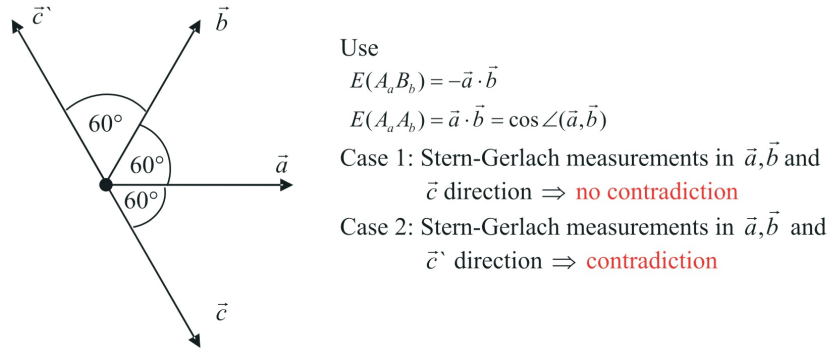

Figure 2.2: Orientations for spin measurement in the two particle 1/2-spin experiment used in Bell's derivation.

Therefore he concludes that no local hidden variable theory is possible that does not contradict quantum mechanics. Or stronger, no objective local theory can agree in all circumstances with the predictions of quantum mechanics.
The Bell paper was a milestone on the way to resolve the dispute between the physicists following Bohr and the local realists inspired by Einstein's believe in the incompleteness of quantum mechanics. For the first time in history, the quantum mechanical completeness question seemed to be translated to an experimentally testable relation.

In the following years, many different versions of Bell type inequalities were developed whereas the inequality of Clauser, Horne, Shimony and Holt (CHSH)[9] is the most significant generalization.

2.5 The Clauser-Horne-Shimony-Holt inequality

The CHSH inequality is a generalization of the Bell inequality. The authors aim to generalize Bell's theorem such that it can be applied to realizable experiments. In the following, the main steps in the derivation of the generalized Bell inequality and the mapping of this inequality to a real experiment are shown.
CHSH use for their derivation of the generalized Bell inequality the experimental setup seen in Figure 2.3. It is assumed that a source sends correlated information

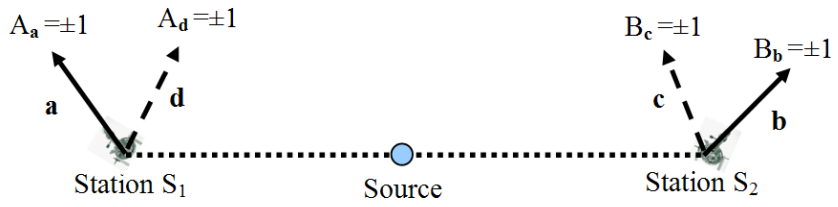

Figure 2.3: Clauser-Horne-Shimony-Holt setup for the derivation of the generalized Bell inequality.

to two independent measuring apparatuses. Each of the apparatuses has adjustable parameters ($\mathbf{s1} = \mathbf{a}$ or $\mathbf{d}$ and $\mathbf{s2} = \mathbf{b}$ or $\mathbf{c}$). CHSH introduce a set of hidden source parameters Λ. The probability distribution $\rho(\lambda)$ of these hidden variables is assumed to be independent of the setting parameters ($\mathbf{s1}$, $\mathbf{s2}$). Further, it is assumed that the random variables $A(\mathbf{s1}, \lambda)$ and $B(\mathbf{s2}, \lambda)$ are determined by the setting and source parameters.
Using these assumptions and some basic calculations [9] CHSH arrive at their well known inequality:

$$S = |E(A_{\mathbf{a}}B_{\mathbf{b}}) - E(A_{\mathbf{a}}B_{\mathbf{c}})| + E(A_{\mathbf{d}}B_{\mathbf{b}}) + E(A_{\mathbf{d}}B_{\mathbf{c}}) \leq 2. \tag{2.8}$$

This inequality is for example suitable for experimental tests with correlated photon pairs. Because no single photon measurements are yet possible, the following procedure is suggested by CHSH.
For light experiments (with photons), the measuring stations S_1 and S_2 can consist of polarizers followed by detectors. The values $+1(-1)$ of the random variables $A_{\mathbf{s1}}$

and $B_{\mathbf{s2}}$ denote the transmission (absobtion) of the photons through the polarizer with orientations **s1** and **s2** respectively. If the polarizer is removed, the orientation is defined as $\mathbf{si} = \infty$. It is clear that $A_\infty = +1$ and $B_\infty = +1$. To link (2.8) with the experiment a last assumption[5] is made:"...if a pair of photons emerges from I_a, II_b the probability of their joint detection is independent of a and b. Then if the flux into I_a, II_b is a constant independent of a and b, the rate of coincidence detection R(a,b) will be proportional to $w\left[A(a)_+, B(b)_+\right]$, where $w\left[A(a)_\pm, B(b)_\pm\right]$ is the probability that $A(a) = \pm 1$ and $B(b) = \pm 1$"[6][9]. In the following, CHSH define $R_o = R(\infty, \infty)$, $R_1(\mathbf{s1}) = R(\mathbf{s1}, \infty)$ and $R_2(\mathbf{s2}) = R(\infty, \mathbf{s2})$ and use

$$E(A_\mathbf{a}, B_\mathbf{b}) = w\left[A_{\mathbf{a}+}, B_{\mathbf{b}+}\right] - w\left[A_{\mathbf{a}+}, B_{\mathbf{b}-}\right] - w\left[A_{\mathbf{a}-}, B_{\mathbf{b}+}\right] + w\left[A_{\mathbf{a}-}, B_{\mathbf{b}-}\right] \tag{2.9}$$

and

$$w\left[A_{\mathbf{a}+}, B_{\infty+}\right] = w\left[A_{\mathbf{a}+}, B_{\mathbf{b}+}\right] + w\left[A_{\mathbf{a}+}, B_{\mathbf{b}-}\right] \tag{2.10}$$

and similar expressions to obtain

$$E(A_\mathbf{a} B_\mathbf{b}) = \frac{4R(\mathbf{a}, \mathbf{b})}{R_o} - \frac{2R_1(\mathbf{a})}{R_o} - \frac{2R_2(\mathbf{b})}{R_o} + 1. \tag{2.11}$$

This allows CHSH to express (2.8) in terms of experimental quantities:

$$S = |R(\mathbf{a}, \mathbf{b}) - R(\mathbf{a}, \mathbf{c})| + R(\mathbf{d}, \mathbf{b}) + R(\mathbf{d}, c) - R_1 - R_2 \leq 0. \tag{2.12}$$

Where it is assumed that $R_1(\mathbf{a}) = R_1$ and $R_2(\mathbf{b}) = R_2$ are constant.
In the last part of their paper, CHSH propose a modified version of an earlier experiment performed by Kocher and Commins [19]. Despite this suggestion for a real experiment it took more then a decade before the first experimenter succeeded to test the CHSH inequality.

2.6 The Aspect Experiments

Alain Aspect and his group published between 1981 and 1982 several papers in which they report about optical experiments, that confirm the quantum mechanical predictions for the EPR-Bohm experiment. In combination with the Bell inequality it is generally believed that the Aspect experiments prove the non-existence of hidden variable theories. In the following, two of Aspects papers are summarized. A more detailed discussion and critics of the experiment will be given in chapter 3.
In [2], Aspect uses the experimental setup seen in Figure 2.4 to measure an experimen-

[5] This assumption is nowadays known as fair sampling hypothesis.

[6] In the original paper, I_a and I_b refer to the stations S_1 and S_2 in this report. $A(a)$ is equal to A_{s1} and $B(b)$ corresponds to B_{s2} in this thesis.

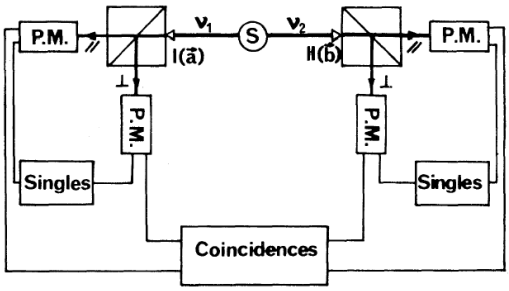

Figure 2.4: "Experimental setup. Two polarimeters I and II, in orientations $\vec{a}$ and $\vec{b}$, perform true dichotomie measurements of linear polarization on photons υ_1 and υ_2. Each polarimeter is rotatable around the axis of the incident beam. The counting electronics monitors the singles and the coincidences." [2]

tal violation of the generalized Bell inequality (2.8). Aspect uses in his experiment a calcium-40 source. The calcium atoms are placed into the excited state $4p^2\ ^1S_0$ by two single-mode lasers. The excited valence electron decays in a two step process (Figure 2.5), releasing a photon at 551.3 nm (green) and a photon at 422.7 nm (blue).

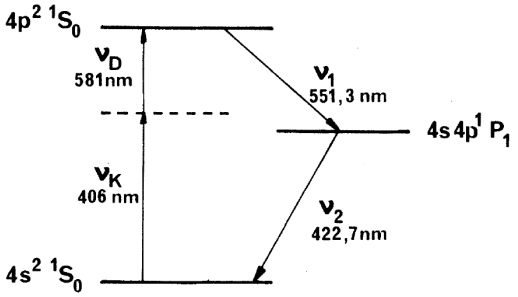

Figure 2.5: "Relevant levels of calcium. The atoms, selectively pumped to the upper level by the nonlinear absorption of υ_K and υ_L, emits the photons υ_1 and υ_2 correlated in polarization." [4]

Because the described process is a $(J = 0) \rightarrow (J = 1) \rightarrow (J = 0)$ cascade, the two emitted photons have correlated polarizations. When a photon arrives at the polarizing beam splitter (PBS) it is transmitted $(+1)$ with a probability of $cos^2(\alpha)$ where α is the angle between the photon polarization and the principle transmission direction of the PBS. Otherwise the photon is reflected (-1).

To test the generalized Bell inequality (2.8), Aspect defines

$$E(A_{\mathbf{a}}B_{\mathbf{b}}) = \frac{R_{++}(\mathbf{a},\mathbf{b}) + R_{--}(\mathbf{a},\mathbf{b}) - R_{+-}(\mathbf{a},\mathbf{b}) - R_{-+}(\mathbf{a},\mathbf{b})}{R_{++}(\mathbf{a},\mathbf{b}) + R_{--}(\mathbf{a},\mathbf{b}) + R_{+-}(\mathbf{a},\mathbf{b}) + R_{-+}(\mathbf{a},\mathbf{b})} \tag{2.13}$$

where $R_{\pm\pm}(\mathbf{a},\mathbf{b})$ are four coincidence rates that are defined as follows. If the two photomultipliers detecting the photons, transmitted through the PBS (in the two polarimeters I and II), register a photon within a 20 ns time window[7] then we have measured a ($A_{\mathbf{a}} = +1$,$B_{\mathbf{b}} = +1$) event and can therefore increase $R_{++}(\mathbf{a},\mathbf{b})$.
Definition (2.13) is allowed because of the assumed validity of the fair sampling theorem. To obtain the maximal violation of (2.8) in optical experiments the polarimeter orientations have to be chosen as $(\mathbf{a},\mathbf{b}) = (\mathbf{d},\mathbf{b}) = (\mathbf{d},\mathbf{c}) = 22.5^o$ and $(\mathbf{a},\mathbf{c}) = 67.5^o$ (Figure 2.6). Aspect's measurement results are $S_{expt} = 2.697 \pm 0.015$. This was the

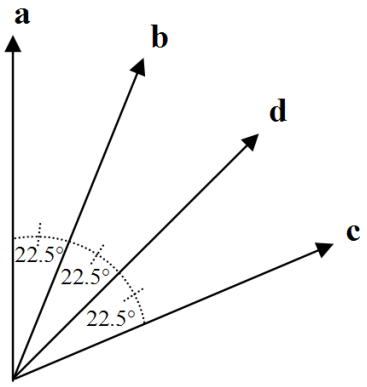

Figure 2.6: Orientations leading to a maximum violation of the generalized Bell inequalities.

largest violation of inequality (2.8) reported until that time.
Despite of this strong experimental violation of (2.8) many physicists were not yet convinced and they claimed that the source might be influenced by the polarimeter orientation and that the violation of (2.8) can therefore be explained classically[8].
In the same year (1982) Aspect published a second paper [3] that disproved this hypothesis. He introduced the method of delayed choice. This means that the polarization orientation of the polarizer is chosen after the source has emitted the photon pair. The polarizer orientation is changed fast enough by employing a trick. Instead of rotating the polarizers, the photons are redirected by an optical switch toward

[7] In this case it is assumed that the two photons are from the same polarization correlated photon pair.

[8] This means with an objective local theory

fixed polarizers in different channels. The optical switching of the light is done by acousto-optical interaction with an ultrasonic standing wave in water [3]. Because the optical switch has a frequency of around 50 MHz (switching between two channels every 10 ns), it can safely be stated that the polarizer orientation changes during the flight of the photons. This means that the polarizer orientation can not have an influence on the generation process of the correlated photon pair.
In this experiment Aspect tests an inequality similar to (2.12). The measured value for the quantity S is $S_{expt} = 0.101 \pm 0.020$ for the polarizer orientations seen in Figure 2.6. This is a violation of inequality (2.12) of 5 standard deviations. Therefore, no hidden variable theory can explain the experimental results.
The Aspect experiments are generally accepted as first experimental proof of the completeness of quantum mechanics. Despite of the fact that the experiments clearly show a violation of the generalized Bell inequalities, many physicists keep doubting the consequences connected to the quantum mechanical explanation of EPR type of experiments. Especially the necessary quantum nonlocality is still alarming many physicists.
During the years after the Aspect experiments many reasons where found, why the Aspect experiment can not be taken as ultimate proof for the non-existence of locality. In chapter 3 some of these loopholes will be explained in more details.
In the next section the latest important theoretical contribution to the question whether or not quantum mechanics is a complete theory is introduced.

2.7 The Greenberger-Horne-Zeilinger Gedankenexperiments

The GHZ Gedankenexperiments are a set of experiments that analyze quantum mechanical systems of three or more correlated spin-1/2 particles. Similar to the Bell type inequalities, the GHZ Gedankenexperiments try to answer the question whether or not a hidden variable theory beyond the quantum mechanical theory exists. The innovative idea in the GHZ experiments is that their arguments only consider perfect correlations rather than the statistical correlations normally used to demonstrate the incompatibility of EPR's propositions with quantum mechanics. Greenberger, Horne, Shimony and Zeilinger attempt to show in their review paper [20] how the Bell theorem can be derived without inequalities. They present two different examples. One is a four-particle spin-entangled state experiment and in their second Gedankenexperiment they use a three-particle interferometer.

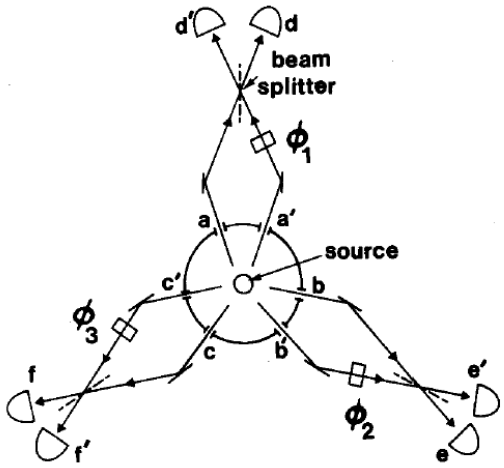

Figure 2.7: Three-particle interferometric GHZ Gedankenexperiment.[20]

Because in this work the maximum number of entangled particles is limited to three, only the three-particle entangled state Gedankenexperiment is explained. The Gedankenexperimental setup used in [20] can be seen in Figure 2.7. It is assumed that the source in the central region consists of a particle that has a (mean) momentum of zero. This particle decays in three particles of equal mass (or into three photons). "If all three particles have the same energy, then, by momentum conservation, they must be emitted 120^o apart. The equal energy requirement can be enforced by placing energy filters at the detectors. The central source is surrounded by an array of six apertures, the three particles 1, 2 and 3 must emerge either through a, b, and c or through a', b', and c'." [20] Therefore, the quantum mechanical description of the state of the three particles beyond the apertures is

$$|\Psi\rangle = \frac{1}{\sqrt{2}}\left[|a\rangle_1 |b\rangle_2 |c\rangle_3 + |a'\rangle_1 |b'\rangle_2 |c'\rangle_3\right] \tag{2.14}$$

where $|a\rangle_1$ stands for particle 1 in beam a, etc. When the transformations[9]

$$|a\rangle_1 \rightarrow \frac{1}{\sqrt{2}}\left[|d\rangle_1 + i\,|d'\rangle_1\right] \tag{2.15}$$

and

$$|a'\rangle_1 \rightarrow \frac{e^{i\phi_1}}{\sqrt{2}}\left[|d'\rangle_1 + i\,|d\rangle_1\right] \tag{2.16}$$

[9]These transformations come from the phase shifters ϕ_i and 50-50 beam splitters seen in Figure 2.7.

are applied to the entangled three particle state (2.14) then the measured three-particle state with eight terms develops. The squared amplitude of the measured states equal the probabilities of detection for the eight possible measurement results:

$$P^{\Psi}_{def}(\phi_1,\phi_2,\phi_3) = \frac{1}{8}\left[1 + sin(\phi_1+\phi_2+\phi_3)\right] \tag{2.17}$$

$$P^{\Psi}_{d'ef}(\phi_1,\phi_2,\phi_3) = \frac{1}{8}\left[1 - sin(\phi_1+\phi_2+\phi_3)\right] \tag{2.18}$$

$$P^{\Psi}_{de'f}(\phi_1,\phi_2,\phi_3) = \frac{1}{8}\left[1 - sin(\phi_1+\phi_2+\phi_3)\right] \tag{2.19}$$

$$P^{\Psi}_{d'e'f}(\phi_1,\phi_2,\phi_3) = \frac{1}{8}\left[1 + sin(\phi_1+\phi_2+\phi_3)\right] \tag{2.20}$$

$$P^{\Psi}_{def'}(\phi_1,\phi_2,\phi_3) = \frac{1}{8}\left[1 - sin(\phi_1+\phi_2+\phi_3)\right] \tag{2.21}$$

$$P^{\Psi}_{d'ef'}(\phi_1,\phi_2,\phi_3) = \frac{1}{8}\left[1 + sin(\phi_1+\phi_2+\phi_3)\right] \tag{2.22}$$

$$P^{\Psi}_{de'f'}(\phi_1,\phi_2,\phi_3) = \frac{1}{8}\left[1 + sin(\phi_1+\phi_2+\phi_3)\right] \tag{2.23}$$

$$P^{\Psi}_{d'e'f'}(\phi_1,\phi_2,\phi_3) = \frac{1}{8}\left[1 - sin(\phi_1+\phi_2+\phi_3)\right] \tag{2.24}$$

To follow the idea of the EPR-Bohm experiment, the result is called $+1$ (-1) if the particle is registered by an unprimed (primed) detector. This definition together with (2.17-2.24) can be used to calculate the expectation value of the product of the three outcomes:

$$E^{\Psi}(\phi_1,\phi_2,\phi_3) = sin(\phi_1+\phi_2+\phi_3) \tag{2.25}$$

It is then easy to see that "perfect correlations are obtained for the following choices of angles:" [20]

$$E^{\Psi}(\phi_1,\phi_2,\phi_3) = +1 \qquad \text{if} \quad \phi_1+\phi_2+\phi_3 = \frac{\pi}{2} \tag{2.26}$$

$$E^{\Psi}(\phi_1,\phi_2,\phi_3) = -1 \qquad \text{if} \quad \phi_1+\phi_2+\phi_3 = \frac{3\pi}{2} \tag{2.27}$$

These equations (2.26-2.27) are then used by GHSZ to create a new EPR test based on an idea proposed by Mermin [10]. It is assumed that the results ($+1$ or -1) of the measurements in the six stations d, d', e, e', f and f' can be described by the three random variables D, E and F. As in the derivation of the Bell inequalities, a hidden source parameter Λ with the possible realization λ is introduced. In addition it is assumed that the values of D, E and F also depend on ϕ_1, ϕ_2 and ϕ_3 respectively. This means that the perfect correlation conditions can be rewritten as

$$D_\lambda(\phi_1)E_\lambda(\phi_2)F_\lambda(\phi_3) = +1 \qquad \text{if} \quad \phi_1+\phi_2+\phi_3 = \frac{\pi}{2} \tag{2.28}$$

$$D_\lambda(\phi_1)E_\lambda(\phi_2)F_\lambda(\phi_3) = -1 \qquad \text{if} \quad \phi_1+\phi_2+\phi_3 = \frac{3\pi}{2}. \tag{2.29}$$

From these perfect correlations (2.28-2.29) the following 4 relations can be obtained:

$$D_\lambda\left(\frac{\pi}{2}\right) E_\lambda\left(\frac{\pi}{2}\right) F_\lambda\left(\frac{\pi}{2}\right) = -1 \tag{2.30}$$

$$D_\lambda(0)\, E_\lambda(0)\, F_\lambda\left(\frac{\pi}{2}\right) = +1 \tag{2.31}$$

$$D_\lambda(0)\, E_\lambda\left(\frac{\pi}{2}\right) F_\lambda(0) = +1 \tag{2.32}$$

$$D_\lambda\left(\frac{\pi}{2}\right) E_\lambda(0)\, F_\lambda(0) = +1. \tag{2.33}$$

If we assume that λ is the same for all four measurements[10] then (2.31), (2.32) and (2.33) can be multiplied and we obtain:

$$D_\lambda\left(\frac{\pi}{2}\right) E_\lambda\left(\frac{\pi}{2}\right) F_\lambda\left(\frac{\pi}{2}\right) = +1. \tag{2.34}$$

But this contradicts the quantum mechanical prediction (2.30). This means that the GHZ argument "concerns only perfect correlations rather than statistical correlations, and it completely dispenses with inequalities." [20]
In the next section the experimental realization of the GHZ Gedankenexperiment is introduced.

2.8 The Pan *et al.* realization of the GHZ Gedankenexperiment

Ten years after the theoretical formulation of the GHZ Gedankenexperiment, Pan *et al.* published in 2000 the first experimental test of quantum nonlocality in three-photon Greenberger-Horne-Zeilinger (GHZ) entanglement [1]. The experimental setup of the optics based GHZ test of quantum nonlocality can be seen in Figure 2.8. In their letter Pan *et al.* show that no local realistic model based on a small number of elements of reality can explain the measured results.
In [1], the experiment is first analyzed with quantum mechanical methods. It is assumed that the entangled three-photon GHZ state is:

$$|\psi\rangle = \frac{1}{\sqrt{2}}\left(|H\rangle_1 |H\rangle_2 |H\rangle_3 + |V\rangle_1 |V\rangle_2 |V\rangle_3\right) \tag{2.35}$$

where H (V) denotes horizontal (vertical) linear polarization. Then four new polarization directions are introduced. Two of them are linear polarizations along H'/V'

[10] Here it should be emphasized that this is only possible in "Gedanken", but can never be measured in a real experiment.

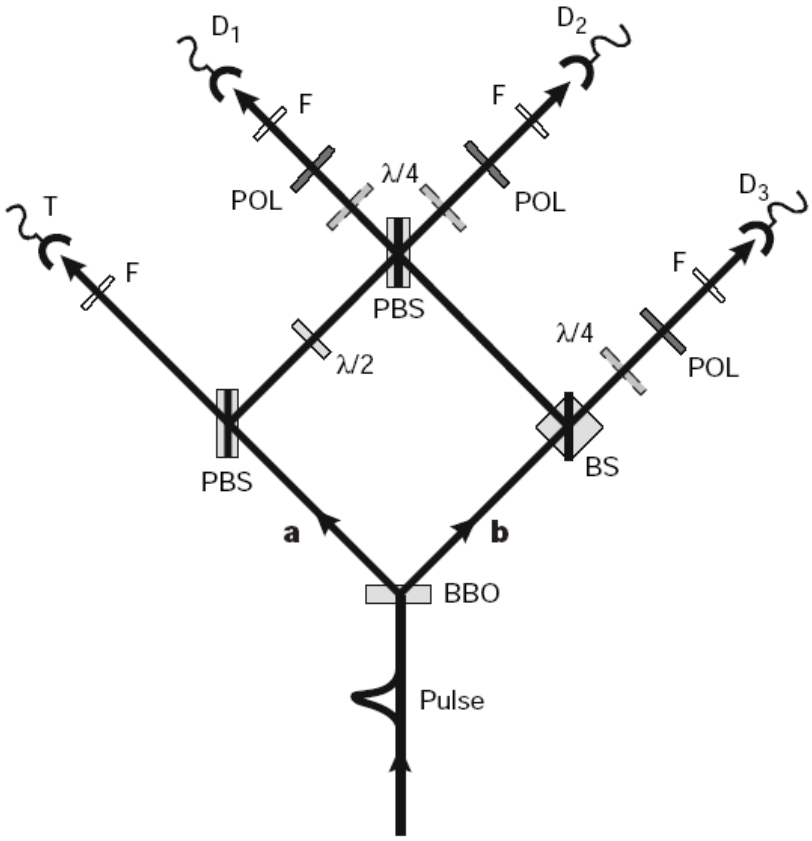

Figure 2.8: Experimental setup for the Greenberger-Horne-Zeilinger (GHZ) tests of quantum nonlocality used by Pan *et al.* [1]. In the actual experiment four polarization correlated photons are generated. After having propagated through a setup with several optical elements (wave-plates and beam splitters), the polarizations of three of the four photons, denoted as photon 1, 2 and 3, are measured by equipments consisting of polarization analyzers and three detectors D_1, D_2 and D_3. Whenever detector D_i clicks, it is known that the registered photon i features the polarization indicated by the polarization analyzers in front of the detector. The fourth photon (registered by detector T) is used to guarantee that photon 1, 2 and 3 are in the entangled three-photon GHZ state. Only when all four detectors T, D_1, D_2 and D_3 register a photon within a certain time window, it is assumed that the three photons 1, 2 and 3 are in the entangled three-photon GHZ state. This detection of four photons is called fourfold coincidence.

($45^o/-45^o$ polarization) and the other two are circular polarizations L/R (left-/right-handed).

$$\left|H'\right\rangle = \frac{1}{\sqrt{2}}\left(|H\rangle + |V\rangle\right) \tag{2.36}$$

$$\left|V'\right\rangle = \frac{1}{\sqrt{2}}\left(|H\rangle - |V\rangle\right) \tag{2.37}$$

$$|R\rangle = \frac{1}{\sqrt{2}}\left(|H\rangle + i\,|V\rangle\right) \tag{2.38}$$

$$|L\rangle = \frac{1}{\sqrt{2}}\left(|H\rangle - i\,|V\rangle\right). \tag{2.39}$$

These linear transformations are used to predict the measurement results in the new basis. The measurement in the linear basis is defined as x measurement and the measurement in the circular basis is denoted as y measurement. In [1] the yyx experiment is predicted by the following quantum state:

$$\begin{aligned}|\psi\rangle = \frac{1}{2}(&|R\rangle_1 |L\rangle_2 \left|H'\right\rangle_3 + |L\rangle_1 |R\rangle_2 \left|H'\right\rangle_3 \\ &+ |R\rangle_1 |R\rangle_2 \left|V'\right\rangle_3 + |L\rangle_1 |L\rangle_2 \left|V'\right\rangle_3).\end{aligned} \tag{2.40}$$

Besides this state for the yyx experiment they also show the quantum mechanical prediction for the xxx experiment:

$$\begin{aligned}|\psi\rangle = \frac{1}{2}(&\left|H'\right\rangle_1 \left|H'\right\rangle_2 \left|H'\right\rangle_3 + \left|H'\right\rangle_1 \left|V'\right\rangle_2 \left|V'\right\rangle_3 \\ &+ \left|V'\right\rangle_1 \left|H'\right\rangle_2 \left|V'\right\rangle_3 + \left|V'\right\rangle_1 \left|V'\right\rangle_2 \left|H'\right\rangle_3).\end{aligned} \tag{2.41}$$

In addition to this quantum mechanical model, a local realistic model is introduced by Pan *et al.*. "The only way then for local realism to explain the perfect correlations predicted by equation (4) is to assume that each photon carries elements of reality for both x and y measurements that determine the specific individual measurement result. For photon i we call these elements of reality X_i with values $+1(-1)$ for $H'(V')$ polarizations and Y_i with values $+1(-1)$ for $R(L)$..." [1]. Then the quantum mechanically predicted relations $Y_1Y_2X_3 = -1$, $Y_1X_2Y_3 = -1$ and $X_1Y_2Y_3 = -1$ are used by Pan *et al.* to restrict the possible combinations of values for the elements of reality and to find the local realistic preditions for the xxx experiment: "Because of Einstein locality any specific measurement for x must be independent of whether an x or y measurement is performed on the other photon. As $Y_iY_i = +1$, we can write $X_1X_2X_3 = (X_1Y_2Y_3)(Y_1X_2Y_3)(Y_1Y_2X_3)$ and obtain $X_1X_2X_3 = -1$. Thus from a local realist point of view the only possible results for an xxx experiment are $V'V'V'$, $H'H'V'$, $H'V'H'$, and $V'H'H'$." [1]

Subsequently Pan *et al.* show the measurement results for the yyx, yxy, xyy and also the xxx experiments. These measurement results are reproduced by the green bars in Figure 4.2.
As it turns out the experimental results [1] do not strictly comply with $yyx = -1$, $yxy = -1$ and $xyy = -1$. In fact, the measured relative frequency of the states predicted by quantum mechanics for the GHZ state is only 0.85 ± 0.04, whereas the so-called spurious events do occur with non-negligible relative frequency of 0.15 ± 0.02. The measured relative frequency of the states predicted by quantum mechanics for equation $xxx = +1$ is 0.87 ± 0.04 with the spurious events occurring with relative frequency of 0.13 ± 0.02. Because "the sum of the fractions of all spurious events in the yyx, yxy, and xyy experiments, that is, 0.45 ± 0.03" [1] is significantly less than 0.87 ± 0.04, the authors interpret their findings as the first three-particle test of local realism following the GHZ argument. In their final analysis they conclude that no objective local model can explain the experimental results and that quantum nonlocality is therefore proven.
The Pan realization of the GHZ Gedankenexperiment will be discussed in great detail in chapter 4. In the next section of this chapter, the main critique of the theorem of Bell, worked out by Karl Hess and Walter Philipp, is explained.

2.9 Critique of the Theorem of Bell

During the last five years Karl Hess and Walter Philipp published several papers about the Bell theorem and the CHSH inequality [21, 22]. Hess and Philipp particularly show in their work that time and setting dependent equipment parameters can not be excluded by standard Bell type proofs. Therefore, the Bell and CHSH inequalities can not be used to decide whether or not local hidden variable theories can exist.
Another main critique regards the assumption that the source parameter Λ has the same realization for different measurements. They show in their work, that the Bell and CHSH inequalities are special cases of a mathematical theorem derived by the mathematician J. Bass [23] in 1955[11]. The main result of Bass gives conditions under which three pair distributions, defined in the Euclidean plane, can be obtained from three random variables, defined on a common probability space. Specialized to Bell's situation the theorem of Bass states that this can be achieved if and only if the covariances $(\sigma_1, \sigma_2, \sigma_3)$ of the three given pair distributions, considered as a point in

[11] Vorobev fully generalized the theorem in 1962 [24].

$\mathbb{R}^3$ belong to the tetrahedron displayed in Figure 2.9.

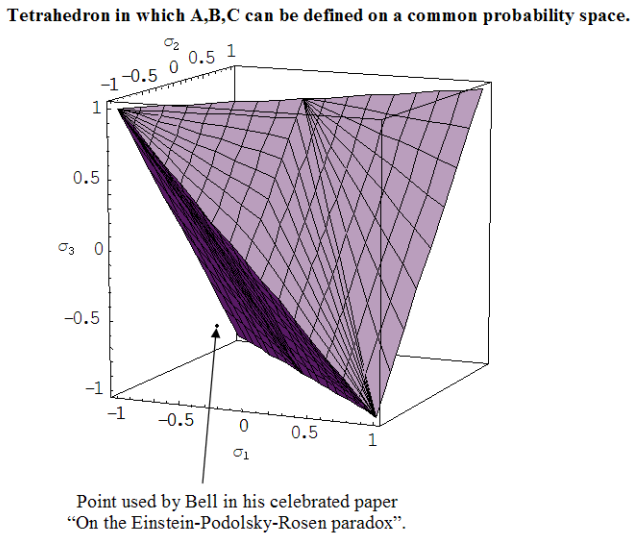

Figure 2.9: Tetrahedron defined by the Bass (Bell) inequalities. $\sigma_{i=1,2,3}$ are the three covariances defining the joint pair distributions of the random variables A, B and C.

Because in Bell's and CHSHs' derivation of their inequalities, the same realization of the source parameter λ determines the value of the involved hidden variables, all hidden variables are defined on a common product probability space. Therefore the famous inequalities of Bell and CHSH are the same as the inequalities derived by J. Bass. This means that the inequalities are only due to the assumption that all measured random variables are defined by the same source parameter and therefore defined on the same probability space. But because in an actual experiment, it is impossible to measure all random variables at the same time, the inequalities can not be tested in an actual experiment. This is because the assumption of the same λ for all measurements does not have to be fulfilled and because the time and setting dependent equipment parameters can be different for different times.

2.10 Conclusion

As history shows, the question of the completeness of quantum mechanics has been of great interests for many decades. Especially the existence of the quantum mechanical nonlocality (due to entanglement) has deep impact on current research topics such as quantum teleportation or quantum computing that are based on the existence of

entanglement.
In the following chapters the Aspect experiment and the Pan *et al.* realization of the GHZ experiment are discussed.

Chapter 3

Analysis of the Aspect Experiments

3.1 Introduction

As described before, Alain Aspect showed for the first time in a series of experiments [2, 3, 4] an experimental violation of the Bell inequalities. The principle experimental setup used by Aspect has been explained in section 2.6. The Aspect experiments are often considered as proof of quantum nonlocality and the nonlocal nature of entanglement. Although the non-intuitive results and explanations are widely accepted, many researchers doubt either the correctness of the experiments [25] or the significance of the inequalities used to rule out local hidden variable theories [21, 22].
Many highly recognized physicists (Einstein, Schrödinger,...) felt, that locality is one of the most important principles not to be violated. This chapter aims to reiterate that the Aspect experiments are not loophole free and that an objective local model may be established which is as plausible as quantum nonlocality (spooky action at a distance).
The model introduced in this chapter shows a modified version of the known detection inefficiency loophole.

3.2 Objective Local Model based on Detection Inefficiency

In this section, an objective local model based on the detection inefficiency loophole (OLMDI) is described. OLMDI was developed on the basis of Maxwell's electromag-

netic wave theory and the well know Jones matrices.
Jones matrices describe how optical elements transform a polarized incident light beam

$$\mathbf{E_i} = \begin{pmatrix} E_i^H \\ E_i^V \end{pmatrix}$$

into the transmitted beam

$$\mathbf{E_t} = \begin{pmatrix} E_t^H \\ E_t^V \end{pmatrix}.$$

Here E_i^H (E_i^V) is the horizontal (vertical) component of the electric field of the incident beam and $\mathbf{E_i}$ is the Jones vector of the incident beam. The Jones matrix $\mathbf{T}$ is a 2x2 matrix. The transmitted beam can be related to the incident beam as follows [26]:

$$\begin{pmatrix} E_t^H \\ E_t^V \end{pmatrix} = \mathbf{T} \begin{pmatrix} E_i^H \\ E_i^V \end{pmatrix} = \begin{pmatrix} t_{11} & t_{12} \\ t_{21} & t_{22} \end{pmatrix} \begin{pmatrix} E_i^H \\ E_i^V \end{pmatrix}. \tag{3.1}$$

In the next subsections, the optical devices used in the Aspect experiments are described. Then, the simulation results are shown and finally, the significance of OLMDI is discussed.

3.2.1 Optical Elements, Source and Detectors

The experimental setup used by Aspect consists mainly of five different types of devices. A photon source (Calcium-40), photon-detectors, polarizing beam splitters, frequency filters and a complex counting electronics.

Calcium-40 Source

As already described in section 2.6, Aspect uses in his experiment a calcium-40 source. Because the described cascade is a $(J = 0) \rightarrow (J = 1) \rightarrow (J = 0)$ cascade, the two resulting photons are correlated in polarization. In the OLMDI model, each photon is described by two 2-dimensional vectors:

$$\begin{pmatrix} E_i^H \\ E_i^V \end{pmatrix} = \begin{pmatrix} E_{norm} cos\left(\alpha_i^E\right) e^{j\gamma_i} \\ E_{norm} sin\left(\alpha_i^E\right) e^{j\gamma_i} \end{pmatrix} \tag{3.2}$$

$$\begin{pmatrix} HV_i^H \\ HV_i^V \end{pmatrix} = \begin{pmatrix} HV_{norm} cos\left(\alpha_i^{HV}\right) e^{j\gamma_i} \\ HV_{norm} sin\left(\alpha_i^{HV}\right) e^{j\gamma_i} \end{pmatrix} \tag{3.3}$$

where i can assume the values A or B. One vector describes the polarization of the photon and the other vector describes a hidden parameter vector (Figure 3.1). We

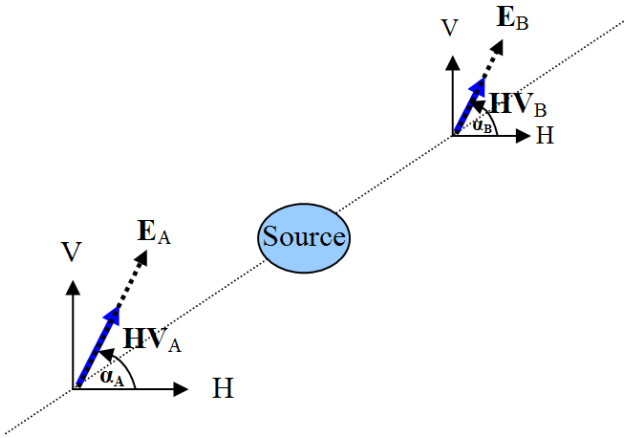

Figure 3.1: The Calcium-40 source used in the Aspect experiments [2, 3, 4] produce two correlated photons A and B.

denote the photon that goes to station S_1 and S_2 (Figure 2.4) as photon A and B respectively. In the actual simulation, $\alpha_A^E = \alpha_A^{HV} = \alpha_B^E = \alpha_B^{HV} = \alpha$. γ_A, γ_B and α are uniformly distributed over $0 - 2\pi$, $E_{norm} = 1$ and $HV_{norm} = \frac{1}{2}$.

Polarizing Beam Splitter

The polarizing beam splitter (PBS) is a non-absorbing optical element. The probability of transmission for a photon is

$$p_{trans} = cos^2(\beta) \tag{3.4}$$

where β is the angle between the principle transmission direction of the PBS and the polarization of the incident photon.
When the photon is transmitted, then the unitary polarization vector $\mathbf{E}_i$ ($i = A$ or B) of the transmitted photon has the same orientation as the principle transmission direction of the PBS. If the incident photon is reflected, the reflected photon has an unitary polarization vector perpendicular to the principle transmission direction of the PBS.
The effect of the PBS on the second (hidden) parameter is rather complicated and it depends on the amount of photons and also the closeness in time and space of these incident photons.
In the Aspect experiments it is assumed that we have only one incident photon per time interval. Therefore, the hidden parameter vector $\mathbf{HV}_i$ of the incident photon is

either transformed by

$$T^{PBS} = a^{PBS} \begin{pmatrix} 1 & 0 \\ 0 & 0 \end{pmatrix} \tag{3.5}$$

where it is assumed that the principle direction of transmission of the PBS is parallel to the horizontal axis H.
If the incident photon is reflected, then the resulting value of $\mathbf{HV}_i^{out}$ is obtained by multiplying $\mathbf{HV}_i$ with

$$R^{PBS} = a^{PBS} \begin{pmatrix} 0 & 0 \\ 0 & i \end{pmatrix}. \tag{3.6}$$

From a basic energy conservation calculation for the hidden variables[1] we obtain $a^{PBS} = \frac{2}{\sqrt{3}}$.

Narrow Bandwidth Filters

The filters seen in Figure 2.4 only allow the transmission of one of the two wavelengths 551.3 nm (green) or 422.7 nm (blue). Thus, the filters guarantee that only green (blue) photons reach the detector in path A (B). The narrow bandwidth filters also help to reduce the environmental noise.

Photodetectors

In optical experiments, silicon avalanche photodiodes are the most common choice. In OLMDI, the detection inefficiency loophole is used to explain the experimental results [2]. Although it is possible to assign a detection inefficiency to the narrow bandwidth filters, in OLMDI the detection inefficiency is assumed to be due to inefficient silicon avalanche photodiodes.
From biological experiments with organic single photon detectors or in other words rods[2], it is known that the detection probability is intensity dependent [27]. From these biological experiments it is also known that the intensity versus detection-probability curve has an S-shape (Figure 3.2) that can be described by

$$p_{detect} = \sum_{n=\delta}^{\infty} \frac{e^{-\alpha I}}{n!} (\alpha I)^n. \tag{3.7}$$

[1] $(a^{PBS})^2 \int_0^{2\pi} \underbrace{cos^2(\delta)}_{P_{transmit}} \underbrace{\frac{1}{4} cos^2(\delta)}_{Energy_{hidden}} + \underbrace{sin^2(\delta)}_{P_{reflect}} \underbrace{\frac{1}{4} sin^2(\delta)}_{Energy_{hidden}} \; d\delta = \frac{1}{4} 2\pi \Rightarrow a^{PBS} = \frac{2}{\sqrt{3}}$

[2] Photo receptors in human eyes.

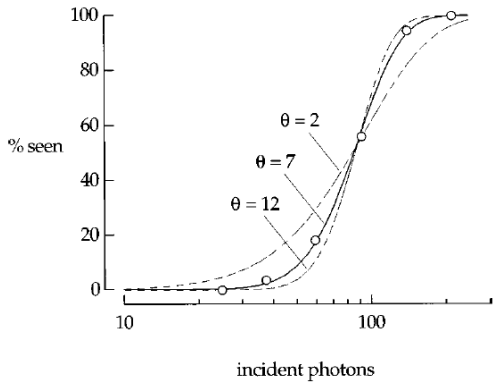

Figure 3.2: "Probability of seeing a flash plotted against the logarithm of the number of photons incident on the front of the eye for several flash strengths."[27]

Here α is a proportionality factor and I denotes the light intensity.
In the Aspect experiments, it is assumed that single indivisible photons hit the detectors. In the presented model, relation (3.7) is used to describe the behavior of the avalanche photodiode detectors. The parameters in (3.7) are interpreted as follows. Instead of the beam intensity, the square of the amplitude of the hidden parameter vector $\mathbf{HV}_i$ is identified with I. In the simulation, the proportionality factors are $\alpha = 36.5$ and $\delta = 7$ (Figure 3.3).

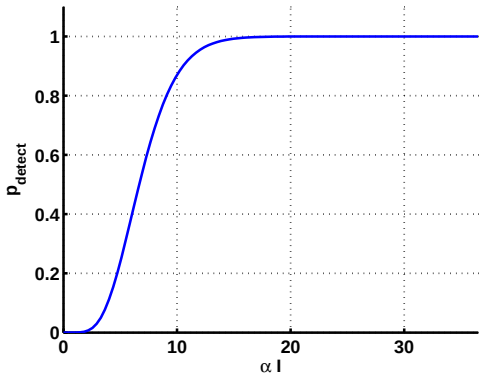

Figure 3.3: Detection probability of a single photon depending on the product of the amplitude square of the hidden parameter vector $I = |\mathbf{HV}_i|^2$ and the proportionality factor α.

Counting Electronics

The fourfold coincidence counting electronics in the Aspect experiments is used to distinguish between uncorrelated single photon counts ($10^4 s^{-1}$) and the true coincidences of correlated photon pairs ($0 - 40 s^{-1}$ where the accidental rates of around $10 s^{-1}$ is already subtracted). The coincidence window is about 20 ns long. Because this is large compared to the lifetime of the intermediate state of the cascade (5 ns), it is assumed that all true coincidences are registered [2]. The significance of the counting electronics will be discussed in section 3.2.3. For the simulation it is assumed that only correlated indivisible photon pairs are generated and that the counting electronics has an efficiency of 100%. This means that only one of the two detectors[3] on each side (A and B) can fire. Whenever detectors on both sides A and B fire simultaneously (within the coincidence time window) a coincidence count is registered[4].
In the next subsection, the main simulation results for the Aspect experiments based on OLMDI are discussed.

3.2.2 OLMDI Simulation Results

In this subsection, the simulation results of the two main experiments of Aspect [2, 3] are discussed. In July 1982 Aspect published a paper that shows a violation of the CHSH inequality (2.8). He used a fourfold coincidence technique, to measure the four coincidence rates $R_{\pm\pm}(\mathbf{a}, \mathbf{b})$. As described in section 2.6, the correlation coefficient along $\mathbf{a}$ and $\mathbf{b}$ can be defined as:

$$E(A_{\mathbf{a}} B_{\mathbf{b}}) = \frac{R_{++}(\mathbf{a}, \mathbf{b}) + R_{--}(\mathbf{a}, \mathbf{b}) - R_{+-}(\mathbf{a}, \mathbf{b}) - R_{-+}(\mathbf{a}, \mathbf{b})}{R_{++}(\mathbf{a}, \mathbf{b}) + R_{--}(\mathbf{a}, \mathbf{b}) + R_{+-}(\mathbf{a}, \mathbf{b}) + R_{-+}(\mathbf{a}, \mathbf{b})}. \tag{3.8}$$

Using this relation (3.8) and the OLMDI model described in subsection 3.2.1, the simulation results shown in Figure 3.4 are obtained.
It can be seen that the simulation comes close to the quantum mechanical prediction

[3] If the detector that registers the transmitted photons fires, then a $+1$ is assigned to the random variable at the measured side A or B. If the detector in the reflected path fires, then a -1 is registered.

[4] It is assumed that the detection inefficiency, which can be a sum of the filter and detector inefficiencies, could also be interpreted such that the magnitude of the hidden variable parameter is inverse proportional to the delay between the impact of the photon on the detector and the time when the photon is really registered by the avalanche diode. If the photon on one side is registered after a long delay (longer than the coincidence time window) compared to the photon on the other side, two singles instead of a correlated pair are registered.

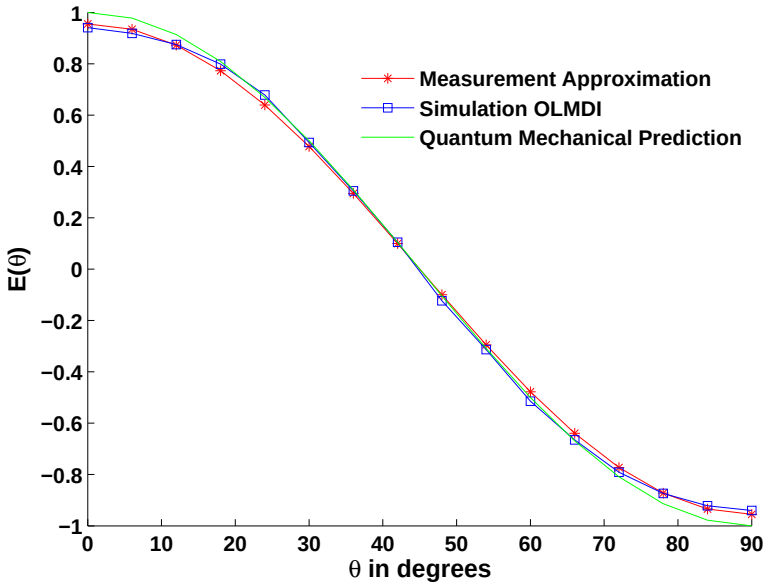

Figure 3.4: Correlation of polarizations as a function of the relative angle between the polarimeters. The simulation with OLMDI is close to the measured results and is clearly a local model that violates the generalized Bell inequality [9]. For each simulated point 30000 correlated photon pairs are generated.

$cos\,(2\theta)$ [5] and it also agrees well with the measured results.
It can easily be verified that OLMDI predicts the experimentally observed rotational invariance of the Aspect experiment. It was also confirmed that the expectation value for the measurements in each station is zero. This means that the two measurement results $+1$ and -1 are registered with equal rates on each side.
The simulation of the value S, defined by the CHSH inequality (2.8), for the four polarizer orientations (Figure 2.6) resulting in the greatest conflict between (2.8) and the quantum mechanical predictions, gives $S_{sim} = 2.8136$.
The simulation also showed that 72.25% of the photons emitted in the direction of one side are registered by one of the detectors ($+1$ or -1). Because the PBS is non-absorbing, the detector efficiency is 72.25%. Before the simulation results are discussed two more simulations using the OLMDI model are carried out.
In [3], the generalized Bell inequality in the form of (2.12) is tested. The measurements show a violation of the inequality $S \leq 0$ by 5 standard deviations. The measured value is $S_{expt} = 0.101 \pm 0.020$. The simulation for the setup given in [3] calculates a value of $S_{sim} = 0.0748$. This value is clearly above the classically allowed maximum of 0. The simulation results of the normalized coincidence rate as a function of the relative orientation of the polarizers are shown in Figure 3.5.

In the following subsection, the simulation results are discussed. It is shown that the detection inefficiency used in OLMDI is within the normally observed detection inefficiencies.

3.2.3 Significance of the Results

First of all it is important to realize that in the Aspect experiments only a small fraction of the observed photons are registered as coincidence counts. The single rate[6] ($10^4 s^{-1}$) is much higher than the measured "true coincidence rates" ($0 - 40 s^{-1}$).
Let us assume that the measured coincidence rate $80 s^{-1}$ of the sum of the four coincidence rates $R_{\pm\pm}(\mathbf{a}, \mathbf{b})$ represents only a small fraction of the emitted correlated photon pairs. We can use OLMDI to calculate the actual rate of emitted correlated photon pairs. If the detector efficiency is 72.25% and the measured coincidence rate is $80 s^{-1}$, then the true rate of polarization correlated photon pairs emitted by the source must be $\frac{80 s^{-1}}{0.7225^2} \approx 154 s^{-1}$. From this rate we can calculate the single rate at each

[5] The quantum mechanical prediction and the simulation assume perfect polarizing beam splitters. In the real experiment, the transmittances are $\epsilon_M^i \approx 0.97$ and $\epsilon_m^i \approx 0.0285$

[6] One station measures a photon but within a given time window , no photon is registered by the other station.

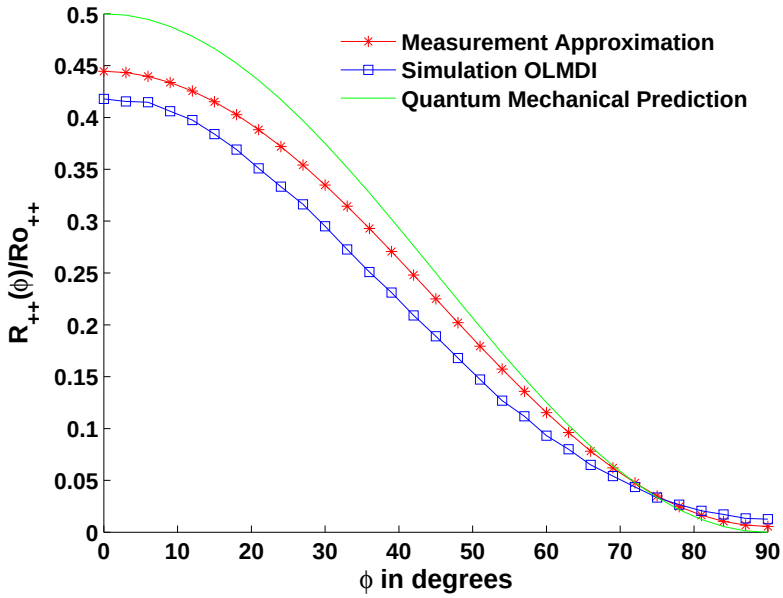

Figure 3.5: Normalized coincidence rate as a function of the relative polarizing beam splitter orientation. The OLMDI simulation and the quantum mechanical prediction assume perfect PBS. The measurement approximation is extracted from [3]. For each simulated point, 100000 correlated photon pairs are generated.

station due to the generated correlated pairs $R_A = R_B = 0.7225 \cdot 154s^{-1} \approx 111s^{-1}$. This rate is at least two orders of magnitude smaller than the measured single rate. Therefore, it is easily possible that 154 correlated photon pairs are generated per second. But because of the detection inefficiency only a summed coincidence rate of $80s^{-1}$ is measured [28].

The author realizes that OLMDI relies on the detection inefficiency loophole and the detection probability enhancement by the polarizing beam splitter[7]. Especially the experimental results shown in Figure 3.5 required the enhancement property of the polarizing beam splitter.

The detection inefficiency loophole is and was often considered as a minor problem, especially because it is assumed that future experiments will close this loophole. But inspite of many elaborated experiments since Aspect's first papers, it was so far not possible[8] to confirm the quantum mechanical predictions with highly efficient detectors [29]. Kwiat reports for example in [30] that the maximum transmission of the interference filters was 65%. Additionally, he reports an efficiency of the silicon avalanche photodiodes in the Geiger mode of 65%. The combined efficiency of the filters and photodetectors are much smaller than the efficiency assumed in the OLMDI model. Weihs states in his 1998 paper [31]: "..., we agree that an ultimate experiment should also have higher detection/collection efficiency, which was 5% in our experiment." Therefore, the suggested OLMDI model is a plausible model for the actual experiments.

3.3 Conclusion

In summary, it was shown that the measurements reported by Aspect are not loophole free. Simulations of some of the actual experiments with the OLMDI model showed that the measured results can be explained without spooky action at a distance (quantum nonlocality).

In the next chapter the Pan *et al.* realization of the GHZ experiment is discussed.

[7] The PBS increases on average the magnitude of the hidden variable vector and increases therefore the detection probability of a single photon.

[8] At least to the best knowledge of the author.

Chapter 4

The Pan *et al.* Realization of the GHZ Gedankenxperiment

4.1 Introduction

Pan *et al.* [1] published in 2000 the first experimental proof of quantum nonlocality based on three photon Greenberger-Horne-Zeilinger (GHZ) entanglement. The basic ideas of GHZ and the main results of the Pan *et al.* measurements have been presented in section 2.7 and in section 2.8 respectively. The GHZ Gedankenexperiment is considered as one of the best experiments to test quantum mechanics versus local realism. Additionally, the experimental realization by Pan *et al.* is regarded as a very important contribution to the establishment of quantum nonlocality.
In this chapter it is shown that the experimental results reported by Pan *et al.* can not be used to decide whether an objective local model or the quantum mechanical model gives a better fit for the observed data. We will use an objective local model based on elements of reality[1] as did Pan *et al.*. A minor modification of the assumptions in the objective local model (local realistic model) of Pan *et al.* results in a modified local realistic model[2] that gives predictions that are statistically closer to the experimental results than the predictions of the quantum mechanical model.
Additionally, a model based on time coordinated equipment parameters (section 4.3)

[1] EPR define an element of physical reality as follows: "If, without in any way disturbing a system, we can predict with certainty (i.e., with probability equal to unity) the value of a physical quantity, then there exists an element of physical reality corresponding to this physical quantity."[5]

[2] This modified local realistic model (local instruction-set model) was developed with the help of an extended objective local model based on the detection inefficiency loophole. This model is explained in appendix A.

is introduced and applied to the experimental realization of the GHZ Gedankenexperiment.

4.2 Local Instruction-Set Model

Pan *et al.* studied in their work the three-photon entangled state also known as 'Greenberger-Horne-Zeilinger' state [11]. The experimental setup used by Pan *et al.* can be seen in Figure 4.1. The main results of the theoretical analysis given by Pan *et al.* are summarized in section 2.8.

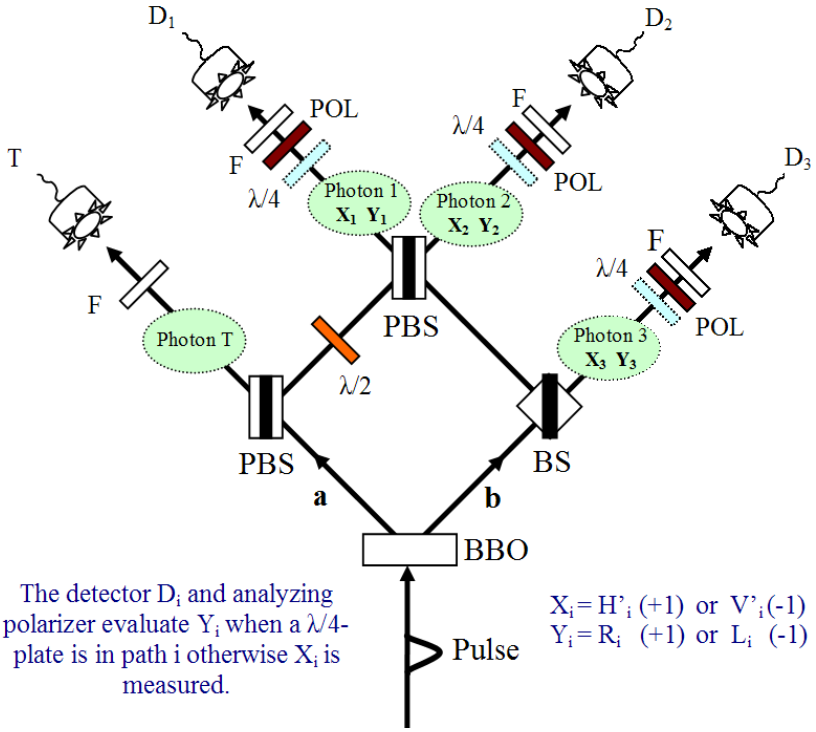

Figure 4.1: Experimental setup for Greenberger-Horne-Zeilinger (GHZ) tests of quantum nonlocality used by Pan *et al.*. The interesting case of fourfold coincidences are indicated by the four photons T, 1, 2 and 3. Because in the path of the trigger photon T, no quarter-wave ($\lambda/4$) plate and polarizer are placed, it will be detected by detector T independently of its polarization. For photon $i = 1$, 2 or 3, the two elements of reality X_i and Y_i are introduced by Pan *et al.*. In a local realistic theory these elements of reality are used to decide whether the photon is absorbed or transmitted by the analyzing polarizer (POL).

Recapitulating it was shown by Pan *et al.* that quantum mechanics predicts $yyx = -1$, $yxy = -1$, $xyy = -1$ and $xxx = +1$. Here x refers to a photon polarization measurement in the linear polarization basis $H' = +1/V' = -1$ ($45^o/-45^o$ polarization) and y denotes a measurement in the circular polarization basis $R = +1/L = -1$ (right-handed/left-handed). The yyx experiment means that for photon 1 and 2, the circular polarizations and for photon 3 the linear polarization are evaluated. The quantum mechanical predictions are shown by the blue bars in Figure 4.2.
The local realistic model introduced by Pan *et al.* predicts for yyx, yxy and xyy the same results as the quantum mechanical model. But it predicts $xxx = -1$ whereas the quantum mechanical model predicts the opposite. The predications of the local realistic model are reproduced by the red bars in Figure 4.2.
Because the experimental results (green bars in Figure 4.2) are in significantly better agreement with the quantum mechanical predictions than with the local realistic predictions, Pan *et al.* interpret their findings as the first three-particle test of local realism following the GHZ argument. In their final analysis they conclude that no objective local model can explain the experimental results and that quantum nonlocality is therefore proven.
However, there exists a logical problem in the assumptions introduced by Pan *et al.* for the local realistic model. Pan *et al.* derive their local realistic model based on the predictions of the competing QMM. Before the relations $yyx = -1$, $yxy = -1$ and $xyy = -1$ are experimentally verified, it is assumed that the local realistic model must also predict these relations. But this procedure conflicts with the basic ideas of a fair scientific comparison between two independent competing models.
In the following a modified local realistic model, based on elements of reality, is presented. This model was developed with an extended objective local model based on detection inefficiencies (EOLMDI). The details of this EOLMDI model can be found in appendix A. The modified local realistic model produces theoretical predictions that are closer to the results of the actual experiment than the predictions of the quantum mechanical model.
We use instruction sets carried by the particles from the common source and therefore guarantee locality while at the same time extending the model of Pan *et al.*. These instruction sets are given in Table 4.1. We only list the combinations of elements of reality that are assigned a non-zero probability. For example, the instruction set $(H_1'R_1|H_2'R_2|H_3'L_3)$ means that the photon going toward detector D_1 (photon 1) has the values $X_1 = H_1'$ and $Y_1 = R_1$ for the two elements of reality representing the linear and the circular polarization of that photon, respectively. Photon 2 has $X_2 = H_2'$

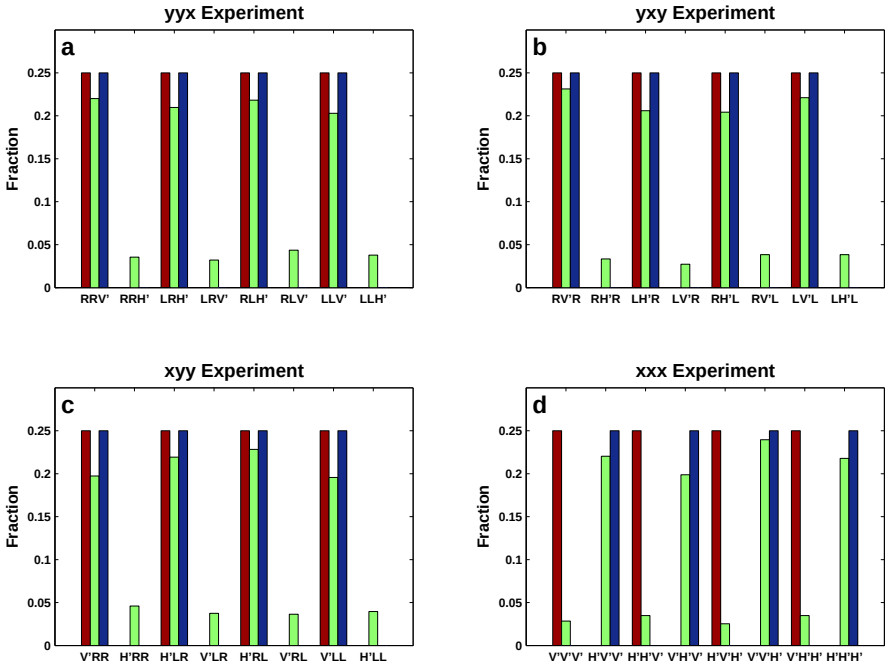

Figure 4.2: All outcomes for the yyx, yxy, xyy and xxx experiments. The blue bars represent the quantum mechanical predictions, the green bars reproduce the experimental results measured by Pan *et al.* and the red bars are the fractions obtained by Pan *et al.*'s local realistic model.

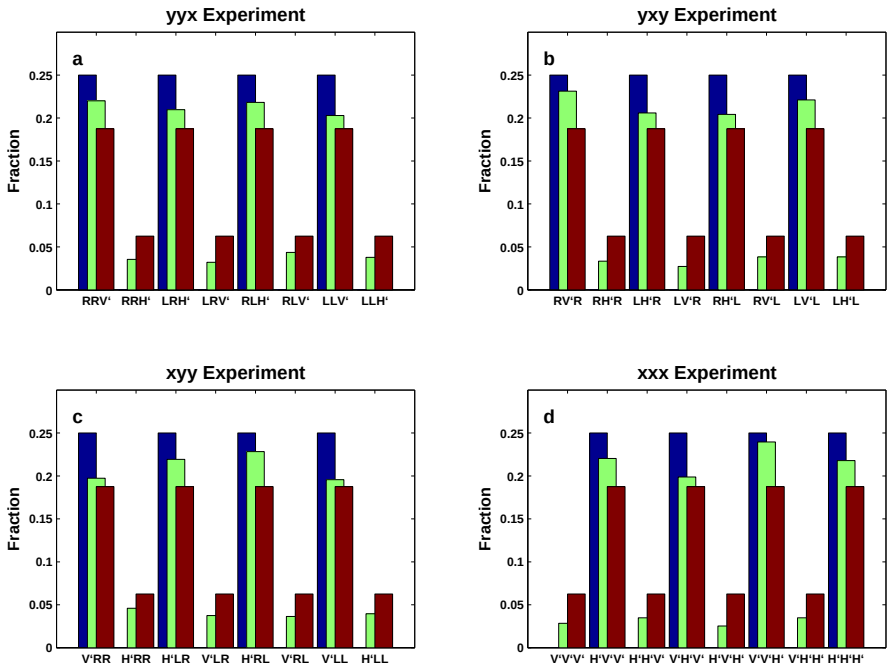

Figure 4.3: All outcomes for the yyx, yxy, xyy and xxx experiments. The blue bars represent the quantum mechanical predictions, the green bars are the experimental results measured by Pan et al. and the red bars are the fractions obtained by the instruction set for the elements of reality shown in Table 4.1.

and $Y_2 = R_2$ and photon 3 has $X_3 = H_3'$ and $Y_3 = L_3$.

It can easily be checked that this table results in a maximum randomness for any individual or two-photon joint measurement.

If we use the instruction sets of Table 4.1 to evaluate the yyx, yxy, xyy and xxx experiments, we obtain the results shown as the red bars in Figure 4.4. It can clearly be seen that the predictions of the modified local realistic model are on average closer to the measurement results of the actual experiment than the quantum mechanical predictions based on the GHZ state.

We have also computed the results for the xxy, xyx, yxx and yyy experiments. For all of these experiments it follows from Table 4.1 that all the eight events (i.e. $H_1'H_2'R_3$, $H_1'H_2'L_3$,...,$V_1'V_2'L_3$ in the xxy experiment) occur with equal probability $\frac{1}{8}$. This is in agreement with the predictions of the quantum mechanical model of Pan *et al.*.

It is realized that a complete analysis of all aspects of the Pan *et al.* experiment may

$X_1\,Y_1 \mid X_2\,Y_2 \mid X_3\,Y_3$	$X_1\,Y_1 \mid X_2\,Y_2 \mid X_3\,Y_3$
$H'_1R_1 \mid H'_2R_2 \mid H'_3L_3$	$V'_1R_1 \mid H'_2R_2 \mid V'_3R_3$
$H'_1R_1 \mid H'_2R_2 \mid V'_3L_3$	$V'_1R_1 \mid H'_2R_2 \mid V'_3L_3$
$H'_1R_1 \mid H'_2L_2 \mid H'_3R_3$	$V'_1R_1 \mid H'_2L_2 \mid H'_3L_3$
$H'_1R_1 \mid H'_2L_2 \mid H'_3L_3$	$V'_1R_1 \mid H'_2L_2 \mid V'_3L_3$
$H'_1R_1 \mid V'_2R_2 \mid V'_3R_3$	$V'_1R_1 \mid V'_2R_2 \mid H'_3R_3$
$H'_1R_1 \mid V'_2R_2 \mid V'_3L_3$	$V'_1R_1 \mid V'_2R_2 \mid V'_3R_3$
$H'_1R_1 \mid V'_2L_2 \mid H'_3R_3$	$V'_1R_1 \mid V'_2L_2 \mid H'_3R_3$
$H'_1R_1 \mid V'_2L_2 \mid V'_3R_3$	$V'_1R_1 \mid V'_2L_2 \mid H'_3L_3$
$H'_1L_1 \mid H'_2R_2 \mid H'_3R_3$	$V'_1L_1 \mid H'_2R_2 \mid H'_3R_3$
$H'_1L_1 \mid H'_2R_2 \mid H'_3L_3$	$V'_1L_1 \mid H'_2R_2 \mid V'_3R_3$
$H'_1L_1 \mid H'_2L_2 \mid H'_3R_3$	$V'_1L_1 \mid H'_2L_2 \mid V'_3R_3$
$H'_1L_1 \mid H'_2L_2 \mid V'_3R_3$	$V'_1L_1 \mid H'_2L_2 \mid V'_3L_3$
$H'_1L_1 \mid V'_2R_2 \mid H'_3L_3$	$V'_1L_1 \mid V'_2R_2 \mid H'_3R_3$
$H'_1L_1 \mid V'_2R_2 \mid V'_3L_3$	$V'_1L_1 \mid V'_2R_2 \mid H'_3L_3$
$H'_1L_1 \mid V'_2L_2 \mid V'_3R_3$	$V'_1L_1 \mid V'_2L_2 \mid H'_3L_3$
$H'_1L_1 \mid V'_2L_2 \mid V'_3L_3$	$V'_1L_1 \mid V'_2L_2 \mid V'_3L_3$

Table 4.1: Instruction sets for the elements of reality X_i and Y_i. Each of the 32 combinations occurs with equal probability ($\frac{1}{32}$). Shaded entries indicate the relevant elements of reality for the yyx experiment. For example, when the RRV' measurement is carried out, the following photon triples would result in a fourfold coincidence count (assuming trigger T clicks): $(H'_1R_1|H'_2R_2|V'_3L_3)$, $(H'_1R_1|V'_2R_2|V'_3R_3)$, $(H'_1R_1|V'_2R_2|V'_3L_3)$, $(V'_1R_1|H'_2R_2|V'_3R_3)$, $(V'_1R_1|H'_2R_2|V'_3L_3)$ and $(V'_1R_1|V'_2R_2|V'_3R_3)$. Adding the probabilities yields $\frac{6}{32}$. On the other hand, when the RRH' measurement is performed, then the photon triples, which would give fourfold coincidences are $(H'_1R_1|H'_2R_2|H'_3L_3)$ and $(V'_1R_1|V'_2R_2|H'_3R_3)$. The sum of the probabilities of these combinations is $\frac{2}{32}$.

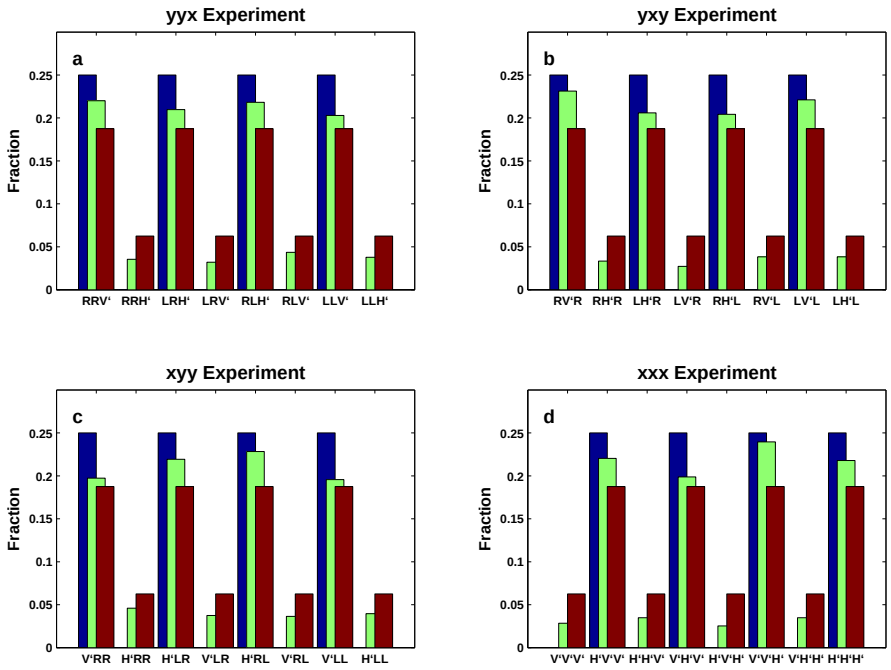

Figure 4.4: All outcomes for the yyx, yxy, xyy and xxx experiments. The blue bars represent the quantum mechanical predictions based on the GHZ state, the green bars are the experimental results measured by Pan *et al.* and the red bars are the fractions obtained by the instruction sets for the elements of reality shown in Table 4.1.

also need to include other observations such as the influence of delays imposed on the photons by the experimental setup. Such delays influence the observed correlations. More general time dependencies are also possible. Nevertheless, the modified local realistic model based on elements of reality can explain the main results reported in [1] with a statistically smaller error than the quantum mechanical model. Therefore, the Pan *et al.* experiment can not be used to draw conclusions about the existence of quantum nonlocality. Moreover, the question whether or not quantum mechanics is a complete theory can not be answered from the reported experimental results because, as we have shown for this particular experiment not even the class of local realistic models based on a small number of instruction sets representing elements of reality can be excluded.
Given this situation, in the following section, another objective local models for the Pan *et al.* realization of the GHZ experiment is presented.

4.3 Time Coordinated Measuring Equipments

From many optical experiments it is well known, that the exact spacial adjustment of the optical elements is crucial for the success of the experiment. In optical measurements investigating entanglement, this spacial coordination has to be in the μm range [1]. In most optical experiments it is assumed that only the transversal alignment is of importance and that the longitudinal alignment[3] is of minor significance. In the Pan *et al.* realization of the GHZ Gedankenexperiment this general behavior is not true. To guarantee that the analyzing polarizers and detectors in the different paths do not influence each other, the measurements in the involved paths have to be within a specified time window. Otherwise, the possible results are distinguishable and no more entangled. In the time coordinated measuring equipment (TCME) model it is assumed that all entangled photon pairs are registered (no detection inefficiency) and that not only the transversal alignment is very important but also the longitudinal alignment.

4.3.1 The TCME Model

The TCME model consists of three main components. The source produces similarly to the model described in section 4.2 certain combinations of photons, each with two elements of reality X_i and Y_i $(i = 1, 2, 3)$. The used source can produce eight different

[3]The transversal alignment denotes the alignment of the optical elements perpendicular to the light beam. The longitudinal alignment is the alignment in the direction of the light beam.

combinations (Table 4.2) that are generated all with equal probability $\frac{1}{8}$.

$X_1\,Y_1 \vert X_2\,Y_2 \vert X_3\,Y_3$	$X_1\,Y_1 \vert X_2\,Y_2 \vert X_3\,Y_3$
$H'_1R_1 \vert H'_2R_2 \vert V'_3L_3$	$V'_1R_1 \vert H'_2L_2 \vert H'_3L_3$
$H'_1R_1 \vert V'_2L_2 \vert H'_3R_3$	$V'_1R_1 \vert V'_2R_2 \vert V'_3R_3$
$H'_1L_1 \vert H'_2L_2 \vert V'_3R_3$	$V'_1L_1 \vert H'_2R_2 \vert H'_3R_3$
$H'_1L_1 \vert V'_2R_2 \vert H'_3L_3$	$V'_1L_1 \vert V'_2L_2 \vert V'_3L_3$

Table 4.2: Instruction sets for the elements of reality X_i and Y_i produced by the source. Each of the eight combinations occurs with equal probability $\frac{1}{8}$. Shaded entries indicate the relevant elements of reality for the yyx experiment.

The polarization analyzers consist only of polarizers for the case of X_i measurements and of $\lambda/4$-wave plates followed by polarizers for the Y_i measurements (Figure 4.1). In the TCME model, the measuring equipment parameters λ_{Xi} and λ_{Yi} are described by the time dependent instructions sets shown in Table 4.3. The evaluation of the source parameters depends on the value of the time dependent measuring equipment parameters that can have two different realizations.
When the measuring equipment behaves (n)ormal, the photon is transmitted through the measuring equipment if the setting of the equipment is equal to the value of the elements of reality associated to the incident photon. For example, if we make a x measurement, and the value of the element of reality X_i is V_i' then the measured result is V_i'.
On the other hand, if for the measuring equipment parameter an (i)nverse behavior is indicated by Table 4.3, measuring results are opposite to the values of the elements of realities associated to the measured photon. For example, if the element of reality associated to the photon has the value V_i', the measured value will be H_i'. Table

Time	t_0	t_1	t_2	t_3	t_4	t_5	t_6	t_7
λ_X	n	n	i	n	n	i	n	i
λ_Y	n	n	i	n	n	n	n	i

Table 4.3: Time and setting dependent measuring equipment parameters λ_X and λ_Y. 'n' denotes the normal reading of the respective element of reality sent by the source (i.e. $V_i' \rightarrow V_i'$). 'i' means that the received element of reality is read inversely (i.e. $V_i' \rightarrow H_i'$) by the measuring equipment.

4.3 is only an example of possible time dependent equipment parameters. It is as-

sumed that the measurement time can be divided in short periods of finite durations. For simplicity, it is assumed that the behavior of the time dependent equipment parameters is periodic and that the sequences described in Table 4.3 are periodically repeated.

It is now shown how this model could relate to the Pan *et al.* experiment. It is well known that optical experiments measuring entanglement are not only expensive but also require great experimental skills. They are so difficult because the exact adjustment (positioning, coordination of the phases of different photons,...) of the involved optical elements is crucial for a successful experiment. In the following, it is shown how the experimental results could be explained with an objective local theory. It is shown that a model based on time coordinated equipment parameters could explain the experimental results reported by Pan *et al.* in [1] even better than the time independent model presented in section 4.2.

Although in [1] the xxx experiment is presented last, it is assumed that in practice, the experimental setup is first adjusted using the xxx experiment. I assume this because the xxx experiment has the smallest number of optical elements[4]. Therefore this experiment seems to be the most natural choice to start with. It is also assumed that in the actual experiment, all optical elements such as the beta-barium borate crystal (BBO), polarizing beam splitters (PBS), beam splitters (BS), narrow bandwidth filters (F), $\lambda/2$-plate and detectors D_i [5] are mounted at a fixed position on an experimental table.

Let us additionally assume, that the analyzing polarizers are also fixed in the longitudinal direction[6] and that the polarizers are only rotated around an axis parallel to the longitudinal direction when the settings (i.e. V_i' or H_i' for the X_i measurement) are changed. It is assumed, that this rotation perpendicular to the longitudinal direction does not influence the longitudinal time coordination (phase shift introduced in Table 4.4) between the three polarization analyzers 1, 2 and 3. As seen in Table 4.4, the general λ_X equipment parameter behavior described in Table 4.3 is applied to the three x measurements in the three paths 1, 2 and 3 (Figure 4.1). As can be seen, the measuring equipment in the three paths are time coordinated. The measuring equipment in path 2 has for example a positive phase shift of $\frac{T}{8}$, where T is the duration of the time interval of one period, with respect to the measuring equipment in path 1. Path 3 has a positive phase shift of $\frac{7T}{8}$ with respect to the measuring

[4]To change from a x measurement to a y measurement, only a correctly adjusted $\lambda/4$-plate has to be placed in front of the analyzing polarizer.

[5]The general behavior of these elements is explained in great details in appendix A.

[6]The direction in which the photons are traveling in each path.

xxx experiment

t	k	k+1	k+2	k+3	k+4	k+5	k+6	k+7
$\lambda_{X1}=\lambda_X(t_{x1}\|x1=mod(t,8))$	n	n	i	n	n	i	n	i
$\lambda_{X2=}\lambda_X(t_{x2}\|x2=mod(t+1,8))$	n	i	n	n	i	n	i	n
$\lambda_{X3=}\lambda_X(t_{x3}\|x3=mod(t+7,8))$	i	n	n	i	n	n	i	n

xyy experiment

t	k	k+1	k+2	k+3	k+4	k+5	k+6	k+7
$\lambda_{X1}=\lambda_X(t_{x1}\|x1=mod(t,8))$	n	n	i	n	n	i	n	i
$\lambda_{Y2=}\lambda_Y(t_{y2}\|y2=mod(t,8))$	n	n	i	n	n	n	n	i
$\lambda_{Y3=}\lambda_Y(t_{y3}\|y3=mod(t+5,8))$	n	n	i	n	n	i	n	n

yxy experiment

t	k	k+1	k+2	k+3	k+4	k+5	k+6	k+7
$\lambda_{Y1}=\lambda_Y(t_{y1}\|y1=mod(t+1,8))$	n	i	n	n	n	n	i	n
$\lambda_{X2=}\lambda_X(t_{x2}\|x2=mod(t+1,8))$	n	i	n	n	i	n	i	n
$\lambda_{Y3=}\lambda_Y(t_{y3}\|y3=mod(t+6,8))$	n	i	n	n	i	n	n	n

yyx experiment

t	k	k+1	k+2	k+3	k+4	k+5	k+6	k+7
$\lambda_{Y1}=\lambda_Y(t_{y1}\|y1=mod(t+7,8))$	i	n	n	i	n	n	n	n
$\lambda_{Y2=}\lambda_Y(t_{y2}\|y2=mod(t+4,8))$	n	n	n	i	n	n	i	n
$\lambda_{X3=}\lambda_X(t_{x3}\|x3=mod(t+7,8))$	i	n	n	i	n	n	i	n

Table 4.4: Time coordinated instuction sets of the time and setting dependent equipment parameters λ_X and λ_Y for the four experiments xxx, xyy, yxy and yyx. $\lambda_X(t_{xi})$ and $\lambda_Y(t_{yi})$ refers to the general x and y measurement behavior described in Table 4.3. k is an integer multiple of 8.

equipment in path 1.
When the eight measurements for the xxx experiment are finished, $\lambda/4$-plates are placed in front of the analyzing polarizers (for the yyx, yxy and xyy experiments) and adjusted (for example the orientation of the optical axis is adjusted and the measuring equipments are time coordinated). It is assumed that this adjustment of the equipment causes the time dependences shown in Table 4.4 [7].
In the following subsection, the simulation results for the above model are discussed.

4.3.2 Simulation Results and Discussion

The simulation of the Pan *et al.* realization of the GHZ Gedankenexperiment with the TCME model results in the fractions shown by the red bars in Figure 4.5. The number of generated photon pairs was adjusted such that the average number of simulated fourfold coincidences was 133 (19) for the quantum mechanically desired (undesired) states[8]. It can be seen that the fluctuation around these mean values is similar to the fluctuations measured in the actual experiments [1] in which roughly the same amount of fourfold coincidences are reported.
An additional simulation with the TCME model shows that the quantum mechanically desired states are observed in a fraction of 0.875 of all cases while the quantum mechanically undesired states occur only in a fraction of 0.125 of all cases. Thus, the predictions of the objective local TCME model for the quantum mechanically desired states reproduce the measured values 0.85 ± 0.04 and 0.87 ± 0.04 for the experiments yyx, yxy, xyy and xxx respectively, within the range of experimental errors. The TCME model predictions of 0.125 for the quantum mechanically undesired states are within the reported measurement errors for the xxx experiment 0.13 ± 0.02. Furthermore, the fraction 0.125 is only 0.005 away from the smallest values contained in the measuring tolerance interval 0.85 ± 0.04.
Simulations with the TCME model also confirmed that a maximum randomness for any individual or two-photon joint measurement is guaranteed.
Pan *et al.* show in their paper an additional measurement result. They report that

[7] In Table 4.4 it is arbitrarily assumed that for all experiments in which y measurements are involved, all y equipment parameters need to be readjusted when changing to a new experiment (i.e. from the yyx to the yxy experiment). It is of course also possible to create a table for the four experiments in which the xxx experiment is first measured and then for each of the experiments yyx, yxy and xyy the two components that change from experiment to experiment are adjusted.

[8] The term quantum mechanically desired state denotes the experimental outcomes that fulfill the quantum mechanical predictions $xyy = -1$, $yxy = -1$, $yyx = -1$ and $xxx = +1$. The quantum mechanically undesired states describe all other outcomes.

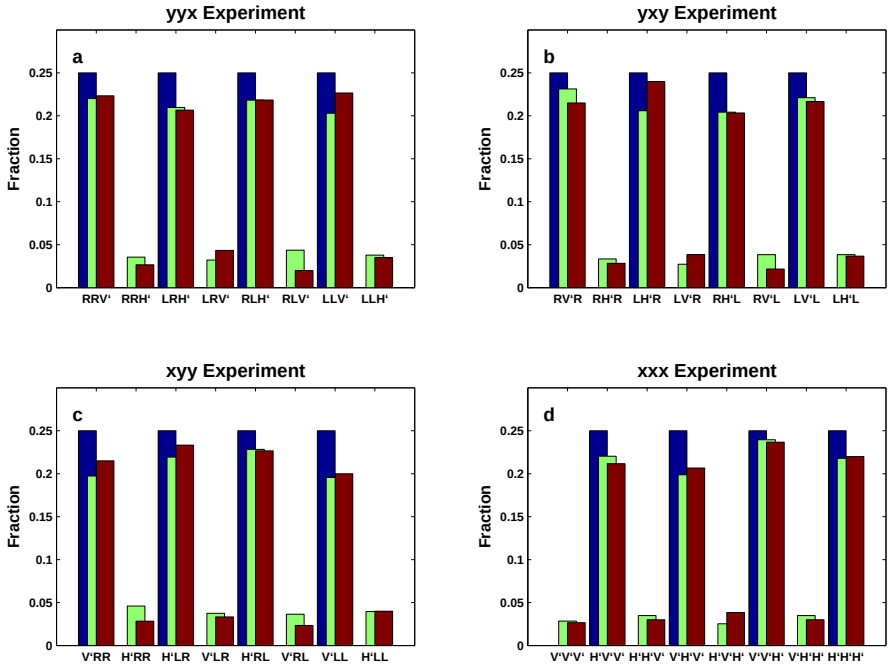

Figure 4.5: All outcomes for the yyx, yxy, xyy and xxx experiments. The blue bars represent the quantum mechanical predictions, the green bars reproduce the experimental results measured by Pan *et al.* and the red bars are the fractions obtained by a simulation with the TCME model.

a translation of the final polarizing beam-splitter introduces a delay between photon 1 and 2 at this final polarizing beam splitter (Figure 4.1). "At large delay, that is, outside the region of coherent superposition, the two possibilities HHH and VVV are distinguishable and no entanglement results."[1] (Figure 4.6).

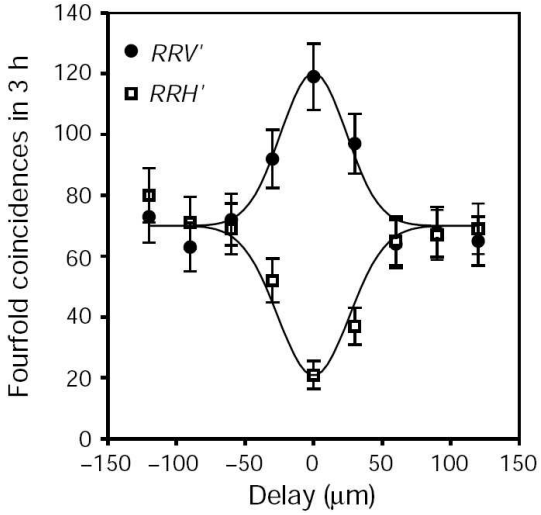

Figure 4.6: yyx experiment measuring circular polarization on photons 1 and 2 and linear polarization on photon 3. The variation of the delay between photons 1 and 2 at the final polarizing beam splitter influences the fourfold coincidences. This is demonstrated on the example of RRV' and RRH' measurements. For more details refer to [1].

The TCME model gives an intuitive explanation of the observed influence of delays imposed on the photons by the experimental setup. The delay between photon 1 and 2 at the final polarizing beam splitter represents the strength of uncoordination between the different time coordinated measuring equipments. The larger the delay the bigger the uncoordination. A simulation implementing this delay-dependent strength of uncoordination[9] results in a delay dependent fourfold coincidence count behavior as shown in Figure 4.7. It can be seen that the simulation results agree with the experimental results obtained by Pan *et al.* (Figure 4.6).
So far, it has been shown that the TCME model can be used to explain the measured results for the four experiments yyx, yxy, xyy and xxx and also the delay dependence

[9]In the simulation, the strength of uncoordination (randomness) in the measurement time t (Table 4.4) is linearly proportional to the delay introduced by the final polarizing beam splitter. Maximum randomness is assumed, when the delay between the photons is bigger than the spacial extension $(3 \cdot 10^8 \frac{m}{s} \cdot 200fs = 60\mu m)$ of the short pulse of ultraviolet light producing the correlated photons.

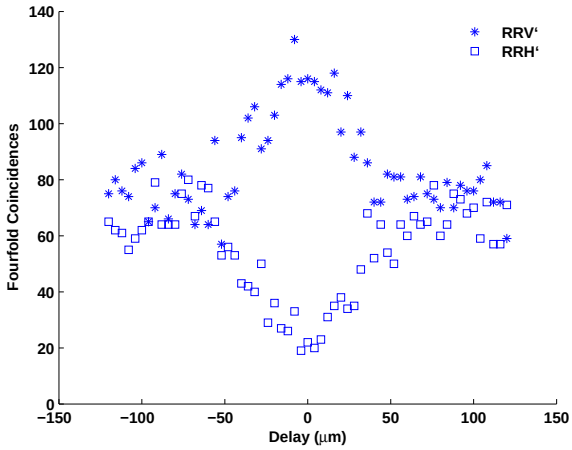

Figure 4.7: Delay dependent fourfold coincidences. The generated number of correlated two photon pairs is adjusted such that at zero delay around 120 (20) fourfold coincidences are registered for the RRV' (RRH') measurements.

of the entanglement. Therefore, the TCME model can be considered as a plausible model.

In the following, additional experimental observations are pointed out. These experimental results are intended to highlight the extreme sensitivity of entanglement to longitudinal adjustments (delay coordiantion).

One of the strongest indications of the necessity of very careful time delay adjustments is given in [32]. The experimental setup and the significant experimental results are shown in Figure 4.8. It can be seen that the number of coincidences depends strongly on the introduced time delay. Therefore by means of this particular entanglement experiment it becomes clear that the optical elements have to be extremely well adjusted to get the observed results.

Despite of the fact that the experimental setup in [32] is different from the setup used in [1], we use the results for the following speculations. Especially because the experiments were done by the same group and with the same optical equipment .

First of all it is interesting to realized that the envelop of the graph a) seen on the right side of Figure 4.8 has a similar shape as the curve seen in Figure 4.6. This means that the coherence region is similarly long in both experiments.

Additionally, the fast fluctuation of the coincidence rate shown in Figure 4.8 a) is noteworthy. A more precise measurement (graph b on the right side in Figure 4.8) reveals that the coincidence rate depends sinusoidally on the time delay. This means

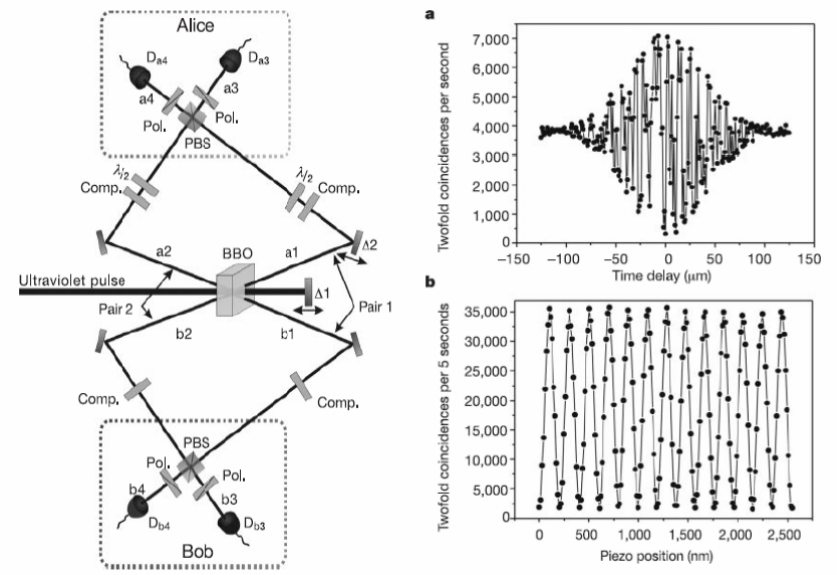

Figure 4.8: Left: Experimental setup for entanglement purification. Right: a) Twofold coincidences per second between the output modes a4 and b4 depending on the delay $\Delta 1$. "The envelope of the observed twofold coincidence varies indicating the visibility of the two-photon coherence."[32] Outside of the coherence region, the components of the Bell states $\frac{1}{\sqrt{2}}\left(|H\rangle_a |H\rangle_b \pm |V\rangle_a |V\rangle_b\right)$ are distinguishable. Therefore no interference occurs. b) A detailed look at the influence of the time delay shows that the twofold coincidence rate varies with a frequency of about 4 times the photon frequency (788nm). It should be emphasized, that the experimental results are extremely delay sensitive. More information can be found in [32].

that a minor change of the time delay (position change in nm range) causes the measurement results to change significantly[10].
In the Pan *et al.* realization of the GHZ Gedankenexperiment, $\lambda/4$-plates have to be added in front of the analyzing polarizers to change from a x to a y measurement. It is well known that $\lambda/4$-plates consist of birefringent materials. Therefore they cause a photon delay. All these observations give us some freedom for speculations and questions.

- Does the time delay introduced by the $\lambda/4$-plate for the y experiment change the outcomes of the Pan *et al.* measurements such that the three experiments yyx, yxy and xyy are on similar probability spaces (all have two $\lambda/4$-plates) but the xxx experiment is on a different probability space?

- Do the experiments in [32] confirm the suggested TCME model, that requires extremely careful adjustments of the involved measuring equipment? The TCME model requires an adjustment of the measuring equipment before each of the four experiments yyx, yxy, xyy and xxx. The above observations make it plausible that these adjustments are indeed necessary and done in the actual experiment. Especially because the time delay introduced by the $\lambda/4$-plate has to be taken into account. Finally, does this mean that the careful adjustments before each of the four experiments is the reason why the quantum mechanically predicted results are observed?

- Could a temperature change in the laboratory have changed the equipment coordination?

Of course, we are aware that the above are only speculations and I emphasize that the aim of this project is not to doubt quantum mechanics. However, the questions above show that the introduction of time dependent equipment parameters raises the bar of requirements that are necessary to show nonlocality.
Considering as example the Pan *et al.* realization of the GHZ Gedankenexperiment, the TCME model shows that time and setting dependent source parameters can reproduce the experimentally observed results within the measuring error. We do not claim, that the TCME model is the objective local model that perfectly describes

[10] This can also explain the irritating observation, that in [33] a ratio of 12:1 between the quantum mechanically desired and undesired states was observed whereas in [1] a ratio of about 11:2 is reported. This can be explained by a better adjustment (resulting in a higher visibility) of the optical elements in [33] compared to the adjustments done in [1].

nature but it gives us some hints how such an objective local hidden variable theories could look like.
As pointed out by Hess and Philipp [34], the major problem of all popular non-existence proofs of local hidden variable theories is the assumption that all measurements/experiments are based on one common probability space. It will be shown in chapter 5 that the theoretical reasoning by Pan *et al.*, why no local realistic model is possible, is also based on this common-probability-space assumption.

4.4 Conclusion

As a summary of this chapter it can be stated that the original conclusion of Pan *et al.* is based on a simple local realistic model based on elements of reality. A small modification in the assumptions[11] for the local realistic model results in predictions for the four experiments xyy, yxy, yyx and xxx that are statistically closer to the reported experimental observations than the quantum mechanical predictions [1].
Additionally, it was shown that a time and setting dependent equipment parameter model can even explain the experimental results within the statistical measurement error. The only requirement for this TCME model is that the four experiments are defined on different probability spaces. It is speculated that this is achieved by adjusting the experimental setup for each experiment. Recently published experimental results [32] show that these adjustments might indeed be required.
In conclusion, it is believed that the Pan *et al.* experiment can not be used to draw conclusions about the existence of quantum nonlocality. Moreover, the question whether or not quantum mechanics is a complete theory can not be answered from the reported experimental results because as shown in section 4.2 not even the class of local realistic models based on a small number of instruction sets representing elements of reality can be excluded. It was also shown that it is possible to reproduce the experimental results reported by Pan *et al.* with objective local models.
In the following chapter, the Pan *et al.* realization of the GHZ Gedankenexperiment is investigated with the tools of classical information theory.

[11] The objective local model does not have to fulfill the quantum mechanical predictions $xyy = -1$, $yxy = -1$ and $yyx = -1$.

Chapter 5

Entropy Analysis of the Pan *et al.* Experiment

5.1 Introduction

Information theory or the mathematical theory of communication was developed in the 1940's by Claude E. Shannon. In 1948 and 1959 Shannon published two classical papers [12, 13] that build the foundation of modern communication theory. The information theory introduced by Shannon is often called classical information theory. Although Shannon was mainly concerned with problems related to electronic communication, his theory can be used in any classical communication problem. Information theory can be viewed as a branch of applied probability theory.

Because quantum mechanics is in principle a probability theory we can ask the question whether Shannon's classical information theory can be used to analyze quantum mechanical communication problems such as teleportation. However, it was stated in previous works [35] that Shannon's classical information theory can not be used for quantum mechanical phenomena like entanglement and superdense coding. This is because negative entropy[1] values are obtained, which are forbidden in Shannon's classical information theory.

It has already been realized by Schumacher [36] that the von Neumann entropy has an information-theoretical meaning. Von Neumann defined the entropy of a quantum state described by the density operator ρ as $S(\rho) \equiv -tr(\rho \cdot log_2(\rho))$. Von Neumann's entropy is currently the entropy of choice to describe conditional entropies in quan-

[1] Entropy is the quantity of information. It is proportional to the amount of uncertainty or freedom of choice of a system. Shannon defined entropy as $H = \sum_i p_i log_2(p_i)$ where p_i is the probability of an event i the occur.

tum entangled systems such as the Bell state or the entangled three-photon GHZ state. This because the von Neumann entropy is allowed to assume negative values. Despite of the fact that Shannon's classical information theory is considered to be inadequate for quantum mechanical information analysis, in this chapter, the classical information theory is used to analyze the entangled three-photon GHZ state. Especially the question whether or not the four experiments yyx, yxy, xyy and xxx of the Pan *et al.* implementation of the GHZ Gedankenexperiment can be defined on one common probability space is of main interest. This question is answered using standard probability theory and Shannon's classical information theory.
In the first section, Shannon's information theory is introduced. Based on this, several entropy values of the single experiments yxy are calculated. In section 5.4 the four experiments yyx, yxy, xyy and xxx are considered together. The entropies of different classical and quantum mechanical theories for the GHZ Gedankenexperiment are calculated and entropy limits are defined. These limits have to be fulfilled to allow classical information theoretical interpretations and more importantly simple classical models based on elements of reality defined on one common probability space. In the following section, a simple proof based on standard probability theory is used to show that the contradiction between the local realistic model described in [1] and the quantum mechanical model is due to the assumed definition of all four experiments yyx, yxy, xyy and xxx on one common probability space. At the end, the findings are summarized.

5.2 Shannon's Information Theory

Claude E. Shannon published in 1948 a key paper about information theory. In this paper he considers the fundamental problem of communication, which is to use a signal that is produced at point A and to reproduce it at a remote point B. He explains his theory using the example of a simple communication system shown in Figure 5.1. This general communication system consists of five parts:

1. "An information source which produces a message or sequence of messages to be communicated to the receiving terminal." [14]

2. The transmitter converts the message into a signal suitable for transmission over the communication channel.

3. The channel is the medium (i.e. coaxial cable) used to transmit the signal from the transmitter to the receiver.

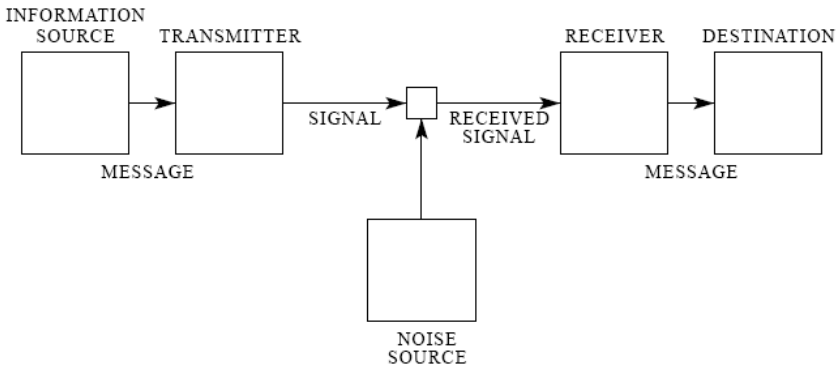

Figure 5.1: Schematic diagram of a general communication system [14].

4. The receiver is the inverse of the transmitter.

5. The destination is the intended receiver of the message.

Shannon classifies in his historic paper three different categories of communication systems: discrete, continuous and mixed [14]. For the analysis of the three-photon Greenberger-Horne-Zeilinger entanglement only the discrete communication theory in which the message and the signal consist of discrete symbols is required.
In the following some definitions are introduced to make the reader familiar with the major concepts of Shannon's information theory.

An ensemble X: Consists of a random variable X with a set of possible *outcomes* $\Omega_X = \{b_1, b_2, ..., b_I\}$, having probabilities $\{p_1, p_2, ..., p_I\}$, with $P(x = b_i) = p_i$, $p_i \geq 0$ and $\sum_{i=1}^{I} p_i = 1$

Entropy: The concept of entropy is the basis of classical information theory. Entropy describes the quantity of information in communication theory. Entropy is often associated with the amount of freedom of choice when selecting or constructing a message. In physics, entropy denotes the degree of randomness or uncertainty.
$H(X)$ denotes the entropy of the random variable X. The entropy of the set of probabilities $p_1, ..., p_n$ for a random variable is defined as[2]

$$H = -\sum_{i=1}^{n} p_i log_2(p_i). \tag{5.1}$$

[2]H is maximized when the freedom of choice is at a maximum. This means that H is maximized when all probabilities p_i are equal. The convention $0 \cdot log_2(0) = 0$ is used in entropy calculations.

Capacity of a Channel: Defines the maximum amount of information that can be transmitted over an information channel within a given time. Capacity is normally measured in bits per seconds.

Discrete Source: Generates successive symbols chosen from a finite set according to certain probabilities (stochastic process) depending often on preceding choices as well as the particular symbols in question.

Markoff Process=Markoff Chain: A stochastic process in which the probabilities depend on the previous events [14].

Ergodic Process: Special class of Markoff processes. In an ergodic process, any large enough sample of a sequence of symbols tends to have the same statistical behavior as the sequence as a whole.

Equivocation: Entropy of the message relative to the signal. It measures the average uncertainty in the message when the signal is known.

Joint entropy: The joint entropy of the random variables X and Y is defined as

$$H(X,Y) = -\sum_{x,y\in\Omega_X,\Omega_Y} p(x,y)log_2(p(x,y)). \tag{5.2}$$

Here $p(x,y)$ is the probability of joint occurrence of x and y. The joint entropy of X and Y is smaller than the sum of the individual entropies X and Y. Only when the random variables X and Y are independent, $H(X,Y) = H(X)+H(Y)$ is valid [37].

Conditional Entropy: The conditional entropy is a measure of how uncertain we are, on average, about the value of X when Y is known. The conditional entropy of X on knowing Y is therefore defined as

$$\begin{aligned} H(X|Y) &= -\sum_{x,y\in\Omega_X,\Omega_Y} p(x,y)log_2(p(x|y)) \\ &= H(X,Y) - H(Y) \end{aligned} \tag{5.3}$$

where $p(x|y)$ is the probability distribution of x conditional on knowing y [38].

Mutual Information: The mutual information between X and Y measures how much information X and Y have in common. The mutual information of X

and Y is obtained as follows [39]:

$$\begin{aligned} I(X:Y) = H(X:Y) &= H(X) - H(X|Y) \\ &= H(X) + H(Y) - H(X,Y) \end{aligned} \tag{5.4}$$

Shannon introduced in his extensive paper many other definitions and proved 23 theorems (i.e. the Noisy Channel Coding Theorem). For the analysis of the three-photon Greenberger-Horne-Zeilinger entanglement the above definitions are sufficient. Before the classical information theory is applied to the Pan *et al.* realization of the GHZ Gedankenexperiment, one of the most useful tool for entropy calculations, the entropy Venn diagram [35, 40] is introduced. In classical information problems, Venn diagrams can be used to quickly find relations between different entropies. Consider for example the binary entropy Venn diagram for the two random variables X and Y seen in Figure 5.2. Each area corresponds to a specific entropy. Relations between

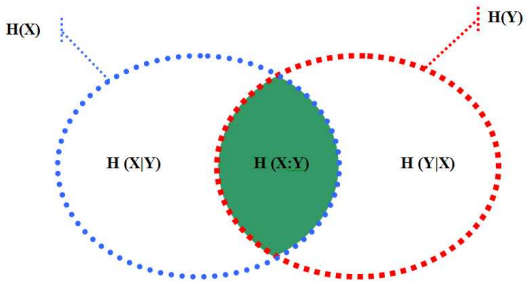

Figure 5.2: Binary entropy Venn diagram for the random variables X and Y. All terms $H(\bullet)$ denote non-negative entropies in the sense of classical Shannon information theory.

entropies can be found by simply adding or subtracting the areas corresponding to the different entropies. Using this simple method, the following entropy relations for the two random variables X and Y can be found:

$$H(X) = H(X|Y) + H(X:Y) \tag{5.5}$$

$$H(Y) = H(Y|X) + H(X:Y) \tag{5.6}$$

$$H(X,Y) = H(X) + H(Y) - H(X:Y). \tag{5.7}$$

In the next sections, the classical Shannon information theory is applied to the Pan *et al.* realization of the GHZ Gedankenexperiment. It is clear that classical information theory results in forbidden negative entropies[3] when applied to quantum entangled

[3] In classical Shannon information theory, mutual entropies of three or more random variables can be negative [41, 42] but conditional entropies are positive semidefinite [43].

systems. It is also known [35] that such quantum mechanical systems can be analyzed with quantum (von Neumann) conditional entropies $S(\rho) \equiv -tr(\rho \cdot log_2(\rho))$ [4]. Nevertheless, an information theoretical analysis based on Shannon's classical information theory can give interesting theoretical results such as the entropic Bell inequalities described in [41].

5.3 Entropy of Single Experiment

Pan *et al.* report in their paper [1] measurements for four different experiments. To start the information theoretical analysis of the Pan *et al.* realization of the GHZ Gedankenexperiment, only one of the four experiments is considered. Since all four experiments have a similar probability distribution, the following analysis of the yxy experiment can easily be adapted to the yyx, xyy and xxx experiments.
For each of the experiments, it is assumed that the measurement result is determined by an element of reality. The element of reality determining the result of the x (y) measurement in path i, is denoted as X_i (Y_i). The elements of reality X_i (Y_i) can assume the values $+1/-1$ for H'/V' (R/L) polarizations. Thus, eight different realizations are possible for the triple $Y_1X_2Y_3$. Because the eight settings of one experiment (i.e. yxy) can be measured by simply rotating the polarizers but without adding new optical elements to the experimental setup, it is assumed that measurements for all eight settings can be defined on one common probability space (classical system). Therefore an entropy Venn diagram can be used to find the entropy relations for the three random variables Y_1, X_2 and Y_3 (Figure 5.3).
Before any entropy for the entangled three-photon GHZ state is calculated, the involved entropies and their relations are defined:

$$H(Y_1) = -p(R_1) \cdot log_2(p(R_1)) - p(L_1) \cdot log_2(p(L_1)) \tag{5.8}$$

$$H(X_2) = -p(H_2') \cdot log_2(p(H_2')) - p(V_2') \cdot log_2(p(V_2')) \tag{5.9}$$

$$H(Y_3) = -p(R_3) \cdot log_2(p(R_3)) - p(L_3) \cdot log_2(p(L_3)) \tag{5.10}$$

$$\tag{5.11}$$

$$H(Y_1, X_2) = -\sum_{\substack{Y_1 \in \{R_1, L_1\} \\ X_2 \in \{H_2', V_2'\}}} p(Y_1, X_2) log_2(p(Y_1, X_2)) \tag{5.12}$$

$$H(Y_1, Y_3) = -\sum_{\substack{Y_1 \in \{R_1, L_1\} \\ Y_3 \in \{R_3, L_3\}}} p(Y_1, Y_3) log_2(p(Y_1, Y_3)) \tag{5.13}$$

[4] Von Neumann entropies can assume negative values.

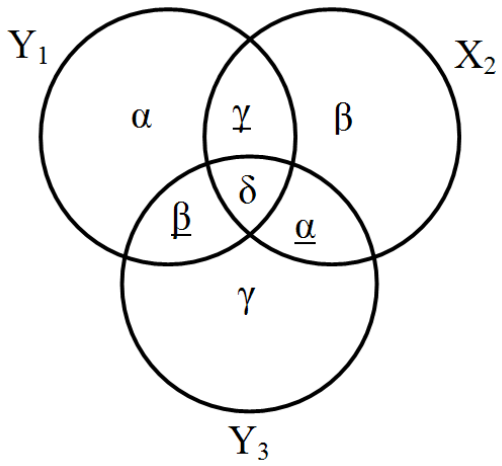

Figure 5.3: Ternary entropy diagram for the three random variables Y_1, X_2 and Y_3. α, $\underline{\alpha}$, β, $\underline{\beta}$, γ, $\underline{\gamma}$, δ are defined in the text.

$$H(X_2,Y_3) = -\sum_{\substack{X_2\in\{H_2',V_2'\}\\ Y_3\in\{R_3,L_3\}}} p(X_2,Y_3)log_2(p(X_2,Y_3)) \tag{5.14}$$

$$H(Y_1,X_2,Y_3) = -\sum_{\substack{Y_1\in\{R_1,L_1\}\\ X_2\in\{H_2',V_2'\}\\ Y_3\in\{R_3,L_3\}}} p(Y_1,X_2,Y_3)log_2(p(Y_1,X_2,Y_3)) \tag{5.15}$$

$$\underline{\gamma}+\delta = H(Y_1:X_2) = H(Y_1)+H(X_2)-H(Y_1,X_2) \tag{5.16}$$

$$\underline{\alpha}+\delta = H(X_2:Y_3) = H(X_2)+H(Y_3)-H(X_2,Y_3) \tag{5.17}$$

$$\underline{\beta}+\delta = H(Y_1:Y_3) = H(Y_1)+H(Y_3)-H(Y_1,Y_3) \tag{5.18}$$

$$\alpha = H(Y_1|X_2,Y_3) = H(Y_1,X_2,Y_3)-H(X_2,Y_3) \tag{5.19}$$

$$\beta = H(X_2|Y_1,Y_3) = H(Y_1,X_2,Y_3)-H(Y_1,Y_3) \tag{5.20}$$

$$\gamma = H(Y_3|Y_1,X_2) = H(Y_1,X_2,Y_3)-H(Y_1,X_2) \tag{5.21}$$

$$\underline{\alpha} = H(X_2:Y_3|Y_1) = H(Y_1,X_2)+H(Y_1,Y_3) -H(Y_1)-H(Y_1,X_2,Y_3) \tag{5.22}$$

$$\underline{\beta} = H(Y_1:Y_3|X_2) = H(Y_1,X_2)+H(X_2,Y_3) -H(X_2)-H(Y_1,X_2,Y_3) \tag{5.23}$$

$$\underline{\gamma} = H(Y_1:X_2|Y_3) = H(Y_1,Y_3)+H(X_2,Y_3) -H(Y_3)-H(Y_1,X_2,Y_3) \tag{5.24}$$

$$\delta = H(Y_1:X_2:Y_3) = H(Y_1)+H(X_2)+H(Y_3)-H(Y_1,X_2)$$

$$-H(Y_1, Y_3) - H(X_2, Y_3) + H(Y_1, X_2, Y_3) \quad (5.25)$$

For a classical system it is known that all Shannon entropies except δ are non-negative.

Quantum mechanical entanglement is one of the most interesting phenomena currently under investigation in physics. Entanglement is so important to understand because it forms the basis of quantum teleportation and certain quantum computational algorithms. To the author's best knowledge, no general information theoretical interpretation of quantum entanglement has been developed.

Quantum entanglement is strongly related to nonclassical correlations between separated quantum systems. Practically, this means that the measurement of an entangled state in station A influences[5] the possible outcome of a remote measurement in station B. This correlation between measurement outcomes of classically independent observers can be expressed in the language of information theory. It is expected that the mutual information of three independent observers A, B and C is different from the mutual information obtained when the observers measure an entangled system. Such an entangled system is, for example, described by the entangled three-photon GHZ state.

In Table 5.1 and 5.2, the entropies for the yxy experiment respectively the entangled three-photon GHZ state measured in the H-V basis are listed. From these tables, several interesting results can be derived.

- The entropy calculation for the transformed entangled three-photon GHZ state[6]

$$\begin{aligned}|\psi\rangle = \frac{1}{2}(&|R\rangle_1 \left|V'\right\rangle_2 |R\rangle_3 + |L\rangle_1 \left|H'\right\rangle_2 |R\rangle_3 \\ &+ |R\rangle_1 \left|H'\right\rangle_2 |L\rangle_3 + |L\rangle_1 \left|V'\right\rangle_2 |L\rangle_3)\end{aligned} \quad (5.26)$$

  results in different entropy values than the entropy calculation for the original entangled three-photon GHZ state[7]

$$|\psi\rangle = \frac{1}{\sqrt{2}} \left(|H\rangle_1 |H\rangle_2 |H\rangle_3 + |V\rangle_1 |V\rangle_2 |V\rangle_3\right). \quad (5.27)$$

  As required by the second law of thermodynamics, the joint entropies (uncertainties) of the transformed state are larger than the joint entropies of the original state. Another interesting observation is the change of the mutual information between two random variables. For the original state, the mutual information of two random variables (elements of reality) is $H(X_{o1} : X_{o2})$=$H(X_{o1} : X_{o3})$=

[5] The entangled state is reduced.

[6] In the following referred to as transformed state.

[7] In the following denoted as original state.

	$H(X_{o1})$	$H(X_{o2})$	$H(X_{o3})$	$H(X_{o1}, X_{o2})$	$H(X_{o1}, X_{o3})$	$H(X_{o2}, X_{o3})$	$H(X_{o1}, X_{o2}, X_{o3})$
Original GHZ State	**1**	**1**	**1**	**1**	**1**	**1**	**1**
	$H(Y_1)$	$H(X_2)$	$H(Y_3)$	$H(Y_1,X_2)$	$H(Y_1,Y_3)$	$H(X_2,Y_3)$	$H(Y_1,X_2,Y_3)$
QM ($Y_1X_2Y_3$=-1)	**1**	**1**	**1**	**2**	**2**	**2**	**2**
Rademacher Functions	**1**	**1**	**1**	**2**	**2**	**2**	**2**
Max. H(•) for Y_1,X_2,Y_3	**1**	**1**	**1**	**2**	**2**	**2**	**3**
LIS	**1**	**1**	**1**	**2**	**2**	**2**	**2.81**
TCME for λ_{Y1X2Y3}=nnn	**1**	**1**	**1**	**2**	**2**	**2**	**2**
TCME for λ_{Y1X2Y3}=iii	**1**	**1**	**1**	**2**	**2**	**2**	**2**
TCME for λ_{Y1X2Y3}=nii	**1**	**1**	**1**	**2**	**2**	**2**	**2**
TCME for λ_{Y1X2Y3}=iin	**1**	**1**	**1**	**2**	**2**	**2**	**2**
TCME overall	**1**	**1**	**1**	**2**	**2**	**2**	**2.54**
Experiment (Pan *et al.*)	**1**	**1**	**1**	**2**	**2**	**2**	**2.61**

Table 5.1: Single and joint entropies for the original entangled three-photon GHZ state $|\psi\rangle = \frac{1}{\sqrt{2}}(|H\rangle_1|H\rangle_2|H\rangle_3 + |V\rangle_1|V\rangle_2|V\rangle_3)$ and for the yxy experiment. All models require a maximum randomness for any individual or two-photon joint measurement. QM ($Y_1X_2Y_3 = -1$): Elements of reality X_i and Y_i have to fulfill the quantum mechanical predictions. Rademacher functions: $Y_1 = -r_1(t)$, $Y_2 = r_1(t)r_3(t)$ and $Y_3 = r_3(t)$ where $r_k(t) = sign\left[sin\left(2^k\pi t\right)\right]$. Max. $H(\bullet)$ for Y_1, X_2, Y_3: Joint probability spaces of the three random variables Y_1, X_2, Y_3 are such that a maximum entropy results. LIS: Values of the elements of reality are assigned according to the rules of the local instruction-set model (section 4.2). TCME: Values of X_i and Y_i are assigned according to the TCME model (section 4.3). Four equipment parameter combinations (nnn, iii, nii and iin) are possible for the yxy experiment. The overall TCME entropy calculation considers the distribution of the values of elements of reality in the long run. Experiment (Pan *et al.*): Entropies for the measurement results reported by Pan *et al.*.

	α_o	$\underline{\alpha}_o$	β_o	$\underline{\beta}_o$	γ_o	$\underline{\gamma}_o$	δ_o
Original GHZ State	**0**	**0**	**0**	**0**	**0**	**0**	**1**
	α	$\underline{\alpha}$	β	$\underline{\beta}$	γ	$\underline{\gamma}$	δ
QM ($Y_1X_2Y_3$=-1)	**0**	**1**	**0**	**1**	**0**	**1**	**-1**
Rademacher Functions	**0**	**1**	**0**	**1**	**0**	**1**	**-1**
Max. H(•) for Y_1,X_2,Y_3	**1**	**0**	**1**	**0**	**1**	**0**	**0**
LIS	**0.81**	**0.19**	**0.81**	**0.19**	**0.81**	**0.19**	**-0.19**
TCME for λ_{Y1X2Y3}=nnn	**0**	**1**	**0**	**1**	**0**	**1**	**-1**
TCME for λ_{Y1X2Y3}=iii	**0**	**1**	**0**	**1**	**0**	**1**	**-1**
TCME for λ_{Y1X2Y3}=nii	**0**	**1**	**0**	**1**	**0**	**1**	**-1**
TCME for λ_{Y1X2Y3}=iin	**0**	**1**	**0**	**1**	**0**	**1**	**-1**
TCME overall	**0.54**	**0.46**	**0.54**	**0.46**	**0.54**	**0.46**	**-0.46**
Experiment (Pan *et al.*)	**0.61**	**0.39**	**0.61**	**0.39**	**0.61**	**0.39**	**-0.39**

Table 5.2: Conditional entropies (α, β, γ), conditional informations ($\underline{\alpha}$, $\underline{\beta}$, $\underline{\gamma}$) and mutual information δ for the original entangled three-photon GHZ state $|\psi\rangle = \frac{1}{\sqrt{2}}(|H\rangle_1|H\rangle_2|H\rangle_3 + |V\rangle_1|V\rangle_2|V\rangle_3)$ and the yxy experiment. QM ($Y_1X_2Y_3 = -1$): Elements of reality X_i and Y_i have to fulfill the quantum mechanical predictions. Rademacher functions: $Y_1 = -r_1(t)$, $Y_2 = r_1(t)r_3(t)$ and $Y_3 = r_3(t)$ where $r_k(t) = sign\left[sin\left(2^k\pi t\right)\right]$. Max. $H(\bullet)$ for Y_1, X_2, Y_3: Joint probability spaces of the three random variables Y_1, X_2, Y_3 are such that a maximum entropy results. LIS: Values of the elements of reality are assigned according to the rules of the local instruction-set model (section 4.2). TCME: Values of X_i and Y_i are assigned according to the TCME model (section 4.3). Four equipment parameter combinations (*nnn*, *iii*, *nii* and *iin*) are possible for the yxy experiment. The overall TCME entropy calculation considers the distribution of the values of elements of reality in the long run. Experiment (Pan *et al.*): Entropies for the measurement results reported by Pan *et al.*.

$H(X_{o2} : X_{o3}) = 1$ while it is $H(Y_1 : X_2)$=$H(Y_1 : Y_3)$= $H(X_2 : Y_3) = 0$ for the transformed state. Consequently, the transformation reduces the information shared by two variables. In terms of quantum mechanics this means that a measurement at one detector reduces the original state such that the outcomes at the other detectors are known ($H(X_{o1}, X_{o2}|X_{o3}) = H(X_{o2}, X_{o3}|X_{o1}) = H(X_{o1}, X_{o3}|X_{o2}) = 0$). Whereas for the transformed state, measurements at two detectors are required, to determine the result of the third detector ($\alpha = \beta = \gamma = 0$ but $H(Y_1, X_2|Y_3) = H(X_2, Y_3|Y_1) = H(Y_1, Y_3|X_2) = 1$). The change of the mutual information between the three random variables can also be seen when comparing δ and δ_o. The mutual information in the case of the original state is $\delta_o = 1$ (1. order entanglement) while we obtain $\delta = -1$ for the transformed state (2. order entanglement). Thus $H(Y_1 : X_2 : Y_3)$ can be negative [42].

Some may not be comfortable with this fact because it is difficult to interpret $H(Y_1 : X_2 : Y_3) < 0$ as a measure of information. Nevertheless, if the definition $H(Y_1 : X_2 : Y_3) = H(Y_1 : X_2) - H(Y_1 : X_2|Y_3)$ is used to interpret a negative mutual entropy of three random variables, then it means that $H(Y_1 : X_2) < H(Y_1 : X_2|Y_3)$. Therefore, the mutual information of three variables can only be negative, when the knowledge of i.e. Y_3 causes an increase in the conditional mutual information between Y_1 and X_2 compared to the mutual information of Y_1 and X_2 not knowing Y_3.

The difference between $\delta = -1$ for the transformed state and $\delta_o = 1$ for the original state can be explained as follows.

When a measurement at one detector (i.e. D_1) is done for the original state, then it is known from quantum mechanics that the act of measurement reduces the entangled quantum mechanical state to a uniquely defined quantum state $|H\rangle_1 |H\rangle_2 |H\rangle_3$ or $|V\rangle_1 |V\rangle_2 |V\rangle_3$. Therefore, when knowing the measurement result in one station, the outcome in the second station is uniquely defined. This means that two random variables (i.e. X_{o1} and X_{o2}) have a mutual information $H(X_{o1} : X_{o2}) = 1$. On the other hand side, if the measurement result in a third station is known (i.e. X_{o3}), then the measurement results for the remaining variables are known. This means that the additional knowledge of X_{o1} does not increase the information known about X_{o2} when X_{o3} is known. Therefore $H(Y_1 : X_2|Y_3) = 0$ and $H(Y_1 : X_2 : Y_3) = 1$.

A similar analysis for the transformed state shows that the knowledge of the measurement result of one random variable (i.e. Y_1) does not determine the

measurement result of the another random variables (i.e. X_2). Therefore, the two individual measurements are completely independent $H(Y_1 : X_2)$= $H(Y_1 : Y_3) = H(X_2 : Y_3) = 0$.
On the other hand side, if a third random variable (i.e. Y_3) is know, then the measurement of one of the two remaining random variables (i.e. Y_1 or X_2) reduces the state such that the value of the third random variable is uniquely defined due to entanglement. Therefore, the conditional information for the transformed state in the yxy experiment is $H(Y_1 : X_2|Y_3) = H(Y_1 : Y_3|X_2) = H(X_2 : Y_3|Y_1) = 1$ and $H(Y_1 : X_2 : Y_3) = -1$.
Because the predicted outcomes for the eight settings of the yxy experiment are the same for the quantum mechanical model and the model based on Rademacher functions, the entropies are the same in both cases. Thus the above analysis for the transformed state is also valid for the Rademacher function model.
In conclusion, it was shown that in general, a negative mutual information $H(X : Y : Z) = H(X : Y) - H(X : Y|Z)$ means that the two random variables X and Y have more mutual information when a third random variable Z is know than when the random variable Z is not known. For the given example, it means that a measurement of the original state at one station determines the outcomes at the other two detectors whereas in the case of the transformed state, the knowledge of two random variables is required to uniquely determine the outcome at the remaining detector. This can be interpreted as a reduction of entanglement between the random variables by the linear transformations (2.36 - 2.39).

- The comparison of the entropies for the transformed quantum mechanical state and the maximum joint entropy of three random variables case shows that the quantum mechanical condition $Y_1X_2Y_3 = -1$ only reduces the joint entropy $H(Y_1, X_2, Y_3)$. A maximum randomness destroys all conditional informations $\underline{\alpha}$, $\underline{\beta}$ and $\underline{\gamma}$ and the mutual entropy $\delta = 0$. Additionally, the conditional entropies $\alpha = \beta = \gamma = 1$ are maximized for the case of maximum randomness.

- The information theoretical analysis of the predictions of the TCME model for the yxy experiment shows a very interesting property of the entropies of time and setting dependent equipment parameter model. As described in section 4.3, the measuring equipments are adjusted such that the equipment parameter combination is $\frac{5}{8}$ of the time nnn and $\frac{1}{8}$ of the time iii, nii or iin, respectively.

For each of these combinations, the entropy values are the same as for the transformed entangled three-photon GHZ state[8]. An analysis of the overall (over a long period of time) distribution for the *yxy* experiment, obtained by the simulation with the TCME model shows (Figure 4.5) that the overall entropies are not weighted averages of the single time entropies. This can for example be seen when considering α in Table 5.2. The weighted average of the four entropies $\alpha_{nnn} = 0$, $\alpha_{iii} = 0$, $\alpha_{nii} = 0$ and $\alpha_{iin} = 0$ is zero and not $\alpha_{overall} = 0.54$. This behavior is mathematically expressed in the following remark.

Remark 5.1 *The random variable A with values* $\{a_1, a_2, ..., a_N\}$ *is given. It is assumed that the time* $t \in \{t_1, ...t_M\}$ *can be divided into M different intervals* t_i. $p_i = P(t = t_i)$ *is the probability that the random variable A is measured during the time interval* t_i. *Additionally, the probabilities* p_i *satisfy* $\sum_{i=1}^{M} p_i = 1$. *It is also assumed that A is at each time* t_i *defined on a certain probability space. Therefore the conditional probability distribution of* $(A|t)$ *has to fulfill* $\sum_{i=1}^{N} p(a_i|t) = 1$ *at any time t.*
The entropy of A at a given time t is defined as

$$H(A|t) = -\sum_{i=1}^{N} p(a_i|t) log_2(p(a_i|t)). \tag{5.28}$$

The entropy of A over all t is

$$H(A) = -\sum_{i=1}^{N} \left(\sum_{k=1}^{M} p(t_k) p(a_i|t_k) log_2 \left(\sum_{k=1}^{M} p(t_k) p(a_i|t_k) \right) \right). \tag{5.29}$$

It can easily be checked that this is in general [9] *not equal to*

$$H_{ta}(A) = -\sum_{k=1}^{M} p(t_k) \left[\sum_{i=1}^{N} p(a_i|t_k) log_2 \left(p(a_i|t_k) \right) \right] = \sum_{k=1}^{M} p(t_k) H(A|t_k). \tag{5.30}$$

(5.28) and (5.29) and accordingly (5.29) and (5.30) are only equal when the probability distribution for A is the same at all times t

$$p(A|t) = p(A). \tag{5.31}$$

[8] During the times $t = k + 4$, the only possible values for the elements of reality predicted by the TCME model for the *yxy* experiment are $Y_1X_2Y_3 = \{R_1H_2'R_3, R_1H_2'L_3, L_1V_2'L_3, L_1H_2'R_3\}$.

[9] For example: Assume $p(A = a_1|t_1) = \frac{1}{4}$, $p(A = a_2|t_1) = \frac{3}{4}$, $p(A = a_1|t_2) = \frac{1}{2}$, $p(A = a_2|t_2) = \frac{1}{2}$, $p(t_1) = \frac{1}{2}$ and $p(t_2) = \frac{1}{2}$. Then, $H(A) = 0.95 \neq H_{ta}(A) = 0.91$.

Remark 5.1 is important because of the following reason. In [41], the authors derive the CHSH inequality for mutual entropies

$$H(A_{\mathbf{a}} : B_{\mathbf{b}}) - H(A_{\mathbf{a}} : B_{\mathbf{c}}) + H(A_{\mathbf{d}} : B_{\mathbf{b}}) + H(A_{\mathbf{d}} : B_{\mathbf{c}}) \leq 2. \tag{5.32}$$

This inequality is only valid when the four random variables $A_{\mathbf{a}}$, $A_{\mathbf{d}}$, $B_{\mathbf{b}}$ and $B_{\mathbf{c}}$ are defined for all times on the same common probability space. If the four variables are defined on different probability spaces at different times and settings, inequality (5.32) can be fulfilled at each time t but violated for the overall experiment. Therefore, any entropic Bell inequalities can be violated by the long run distributions, but remain valid at discrete times t. Thus, from an overall violation of entropic Bell inequalities, no conclusion about locality can be drawn. It can only be checked whether or not the overall experimental results can be explained by a model that has all measurements defined on one common probability space.

- The Pan *et al.* measurement results for the yxy experiment show that the experimental entanglement is not as pure as quantum mechanical predicted. When considering δ as a measure of entanglement, it means that the measured value of $\delta_{exp} = -0.39$ is between the perfectly entangled transformed state $\delta_{QM} = -1$ and $\delta_{max} = 0$ when the three variables Y_1, X_2 and Y_3 are independent.

In conclusion, it was shown that the mutual information $\delta = H(A : B : C)$ of three random variables A, B and C can be interpreted with the definition $H(A : B : C) = H(A : B) - H(A : B|C)$. A value of $\delta \neq 0$ denotes systems for which the knowledge of one random variable changes the mutual information between the other random variables compared to the mutual information of these two random variables not knowing the value of the third random variable. Additionally, a comparison of the entropies at a given time t and the overall entropies showed that the overall entropy can in general not be used to determine the values of the individual entropies and vis versa.
In the following section, classical information theory is used to answer the question whether or not all four experiments yyx, yxy, xyy and xxx can be defined on one common probability space.

5.4 Generalized Entropic Bell Test

In this section, a generalized entropic Bell test is developed and applied to the Pan *et al.* realization of the GHZ Gedankenexperiment. For the derivation of the gener-

alized entropic Bell test, Shannon's classical information theory is used.
The generalized entropic Bell test states *necessary* conditions for the existence of a local realistic model for the experiment under investigation. The generalized entropic Bell test can be used to check whether or not local realistic models based on source (elements of reality) and setting parameters defined on one common probability space can exist. The test is based on the following idea.
At the beginning it is assumed that all investigated experiments can be explained with a local realistic model with all random variables defined on one common probability space. If this assumption is correct, classical Shannon information theory can be applied and non of the calculated entropies should contradict the non-negativity theorem for certain entropies. Therefore, if any of these entropies is negative it is known that the assumption was incorrect and the experiments can not be explained with a local realistic model based on source and setting parameters defined on one common probability space.
Therefore, the question whether or not an observed probability distribution for random variables can be explained by a local realistic model defined on one probability space can be reduced to the sign test of the generalized entropic Bell test. For example, a negative value of $H(A:B|D)$ for the four random variables A, B, C and D indicates, that the experiment can not be explained by a local theory that is only based on source (elements of reality) and setting parameters.
In the following, the generalized entropic Bell test is applied to the experimental results obtained by Pan *et al.*. The four experiments measured in [1] are considered to be described by four random variables:

$$\begin{aligned} A = Y_1Y_2X_3 &\in \{R_1R_2V_3', R_1R_2H_3', L_1R_2H_3', L_1R_2V_3', \\ &\quad R_1L_2H_3', R_1L_2V_3', L_1L_2V_3', L_1L_2H_3'\} \qquad (5.33) \\ B = Y_1X_2Y_3 &\in \{R_1V_2'R_3, R_1H_2'R_3, L_1H_2'R_3, L_1V_2'R_3, \\ &\quad R_1H_2'L_3, R_1V_2'L_3, L_1V_2'L_3, L_1H_2'L_3\} \qquad (5.34) \\ C = X_1Y_2Y_3 &\in \{V_1'R_2R_3, H_1'R_2R_3, H_1'L_2R_3, V_1'L_2R_3, \\ &\quad H_1'R_2L_3, V_1'R_2L_3, V_1'L_2L_3, H_1'L_2L_3\} \qquad (5.35) \\ D = X_1X_2X_3 &\in \{V_1'V_2'V_3', H_1'V_2'V_3', H_1'H_2'V_3', V_1'H_2'V_3', \\ &\quad H_1'V_2'H_3', V_1'V_2'H_3', V_1'H_2'H_3', H_1'H_2'H_3'\} \qquad (5.36) \end{aligned}$$

As can be seen, for each random variable the sample space consists of 8 possible events. Additionally, the four random variables are based on the same six elements of reality X_i and Y_i $(i = 1, 2, 3)$. Therefore, the four random variables A, B, C

and D are not independent. When the four experiments can be explained with a local realistic model based on elements of reality defined on one common probability space, the classical information theoretical analysis of the four experiments should result in values for the entropies $H(A:B)$, $H(A:B|C)$, $H(A:B|C,D)$, $H(A|B)$, $H(A,B|C)$, $H(A,B,C,|D)$, $H(A|B,C)$, $H(A,B|B,C)$ and $H(A|B,C,D)$ that are all non-negative.

Because it is assumed, that Shannon's classical information theory is valid, the quaternary entropy Venn diagram (Figure 5.4) can be used to derived the relations

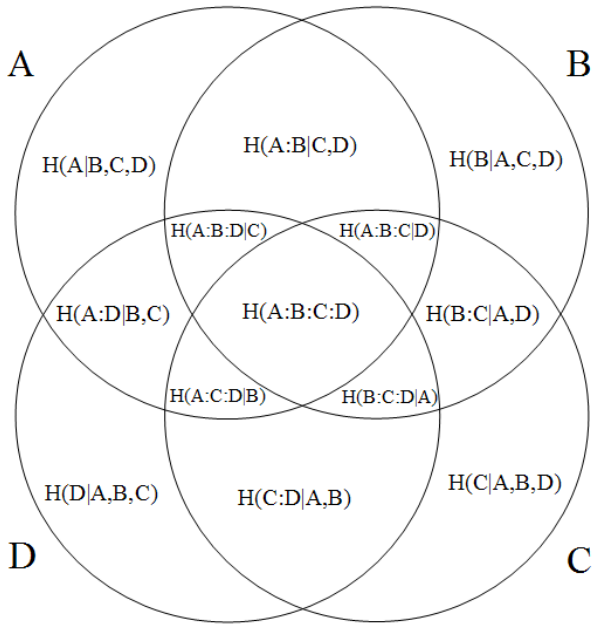

Figure 5.4: Quaternary entropy diagram for the four random variables A, B, C and D.

between different entropies:

$$H(A:B|C) = H(A,C)+H(B,C)-H(C)-H(A,B,C) \geq 0 \quad (5.37)$$

$$\begin{aligned} H(A:B|C,D) &= H(A,C,D)+H(B,C,D) \\ &\quad -H(C,D)-H(A,B,C,D) \geq 0 \end{aligned} \quad (5.38)$$

$$\begin{aligned} H(A:B:C|D) &= H(A,D)+H(B,D)+H(C,D) \\ &\quad +H(A,B,C,D)-H(D)-H(A,B,D) \\ &\quad -H(A,C,D)-H(B,C,D) \end{aligned} \quad (5.39)$$

$$H(A:B:C) = H(A)+H(B)+H(C)+H(A,B,C)$$

$$
\begin{aligned}
& -H(A,B) - H(A,C) - H(B,C) && (5.40)\\
H(A:B:C:D) &= H(A) + H(B) + H(C) + H(D)\\
& -H(A,B) - H(A,C) - H(A,D)\\
& -H(B,C) - H(B,D) - H(C,D)\\
& +H(A,B,C) + H(A,B,D) + H(A,C,D)\\
& +H(B,C,D) - H(A,B,C,D) && (5.41)\\
H(A|B,C) &= H(A,B,C) - H(B,C) \geq 0 && (5.42)
\end{aligned}
$$

Here, the joint entropies of A, B, C and D are defined similarly to (5.8-5.15). The strong subadditivity theorem [43] of the classical Shannon information theory states that the conditional informations (5.37) and (5.38) are non-negative. The monotonicity of Shannon entropies implies that conditional entropies (i.e. $H(A|B,C)$) are positive semidefinite [43]. Thus, if the strong subadditivity condition is violated, it is known that the analyzed system is not on one probability space. This generalized entropic Bell (sign) test of $H(A:B|C)$, $H(A:B|C,D)$ or $H(A|B,C)$ is a simple method to decide whether the Pan *et al.* realization of the GHZ state can be explained by a simple local realistic model with parameters defined on one common probability space or if different probability spaces are required [10].

The main entropies for different classical models used in the generalized entropic Bell test of the Pan *et al.* realization of the GHZ Gedankenexperiment are summarized in Table 5.3 (a detailed calculation of the listed entropies is given in appendix B).

All simple classical models assume that the source parameters (elements of reality) and the measuring equipment settings are defined for all four experiments A, B, C and D on one common product probability space. As can be seen, the conditional information $H(D|A,B)$ is negative for the local elements of reality model that allows only the quantum mechanically predicted result $D = X_1X_2X_3 = +1$. Therefore, the quantum mechanical predictions derived in [1] can not be explained with a classical model that is only based on source and setting parameters defined on the same common probability space at all times t.

To check the generalized entropic Bell test, the conditional entropies for the distributions given by the local realistic model introduced by Pan *et al.* (POLT) and the local instruction-set (LIS) model are calculated. It is expected that all conditional informations are non-negative because the models are based on source and setting parameters that are for all four experiments defined on one common probability space.

[10] In the language of quantum mechanics it reduces to the question whether or not quantum nonlocality is required to explain the experimental results.

	Local EoR model with $A=Y_1Y_2X_3=-1, B=Y_1X_2Y_3=-1, C=X_1Y_2Y_3=-1, D=X_1X_2X_3=-1$	Local EoR model with $A=Y_1Y_2X_3=-1, B=Y_1X_2Y_3=-1, C=X_1Y_2Y_3=-1, D=X_1X_2X_3=+1$	LIS
H(A)=H(B)=H(C)	**2**	**2**	**2.26**
H(D)	**2**	**0**	**2.26**
H(A,B)=H(A,C)=H(B,C)	**3**	**3**	**4.5**
H(A,D)=H(B,D)=H(C,D)	**3**	**0**	**4.5**
H(A,B,C)	**3**	**3**	**5**
H(A,C,D)=H(B,C,D)	**3**	**0**	**5**
H(A,B,C,D)	**3**	**0**	**5**
H(A:B|C)	**1**	**1**	**1.74**
H(A:B|D)=H(A:C|D)=H(B:C|D)	**1**	**0**	**1.74**
H(D|A,B)	**0**	**-3**	**0.5**

Table 5.3: Conditional and mutual informations for different models based on elements of reality (EoR). The local EoR model with $A = Y_1Y_2X_3 = -1$, $B = Y_1X_2Y_3 = -1$, $C = X_1Y_2Y_3 = -1$ and $D = X_1X_2X_3 = -1$ is the local realistic model introduced by Pan *et al.* (POLT). The local EoR model with $A = Y_1Y_2X_3 = -1$, $B = Y_1X_2Y_3 = -1$, $C = X_1Y_2Y_3 = -1$ and $D = X_1X_2X_3 = +1$ is a local model that is based on the same source parameters as POLT. The only difference is that the allowed outcomes are not only for the A, B and C experiment restricted to the quantum mechanically predicted states but also the D experiment is restricted to the quantum mechanically desired states $D = X_1X_2X_3 = +1$. The LIS model is explained in section 4.2

The calculated entropies for POLT and the LIS model (Table 5.3) confirmed that the *necessary* conditions of the generalized Bell test are fulfilled for both models.
In conclusion, it was shown that the non-negativity of certain Shannon entropies (5.37,5.38,5.42) is a necessary condition for the existence of local realistic models based on elements of reality defined on one common product probability space. This generalized entropic Bell test was used to show that the quantum mechanical predictions for the Pan *et al.* realization of the GHZ Gedankenexperiment can not be explained by a simple local realistic model only based on elements of reality defined on one common probability space.
In the following section, another simple test to check whether or not all four experiments yyx, yxy, xyy and xxx reported by Pan *et al.* can be explained by source and setting parameters defined on one common probability space is presented.

5.5 Non-Existence of one Common Probability Space

In the last section it was shown how the generalized entropic Bell test can be used to decide if a physical experiment can be explained with a theory based on one common probability space for all measurements. In this section, a similar test based on an idea of Jean Bass[23] is applied to the Pan *et al.* realization of the GHZ Gedankenexperiment. In [34] the authors show that the celebrated theorem of Bell is only a special case of a theorem of Bass. The authors show that given certain joint distributions for the three pairs (A, B), (A, C) and (B, D) of random variables, "it is not possible to find three random variables A, B and C, defined on a common probability space" [34].
In this section it is assumed that the four experiments yyx, yxy, xyy and xxx can be defined as random variables $A = Y_1Y_2X_3$, $B = Y_1X_2Y_3$, $C = X_1Y_2Y_3$ and $D = X_1X_2X_3$. We show with basic probability theory that these four random variables can not be defined on one common probability space while fulfilling the quantum mechanically predicted relations $A = Y_1Y_2X_3 = -1$, $B = Y_1X_2Y_3 = -1$, $C = X_1Y_2Y_3 = -1$ and $D = X_1X_2X_3 = +1$ [1].
When the four experiments xyy, yxy, yyx and xxx can be defined on one common probability space theorem 5.1 has to be fulfilled.

Theorem 5.1 *The random variables A, B, C and D can be defined on one common*

probability space if and only if

$$\sum_{\substack{a \in A \\ b \in B \\ c \in C}} P(a,b,c,d) = P(d) \tag{5.43}$$

is valid. The joint probability of the four random variables A, B, C and D is given by $P(a,b,c,d)$. $P(d)$ defines the probability distribution of the random variable D.

The probabilities $P(X_1X_2X_3)$ can be obtained from the quantum mechanical prediction given by Pan *et al.*

$$\begin{aligned} |\psi\rangle = \frac{1}{\sqrt{2}} \; & (|H'\rangle_1 |H'\rangle_2 |H'\rangle_3 + |H'\rangle_1 |V'\rangle_2 |V'\rangle_3 \\ & + |V'\rangle_1 |H'\rangle_2 |V'\rangle_3 + |V'\rangle_1 |V'\rangle_2 |H'\rangle_3). \end{aligned} \tag{5.44}$$

From this quantum mechanical state (5.44) we obtain

$$P(X_1X_2X_3 = -1) = 0 \tag{5.45}$$

$$P(X_1X_2X_3 = +1) = \frac{1}{4}. \tag{5.46}$$

To calculate the joint probabilities of the four experiments A, B, C and D, the following definition based on conditional probabilities is used

$$P(a,b,c,d) = P(d|c,b,a) \cdot P(c|b,a) \cdot P(b|a) \cdot P(a). \tag{5.47}$$

We know from Pan *et al.* that the three experiments A, B and C can be defined on one probability space while also fulfilling the quantum mechanical relations $A = Y_1Y_2X_3 = -1$, $B = Y_1X_2Y_3 = -1$ and $C = X_1Y_2Y_3 = -1$. Additionally, whenever the values of the elements of reality of the three experiments A, B and C are known, the result of the D experiment is also known[11]. Therefore $P(d|a,b,c) = 1$ for $d \in \{X_1X_2X_3 = -1\}$ and $P(d|a,b,c) = 0$ for $d \in \{X_1X_2X_3 = +1\}$. When assuming that the measurement results are determined by the elements of reality associated with the photons 1, 2 and 3 (see section 4.2) it can easily be checked that

$$P(R_1R_2V_3') = P(L_1R_2H_3') = P(R_1L_2H_3') = P(L_1L_2V_3') = \frac{1}{4} \tag{5.48}$$

$$\begin{aligned} P(R_1V_2'R_3|R_1R_2V_3') &= P(R_1H_2'L_3|R_1R_2V_3') = \\ P(L_1H_2'R_3|L_1R_2H_3') &= P(L_1V_2'L_3|L_1R_2H_3') = \\ P(R_1V_2'R_3|R_1L_2H_3') &= P(R_1H_2'L_3|R_1L_2H_3') = \\ P(L_1H_2'R_3|L_1L_2V_3') &= P(L_1V_2'L_3|L_1L_2V_3') = \frac{1}{2} \end{aligned} \tag{5.49}$$

[11] It is assumed that for all experiments the same values for the elements of reality are evaluated. This method is known as counterfactual reasoning.

$$
\begin{aligned}
P(V_1' R_2 R_3 | R_1 V_2' R_3, R_1 R_2 V_3') &= P(H_1' R_2 L_3 | R_1 H_2' L_3, R_1 R_2 V_3') = \\
P(V_1' R_2 R_3 | L_1 H_2' R_3, L_1 R_2 H_3') &= P(H_1' R_2 L_3 | L_1 V_2' L_3, L_1 R_2 H_3') = \\
P(H_1' L_2 R_3 | R_1 V_2' R_3, R_1 L_2 H_3') &= P(V_1' L_2 L_3 | R_1 H_2' L_3, R_1 L_2 H_3') = \\
P(H_1' L_2 R_3 | L_1 H_2' R_3, L_1 L_2 V_3') &= P(V_1' L_2 L_3 | L_1 V_2' L_3, L_1 L_2 V_3') = 1 \qquad (5.50)
\end{aligned}
$$

when $A = Y_1 Y_2 X_3 = -1$, $B = Y_1 X_2 Y_3 = -1$ and $C = X_1 Y_2 Y_3 = -1$ are fulfilled. These results together with (5.47) give

$$
\begin{aligned}
P(a, b, c, d) &= \frac{1}{8} \quad \text{if} \quad d \in \{X_1 X_2 X_3 = -1\} \qquad (5.51) \\
P(a, b, c, d) &= 0 \quad \text{if} \quad d \in \{X_1 X_2 X_3 = +1\}. \qquad (5.52)
\end{aligned}
$$

Finally, we can use theorem 5.1 to check if all four experiments A, B, C and D can be defined on one common probability space and at the same time fulfill the quantum mechanical relations $A = Y_1 Y_2 X_3 = -1$, $B = Y_1 X_2 Y_3 = -1$, $C = X_1 Y_2 Y_3 = -1$ and $D = X_1 X_2 X_3 = +1$. From (5.43) and (5.52) we obtain for example $P(H_1' V_2' V_3') = 0$. But this contradicts (5.46). Therefore, the four experiments A, B, C and D can not be defined on one probability space when they have to fulfill the quantum mechanical predications.

Theorem 5.1 was also used to check whether the four experiments A, B, C and D can be defined on one common probability space or not, when the fractions predicted by the LIS model (section 4.2) have to be reproduced. The calculations confirmed that for the distributions predicted by LIS, all four experiments can be defined on the same probability space.

5.6 Conclusion

It was shown that classical Shannon information theory is helpful to analyze entanglement of quantum states. The entangled three-photon GHZ state was used as an example for this entanglement analysis. The information theoretical analysis of the yxy experiment showed that the linear transformations (2.36-2.39) change the mutual information between the three random variables (Y_1, X_2 and Y_3) of the original state and the transformed state. This change can be interpreted as a change in the strength of the entanglement between the three random variables. Additionally it was demonstrated that an entropy analysis of a specific physical experiment can not exclude local realistic models that are based on different time dependent probability spaces.

In this chapter, the generalized entropic Bell test and a theorem based on basic probability theory were introduced. Both tests applied to the four experiments measured by Pan *et al.* showed that the quantum mechanical predictions for the four experiments yyx, yxy, xyy and xxx can not be explained by a local realistic model based on elements of reality that are defined on one common probability space. However, time dependent multi-probability space models that still are local realistic are, at least from the view point of mathematics, possible.

Chapter 6

Conclusion and Future Work

In this Master's Thesis, the experimental realization of the GHZ Gedankenexperiment by Pan *et al.* was studied in great detail, resulting in a modified local realistic model based on elements of reality that can explain the actual experimental results reported in [1] with a statistically smaller error than the quantum mechanical model. Therefore, it is believed that the Pan *et al.* experiment can not be used to draw conclusions about the existence of quantum nonlocality. Moreover, the question whether or not quantum mechanics is a complete theory can not be answered from the reported experimental results because, as it is shown for this particular experiment not even the class of local realistic models based on a small number of instruction sets representing elements of reality can be excluded.

Because the presented modified local realistic model can not exactly explain the observed results, two other models were developed. The time coordinated measuring equipments (TCME) model uses the idea of time and setting dependent equipment parameters. It was shown that the experimental data can be obtained when the four experiments yyx, yxy, xyy and xxx are defined on different probability spaces. The proposed time coordinated equipment parameters seem to be plausible because similar entanglement experiments [32] indicate that the exact coordination of the optical elements is required to observe the quantum mechanically expected data. In addition, the TCME model can even explain the influence of delays imposed on the photons by the experimental setup. Such delays are reported [1] to influence the entanglement.

A third objective local model for the Pan *et al.* experiment, which was used for the development of the instruction-set model, is explained in appendix A. This model is based on the known detection inefficiency loophole. The extended objective local model based on detection inefficiency (EOLMDI) uses several unproven speculations.

Therefore, it is believed that EOLMDI could have physical weaknesses. Nevertheless, it does not contradict important postulates such as the indivisibility of photons. Thus, EOLMDI is an interesting variation of the detection inefficiency loophole especially because the basic version of this model (the OLMDI model) can also reproduce the experimental data measured by Aspect and his group. The EOLMDI model shows how difficult it is to implement a loophole free experimental proof of quantum nonlocality.

In summary it has been shown in the first part of this work, that the Pan *et al.* experiment can not be used to prove the existence of quantum nonlocality. Additionally, several objective local models were proposed. These models suggest future directions in the quest for an objective local explanation of quantum mechanical phenomena such as entanglement or quantum nonlocality.

In chapter 5 an information theoretical analysis of the Pan *et al.* experiment was presented. It was shown that classical entropies can be used as a measure of entanglement. The generalized entropic Bell test was defined and applied to the Pan *et al.* experiment. This test and a theoretical analysis based on basic probability theory were used to prove that the four experiments yyx, yxy, xyy and xxx measured by Pan *et al.* can not be defined on one common probability space when they have to fulfill the quantum mechanical predictions.

The results of this thesis show that the use of more sophisticated local hidden variable theories [21, 44] will be absolutely necessary when the question of quantum nonlocality versus objective local explanations is addressed. The past attempts to prove the completeness of quantum mechanics with Bell type inequalities were useful to exclude certain classes of objective local models. However, time dependent models on more than one probability space appear possible. The search for a theory that goes beyond the quantum mechanical model might benefit from improved future quantum optical experiments based on single photons.

Appendix A

Extended Objective Local Model based on Detection Inefficiency

The extended objective local model based on detection inefficiency (EOLMDI) is an extension of OLMDI. It is based on many unproven speculations such as a new photon property that is described by a hidden parameter vector and certain manipulations of this hidden photon parameter by optical elements. However, the EOLMDI model does not contradict important postulates such as the indivisibility of photons or the observed detection inefficiency of these optical experiments. Therefore the EOLMDI model should be seen as an interesting alternative to objective local models that assume 100% detection efficiencies. The model might be used as guideline for more elaborated local models.
In general, the behavior of the detectors, filters, polarizers and source in the EOLMDI model is the same as in the OLMDI model. In the following section A.1, previously discussed optical elements are repeated and the additional elements used in the Pan *et al.* experiment are introduced. At the end of this appendix, the EOLMDI implementation and simulation results are presented.

A.1 Linear Optical Elements

Most of the optical elements used in the Pan *et al.* realization of the GHZ Gedanken-experiment (Figure A.1) can be described with Jones matrices.
The Jones matrix of a linear optical element describes how a polarized incident light beam

$$\mathbf{E_i} = \begin{pmatrix} E_i^H \\ E_i^V \end{pmatrix}$$

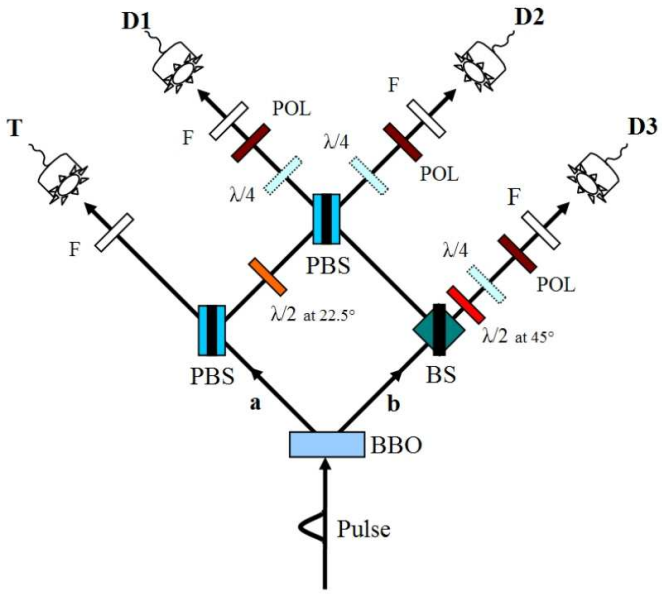

Figure A.1: Experimental setup for Greenberger-Horne-Zeilinger (GHZ) tests of quantum nonlocality [1].

is transformed by that linear optical element into the transmitted beam

$$\mathbf{E_t} = \begin{pmatrix} E_t^H \\ E_t^V \end{pmatrix}.$$

Here E_i^H (E_i^V) is the horizontal (vertical) electrical field component of the incident beam and $\mathbf{E_i}$ is the Jones vector of the incident beam. The Jones matrix $\mathbf{T}$ is a 2x2 matrix. The transmitted beam can be related to the incident beam as follows [26]:

$$\begin{pmatrix} E_t^H \\ E_t^V \end{pmatrix} = \mathbf{T} \begin{pmatrix} E_i^H \\ E_i^V \end{pmatrix} = \begin{pmatrix} t_{11} & t_{12} \\ t_{21} & t_{22} \end{pmatrix} \begin{pmatrix} E_i^H \\ E_i^V \end{pmatrix}. \tag{A.1}$$

Jones matrices describe how the photons are manipulated on average by the corresponding linear optical elements.

For the mathematical description of a physical problem, a reference coordinate system is required. To describe the polarization and other photon parameters, the global reference system seen in Figure A.2 is define. This reference system is the same as the one used by Pan *et al.*. For the computer simulation it is assumed that all transformation matrices of the linear optical elements are given in the H-V basis.

In modern optical quantum experiments, it is assumed that single photons are created and measured. The experimental definition of a single photon is strongly related

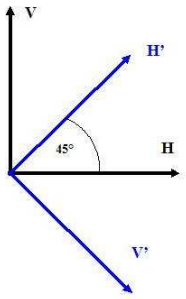

Figure A.2: Global Reference Coordinate System.

to intensity. At light intensities below a certain threshold, it is assumed that single photons (one frequency, short pulse length, ...) are created. It is not in the scope of this project to solve the question what a single photon is. Nevertheless, a mathematical description of single photons is necessary to described the Pan *et al.* experiment. In the EOLMDI model, it is assumed that all emitted photons have the same frequency. Furthermore, we assume that all optical elements are designed to work most efficiently for this frequency ($\lambda = 788nm$). In [1], the authors report that they measure single photons. Therefore, the EOLMDI model has to have indivisible photons. This means that at each optical element it has to be decided whether the photon is transmitted, reflected or absorbed.
In the EOLMDI model, each photon is described by two 2-dimensional vectors[1]

$$\mathbf{E}_i = \begin{pmatrix} E_i^H \\ E_i^V \end{pmatrix} = \begin{pmatrix} E_{norm}^i cos\left(\alpha_i^E\right) \\ E_{norm}^i sin\left(\alpha_i^E\right) \end{pmatrix} \tag{A.2}$$

$$\mathbf{HV}_i = \begin{pmatrix} HV_i^H \\ HV_i^H \end{pmatrix} = \begin{pmatrix} HV_{norm}^i cos\left(\alpha_i^{HV}\right) e^{j\gamma_i} \\ HV_{norm}^i sin\left(\alpha_i^{HV}\right) e^{j\gamma_i} \end{pmatrix}. \tag{A.3}$$

$\mathbf{E}_i$ denotes the polarizations of photon i and $\mathbf{HV}_i$ is a hidden parameter vector assigned to photon i. α_i^E and α_i^{HV} measure the angle of the hidden parameter or polarization vectors in anti-clockwise direction with respect to the horizontal axis H. $E_{norm}^i = 1$ and γ_i is a random phase that can assume any value between 0 and 2π with equal probability. HV_{norm}^i is a real number.
In the following, the optical elements used in the Pan *et al.* realization of the GHZ Gedankenexperiment are described.

[1] This was already described in section 3.2.

A.1.1 Quarter-Wave Plate

A quarter-wave plate (QWP) consists of a birefringent material. The thickness of this plate is adjusted such that the light component polarized in the direction of the larger index of refraction is retarded by $\pi/2$ in phase ($\lambda/4$) with respect to the light component associated with the smaller index.
The Jones matrix for a quarter-wave plate, which has its fast axis oriented in V (vertical) direction[2] is [26]

$$\Lambda_4^V = \begin{pmatrix} 1 & 0 \\ 0 & -i \end{pmatrix}. \tag{A.4}$$

This means that the horizontal, electrical beam component obtains a relative phase shift of $\pi/2$ with respect to the vertical component. It can easily be confirmed that a quarter-wave plate transforms circular (linear) polarized light into linear (circular) polarized light.
In the Pan *et al.* experiment, the quarter-wave plate is oriented such that right (left) circularly polarized light is transformed into H'/V' ($+45^o/-45^o$) polarized light.
When a photon transmits through a quarter-wave plate, both 2-dimensional vectors $\mathbf{E}_i$ and $\mathbf{HV}_i$ are transformed (multiplied) by Λ_4^V.

A.1.2 Half-Wave Plate

A half-wave plate (HWP) consists of a carefully adjusted thickness of a birefringent material such that the light component polarized in the direction of the larger index of refraction is retarded by an odd multiple of π in phase ($\lambda/2$) with respect to that associated with the smaller index. The unitary Jones matrix associated with a half-wave plate is [45]

$$\Lambda_2(\theta) = \begin{pmatrix} \cos(2\theta) & \sin(2\theta) \\ \sin(2\theta) & -\cos(2\theta) \end{pmatrix}. \tag{A.5}$$

Where θ is the angle between the H (horizontal) axis and the fast optical axis of the half-wave plate measured in anticlockwise direction. Half-wave plates are mainly used to rotate linear polarized light by an angle of 2θ [3].
In the simulation of the Pan *et al.* experiment, two half-wave plates are used. The one shown in Figure 1 in [1] has its fast optical axis at an angle of $\theta = 22.5^o$ (Figure A.1), measured anticlockwise from the H (horizontal) axis. This half-wave plate is

[2] As it is used in the Pan *et al.* experiment

[3] Half-wave plates can also be used to transform right (left) circular polarized light into left (right) circular polarized light

used to rotate light that is V (vertically) polarized into light, polarized in V' (-45^o) direction (V (vertical) and H (horizontal) components have equal amplitudes).
The second half-wave plate is placed directly after the beam splitter (BS) (Figure A.1) and is used to rotate the photon polarization $\mathbf{E}_i$ and $\mathbf{HV}_i$ by 90^o [4]. Therefore, a photon that was horizontally (vertically) polarized will after the half-wave plate be vertically (horizontally) polarized. This half-wave plate is used because the state directly after the ploarizaing beam splitter (PBS) and BS is

$$|\psi\rangle = \frac{1}{\sqrt{2}} \left(|H\rangle_1 |H\rangle_2 |V\rangle_3 + |V\rangle_1 |V\rangle_2 |H\rangle_3 \right) \tag{A.6}$$

but the state analyzed in [1] is

$$|\psi\rangle = \frac{1}{\sqrt{2}} \left(|H\rangle_1 |H\rangle_2 |H\rangle_3 + |V\rangle_1 |V\rangle_2 |V\rangle_3 \right). \tag{A.7}$$

There are two possibilities to transform (A.6) into (A.7). Either a half-wave plate, oriented at $\theta = 45^o$ is placed directly after the BS in the path of D3 (this method is used in this work) or it can be assumed that the polarization at D3 is defined at right angles relative to the other stations. This latter method was used by Pan *et al.*.
When a photon transmits through a HWP, the two 2-dimensional vectors $\mathbf{E}_i$ and $\mathbf{HV}_i$ of this photon are multiplied by the HWP Jones matrix (A.5).

A.1.3 Polarizing Beam-Splitter

The general behavior of the non-absorbing polarizing beam-splitter (PBS) was already discussed in section 3.2. Additionally, the behavior for the special case of a single incident photon was shown in the same section. Because EOLMDI is an extension of OLMDI (section 3.2) and not a completely new model, in the following, only the model extensions are discussed.
To apply the PBS model to the Pan *et al.* realization of the GHZ Gedankenexperiment, the PBS behavior for coherent photon pairs has to be defined.
For the case of multiple incident photons overlapping[5] in the PBS it is assumed that all incident photons influence the emitted photons or in simpler words, the PBS manipulates the photons such that the emitted photons have hidden parameter values that are the averages of the hidden parameter values of the incident photons.
To explain the Pan *et al.* experiment, only a few special cases have to be considered.

[4] This means that the fast optical axis of the half-wave plate is oriented at an angle of $\theta = 45^o$ measured anticlockwise from the H (horizontal) axis.

[5] This means that two or more photons are at the same time in the PBS.

As will be explained later, only H (horizontally) or V vertically polarized photons are emitted by the source. This means that the two photons traveling along path **a** or path **b** (Figure A.1) are either vertically or horizontally polarized. As explained in [1] only the case when the two photons in each path are different is of interest. In this case it is guaranteed that the horizontally polarized photon in path **a** is transmitted and the vertically polarized photon is reflected[6]. Therefore, these two photons propagate after the first PBS in different directions.

In the EOLMDI model, it is assumed that the hidden parameter vectors $\mathbf{HV}_i$ and $\mathbf{HV}_k$ of the two incident photons i and k respectively are influenced by the PBS such that the two resulting photons have hidden parameter values that are averages of the two hidden parameter vectors $\mathbf{HV}_i$ and $\mathbf{HV}_k$. Mathematically, this transformation can be described as follows.

Assume the hidden parameter vectors of the two photons propagating along path **a** are defined as

$$\mathbf{HV}_{1\mathbf{a}} = \begin{pmatrix} HV^{1\mathbf{a}}_{norm} e^{j\gamma_{1\mathbf{a}}} cos\left(\alpha^{HV}_{1\mathbf{a}}\right) \\ HV^{1\mathbf{a}}_{norm} e^{j\gamma_{1\mathbf{a}}} sin\left(\alpha^{HV}_{1\mathbf{a}}\right) \end{pmatrix} \tag{A.8}$$

$$\mathbf{HV}_{2\mathbf{a}} = \begin{pmatrix} HV^{2\mathbf{a}}_{norm} e^{j\gamma_{2\mathbf{a}}} cos\left(\alpha^{HV}_{2\mathbf{a}}\right) \\ HV^{2\mathbf{a}}_{norm} e^{j\gamma_{2\mathbf{a}}} sin\left(\alpha^{HV}_{2\mathbf{a}}\right) \end{pmatrix} \tag{A.9}$$

where $\alpha^{HV}_{1\mathbf{a}} = \pi/2$ and $\alpha^{HV}_{2\mathbf{a}} = 0$ or $\alpha^{HV}_{1\mathbf{a}} = 0$ and $\alpha^{HV}_{2\mathbf{a}} = \pi/2$ respectively and $HV^{1\mathbf{a}}_{norm} = HV^{2\mathbf{a}}_{norm} = HV_{norm}$.

The vector $\mathbf{HV}_T$ of the transmitted photon propagating after the first PBS toward detector T is

$$\begin{aligned} \mathbf{HV}_T = & \begin{pmatrix} 1 & 0 \\ 0 & 0 \end{pmatrix} \begin{pmatrix} HV^{1\mathbf{a}}_{norm} e^{j\gamma_{1\mathbf{a}}} cos\left(\alpha^{HV}_{1\mathbf{a}}\right) \\ HV^{1\mathbf{a}}_{norm} e^{j\gamma_{1\mathbf{a}}} sin\left(\alpha^{HV}_{1\mathbf{a}}\right) \end{pmatrix} \\ + & \begin{pmatrix} 1 & 0 \\ 0 & 0 \end{pmatrix} \begin{pmatrix} HV^{2\mathbf{a}}_{norm} e^{j\gamma_{2\mathbf{a}}} cos\left(\alpha^{HV}_{2\mathbf{a}}\right) \\ HV^{2\mathbf{a}}_{norm} e^{j\gamma_{2\mathbf{a}}} sin\left(\alpha^{HV}_{2\mathbf{a}}\right) \end{pmatrix} \end{aligned} \tag{A.10}$$

and the vector $\mathbf{HV}_{\lambda/2}$ of the reflected photon propagating toward the $\lambda/2$-plate (Figure A.1) is

$$\begin{aligned} \mathbf{HV}_{\lambda/2} = & \begin{pmatrix} 0 & 0 \\ 0 & i \end{pmatrix} \begin{pmatrix} HV^{1\mathbf{a}}_{norm} e^{j\gamma_{1\mathbf{a}}} cos\left(\alpha^{HV}_{1\mathbf{a}}\right) \\ HV^{1\mathbf{a}}_{norm} e^{j\gamma_{1\mathbf{a}}} sin\left(\alpha^{HV}_{1\mathbf{a}}\right) \end{pmatrix} \\ + & \begin{pmatrix} 0 & 0 \\ 0 & i \end{pmatrix} \begin{pmatrix} HV^{2\mathbf{a}}_{norm} e^{j\gamma_{2\mathbf{a}}} cos\left(\alpha^{HV}_{2\mathbf{a}}\right) \\ HV^{2\mathbf{a}}_{norm} e^{j\gamma_{2\mathbf{a}}} sin\left(\alpha^{HV}_{2\mathbf{a}}\right) \end{pmatrix}. \end{aligned} \tag{A.11}$$

[6]The decision whether the photon is transmitted or reflected is also in the multi-photon case made according the $p_{trans} = cos^2(\beta)$ relation.

The relevant case for the final PBS (Figure A.1) is when one photon arrives from the path with the $\lambda/2$-plate and the other from the beam-splitter (BS) and when the two emitted photons propagate toward different detectors (D1 and D2). Using the description of the HWP (A.5) and the BS (subsection A.1.4) it can easily be confirmed that the amplitudes of the horizontal and vertical components of the vector $\mathbf{HV}_i$ of the incident photons have amplitudes of $\frac{|HV_{norm}|}{\sqrt{2}}$.
When we assume that the hidden parameter vector of the photon arriving from the BS is $\mathbf{HV}_{BS}^{ref}$ and $\mathbf{HV}_{LPBS}$ for the photon arriving from the $\lambda/2$-plate, the vectors $\mathbf{HV}_i$ of the photons propagating toward detector D1 and D2 can be defined as

$$\mathbf{HV}_{D1} = \begin{pmatrix} 0 & 0 \\ 0 & i \end{pmatrix} \mathbf{HV}_{LPBS} + \begin{pmatrix} 1 & 0 \\ 0 & 0 \end{pmatrix} \mathbf{HV}_{BS}^{ref} \tag{A.12}$$

$$\mathbf{HV}_{D2} = \begin{pmatrix} 1 & 0 \\ 0 & 0 \end{pmatrix} \mathbf{HV}_{LPBS} + \begin{pmatrix} 0 & 0 \\ 0 & i \end{pmatrix} \mathbf{HV}_{BS}^{ref}. \tag{A.13}$$

It can easily be checked that the 'energy' of the hidden parameters is conserved in this two photon case[7].

A.1.4 Beam-Splitter

The beam-splitter (BS) has a similar behavior as the PBS. When a photon arrives at the BS, it is either reflected or transmitted with probability $\frac{1}{2}$. The transmission or reflection probability is independent of the photon polarization. The polarization of the transmitted/reflected photon is equal to the polarization of the incident photon (same orientation and amplitude).
If the two photons arrive simultaneously at the BS and when they have perpendicular polarizations (as assumed in [1]) then the hidden parameter vector of the transmitted photon is the weighted average of the hidden parameter vectors of the two incident photons

$$\begin{aligned} \mathbf{HV}_{BS}^{trans} &= \frac{1}{\sqrt{2}} \begin{pmatrix} 1 & 0 \\ 0 & 1 \end{pmatrix} \begin{pmatrix} HV_{norm}^{\mathbf{1b}} e^{j\gamma_{\mathbf{1b}}} cos\left(\alpha_{\mathbf{1b}}^{HV}\right) \\ HV_{norm}^{\mathbf{1b}} e^{j\gamma_{\mathbf{1b}}} sin\left(\alpha_{\mathbf{1b}}^{HV}\right) \end{pmatrix} \\ &+ \frac{1}{\sqrt{2}} \begin{pmatrix} 1 & 0 \\ 0 & 1 \end{pmatrix} \begin{pmatrix} HV_{norm}^{\mathbf{2b}} e^{j\gamma_{\mathbf{2b}}} cos\left(\alpha_{\mathbf{2b}}^{HV}\right) \\ HV_{norm}^{\mathbf{2b}} e^{j\gamma_{\mathbf{2b}}} sin\left(\alpha_{\mathbf{2b}}^{HV}\right) \end{pmatrix}. \end{aligned} \tag{A.14}$$

[7] The 'energy' of the hidden parameter is defined as $|\mathbf{HV}_i|^2$. The energy conservation law requires that the energy of the hidden parameter of the incident photons is on average equal to the hidden parameter energy of the transmitted photons.

The hidden parameter vector of the reflected photon can be calculated with the following relation:

$$\begin{aligned}\mathbf{HV}_{BS}^{ref} &= \frac{1}{\sqrt{2}}\begin{pmatrix} i & 0 \\ 0 & i \end{pmatrix}\begin{pmatrix} HV_{norm}^{\mathbf{1b}} e^{j\gamma_{\mathbf{1b}}} cos\left(\alpha_{\mathbf{1b}}^{HV}\right) \\ HV_{norm}^{\mathbf{1b}} e^{j\gamma_{\mathbf{1b}}} sin\left(\alpha_{\mathbf{1b}}^{HV}\right) \end{pmatrix} \\ &+ \frac{1}{\sqrt{2}}\begin{pmatrix} i & 0 \\ 0 & i \end{pmatrix}\begin{pmatrix} HV_{norm}^{\mathbf{2b}} e^{j\gamma_{\mathbf{2b}}} cos\left(\alpha_{\mathbf{2b}}^{HV}\right) \\ HV_{norm}^{\mathbf{2b}} e^{j\gamma_{\mathbf{2b}}} sin\left(\alpha_{\mathbf{2b}}^{HV}\right) \end{pmatrix}. \end{aligned} \tag{A.15}$$

This means that the transmitted and reflected photons have the same hidden parameter vector except for a phase shift of $\pi/2$.
A graphical illustration of the four possible outcomes when two photons arrive at the same time at a beam splitter are shown in Figure A.3. Each photon can be

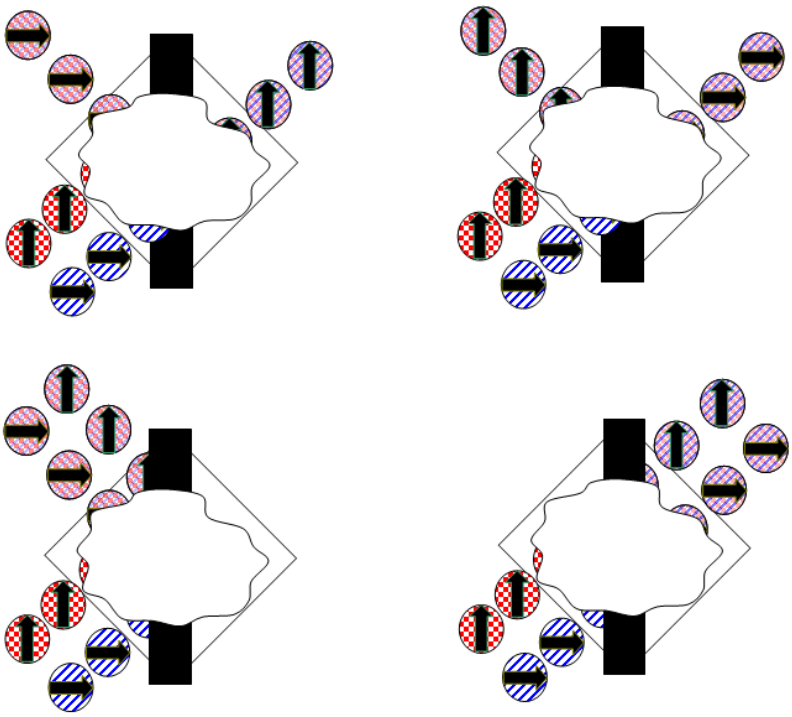

Figure A.3: In the case of two incident photons on a beam splitter, four different outcomes are possible. The shading of the photon (circle) represents the value of the hidden parameter. The arrow represents the photon polarization. It can be seen, that the polarizations of the photons are independent. But the hidden parameter values of the emerging photons are a mixture of the two hidden parameter values of the incident photons.

transmitted or reflected with probability $\frac{1}{2}$. The photons emitted by the BS have the same polarizations as the incident photons. The hidden variable parameters of the emerging photons are statistical mixtures (A.14, A.15) of the incident hidden parameters[8].
It can also be confirmed that on average no hidden parameter energy is absorbed by the BS.

A.1.5 Polarizer

In the Pan *et al.* experiment, linear polarizers (POL) are used to analyze the polarization of the photons. The polarizers are either adjusted in $+45^o$ (H') or -45^o (V') orientation (Figure A.2).
The polarizer behaves similar to a PBS[9] except that it absorbs photons that are not transmitted. The decision whether a photon is absorbed or transmitted depends only on the angle α between the principle transmission direction of the polarizer and the polarization direction of the photon. As in the PBS case, the probability of transmission is $p_{trans} = cos^2(\alpha)$. The polarization of the transmitted photon is parallel to the orientation of the polarizer.
In [1], two different coordinate systems for linear polarization measurements are used. The original state (2.35) is defined in the H-V coordinate system[10]. For the measurements reported in [1], the analyzing polarizers are oriented either in the H' or in the V' direction[11].
The value of the hidden parameter does not have any influence on the transmission probability. But the polarizer transforms the hidden parameter. When transmitting through the polarizer, the hidden parameter vector $\mathbf{HV}_i$ is transformed (multiplied) by the Jones matrix corresponding to the analyzing polarizer orientation:
If the polarizer is adjusted in $+45^o$ (H') orientation, the Jones matrix is

$$POL\,(+45^o) = \frac{B_{POL}}{2}\begin{pmatrix} 1 & 1 \\ 1 & 1 \end{pmatrix}. \tag{A.16}$$

[8] We are aware that such a manipulation of the photons by the BS is strongly speculative and we are not claiming that this is connected to the processes that happen in nature. But because the whole exercise serves the purpose to show that local theories are difficult to exclude it is a useful assumption.

[9] The relevant case in the Pan *et al.* realization of the GHZ experiment is the single photon case described in subsection 3.2.1.

[10] Measurement results in this basis are described in [33].

[11] The orientation of the analyzing polarizer for the R (L) measurements are the same as for the H' (V') measurements.

If the polarizer is oriented in -45^0 direction,

$$POL\,(-45^o) = \frac{B_{POL}}{2}\begin{pmatrix} 1 & -1 \\ -1 & 1 \end{pmatrix} \tag{A.17}$$

has to be used. For H and V measurements

$$POL\,(H) = B_{POL}\begin{pmatrix} 1 & 0 \\ 0 & 0 \end{pmatrix} \tag{A.18}$$

and

$$POL\,(V) = B_{POL}\begin{pmatrix} 0 & 0 \\ 0 & 1 \end{pmatrix} \tag{A.19}$$

respectively are the Jones matrices to be used. For the simulation of the Pan *et al.* realization of the GHZ Gedankenexperiment we use $B_{POL} = \frac{2}{\sqrt{3}}$. This value originates from similar 'energy' considerations as described in section 3.2.

A.1.6 Narrow Bandwidth Filter

The narrow bandwidth filter (NBF) is used to stretch the coherence time. From the Heisenberg uncertainty principle it is known that a particle has either a known frequency or a precisely determined location. Analytically, this can be derived with a Fourier analysis. When a Fourier transformation is applied to a delta-function (describing for example a particle at one location) the resulting spectrum is a white noise. Reverse, if a single frequency is inverse Fourier transformed, its location can not be defined.
The narrow bandwidth filters are used to narrow the frequency range of the detected light beam. This is equivalent to a stretch of the coherence time. A narrow bandwidth filter also helps to reduce the noise.
Although narrow bandwidth filters do normally not have a maximum transmission of 100% [30], for the EOLMDI model a maximum transmission of 100% is assumed. Therefore, the narrow bandwidth filter can be described by an identity matrix[12].

A.2 Detector

It is assumed that the detectors are cooled silicon avalanche photodiodes operated in the Geiger mode [46]. The detectors in the EOLMDI model are supposed to work equal to the detectors described in subsection 3.2.1.

[12]Here it is assumed, that the generated photons have only one frequency that is equal to the transmission frequency of the NBF.

A.3 Source

The source consists of a single nonlinear beta-barium borate (BBO) crystal that down-converts the short UV-pump-laser pulses ($200fs$, $\lambda = 394nm$) to polarization entangled photon pairs. The photons are distributed in two cones of different polarizations. The horizontally polarized and vertically polarized cones intersect at two points. In the experiment, photons from these cone intersections are used as polarization entangled photon pairs.
In the simulation it is assumed that the photons emitted by the BBO crystal are perfectly H (horizontally) or V (vertically) polarized. In addition, whenever the photon in path **a** is polarized in V (H) direction then the entangled photon of the same pair in path **b** is H (V) polarized. Further, it is assumed that the four photons triggering a fourfold coincidence count are generated simultaneously. Mathematically, the four photons of a two-photon-pair are described as follows:
Photon 1 in path **a**:

$$\mathbf{E}_{1\mathbf{a}} = \begin{pmatrix} E^H_{1\mathbf{a}} \\ E^V_{1\mathbf{a}} \end{pmatrix} = \begin{pmatrix} E^{1\mathbf{a}}_{norm} cos\left(\alpha^E_{1\mathbf{a}}\right) \\ E^{1\mathbf{a}}_{norm} sin\left(\alpha^E_{1\mathbf{a}}\right) \end{pmatrix} \tag{A.20}$$

$$\mathbf{HV}_{1\mathbf{a}} = \begin{pmatrix} HV^H_{1\mathbf{a}} \\ HV^H_{1\mathbf{a}} \end{pmatrix} = \begin{pmatrix} HV^{1\mathbf{a}}_{norm} cos\left(\alpha^{HV}_{1\mathbf{a}}\right) e^{j\gamma_{1\mathbf{a}}} \\ HV^{1\mathbf{a}}_{norm} sin\left(\alpha^{HV}_{1\mathbf{a}}\right) e^{j\gamma_{1\mathbf{a}}} \end{pmatrix}. \tag{A.21}$$

Photon 2 in path **a**:

$$\mathbf{E}_{2\mathbf{a}} = \begin{pmatrix} E^H_{2\mathbf{a}} \\ E^V_{2\mathbf{a}} \end{pmatrix} = \begin{pmatrix} E^{2\mathbf{a}}_{norm} cos\left(\alpha^E_{2\mathbf{a}}\right) \\ E^{2\mathbf{a}}_{norm} sin\left(\alpha^E_{2\mathbf{a}}\right) \end{pmatrix} \tag{A.22}$$

$$\mathbf{HV}_{2\mathbf{a}} = \begin{pmatrix} HV^H_{2\mathbf{a}} \\ HV^H_{2\mathbf{a}} \end{pmatrix} = \begin{pmatrix} HV^{2\mathbf{a}}_{norm} cos\left(\alpha^{HV}_{2\mathbf{a}}\right) e^{j\gamma_{2\mathbf{a}}} \\ HV^{2\mathbf{a}}_{norm} sin\left(\alpha^{HV}_{2\mathbf{a}}\right) e^{j\gamma_{2\mathbf{a}}} \end{pmatrix}. \tag{A.23}$$

Photon 1 in path **b**:

$$\mathbf{E}_{1\mathbf{b}} = \begin{pmatrix} E^H_{1\mathbf{b}} \\ E^V_{1\mathbf{b}} \end{pmatrix} = \begin{pmatrix} E^{1\mathbf{b}}_{norm} cos\left(\alpha^E_{1\mathbf{b}}\right) \\ E^{1\mathbf{b}}_{norm} sin\left(\alpha^E_{1\mathbf{b}}\right) \end{pmatrix} \tag{A.24}$$

$$\mathbf{HV}_{1\mathbf{b}} = \begin{pmatrix} HV^H_{1\mathbf{b}} \\ HV^H_{1\mathbf{b}} \end{pmatrix} = \begin{pmatrix} HV^{1\mathbf{b}}_{norm} cos\left(\alpha^{HV}_{1\mathbf{b}}\right) e^{j\gamma_{1\mathbf{b}}} \\ HV^{1\mathbf{b}}_{norm} sin\left(\alpha^{HV}_{1\mathbf{b}}\right) e^{j\gamma_{1\mathbf{b}}} \end{pmatrix}. \tag{A.25}$$

Photon 2 in path **b**:

$$\mathbf{E}_{2\mathbf{b}} = \begin{pmatrix} E^H_{2\mathbf{b}} \\ E^V_{2\mathbf{b}} \end{pmatrix} = \begin{pmatrix} E^{2\mathbf{b}}_{norm} cos\left(\alpha^E_{2\mathbf{b}}\right) \\ E^{2\mathbf{b}}_{norm} sin\left(\alpha^E_{2\mathbf{b}}\right) \end{pmatrix} \tag{A.26}$$

$$\mathbf{HV}_{2\mathbf{b}} = \begin{pmatrix} HV^H_{2\mathbf{b}} \\ HV^H_{2\mathbf{b}} \end{pmatrix} = \begin{pmatrix} HV^{2\mathbf{b}}_{norm} cos\left(\alpha^{HV}_{2\mathbf{b}}\right) e^{j\gamma_{2\mathbf{b}}} \\ HV^{2\mathbf{b}}_{norm} sin\left(\alpha^{HV}_{2\mathbf{b}}\right) e^{j\gamma_{2\mathbf{b}}} \end{pmatrix}. \tag{A.27}$$

$\gamma_{1\mathbf{a}}$, $\gamma_{1\mathbf{b}}$, $\gamma_{2\mathbf{a}}$ and $\gamma_{2\mathbf{b}}$ denote the phases of the four photons. In EOLMDI all four phases are independent of each other and can assume any value in the range of $0 - 2\pi$ with equal probability. It is also assumed that the photons generated by the BBO crystal have $\alpha_i^E = \alpha_i^{HV} = \alpha_i$ where $\alpha_i = m\frac{\pi}{2}$ with $m = 0, 1, 2, 3$. All of the possible values of α_i can be assumed with equal probability. The source is adjusted such that the polarizations of the photon propagating in path **a** and the photon in path **b** (belonging to one entangled photon pair) are entangled at an angle of $\frac{\pi}{2}$ [47]. Therefore the relations

$$\alpha_{1\mathbf{b}} = \alpha_{1\mathbf{a}} + \frac{\pi}{2} \tag{A.28}$$

$$\alpha_{2\mathbf{b}} = \alpha_{2\mathbf{a}} + \frac{\pi}{2} \tag{A.29}$$

have to be fulfilled by all two photon pairs. In the implementation of the EOLMDI model, we use $E^i_{norm} = 1$ and $HV^i_{norm} = 0.5$.
In the next section, several simulation results of the EOLMDI model are discussed.

A.4 Simulation Results and Discussion

The simulation results of the four experiments yyx, yxy, xyy and xxx are shown by the red bars in Figure A.4. The simulation shows that the EOLMDI model can not only explain the experimentally measured results for the yyx, yxy and xyy experiments but also for the xxx experiment. Because the amount of fourfold coincidences was adjusted such that about the same number of fourfold coincidences[13] were observed in the simulation as measured in the actual experiment, a similar variation for the fractions as for the experimental result is observed. The simulation shows that the GHZ terms predicted by quantum mechanics occur in a fraction of 0.75 ± 0.02 of all cases and the undesired states are observed in a fraction of 0.25 ± 0.02.
Although the general behavior of the simulated results is similar to the measured fourfold coincidence fractions, the simulation shows a statistically significantly larger fraction for the quantum mechanically undesired states (0.25 ± 0.02) than the actual experiment (0.15 ± 0.02). One reason for this disagreement between the simulation results and the experimental results might be an inaccurate description of the BBO source. So far, we have assumed that the BBO source has a similar behavior as the calcium-40 source used in the Aspect experiments (section 3.2). But the two sources are physically different. In the experiments carried out by Aspect and his co-workers, a calcium-40 source is used whereas in the Pan *et al.* experiment, a BBO

[13] 132 for quantum mechanically desired states and 44 for quantum mechanically undesired states.

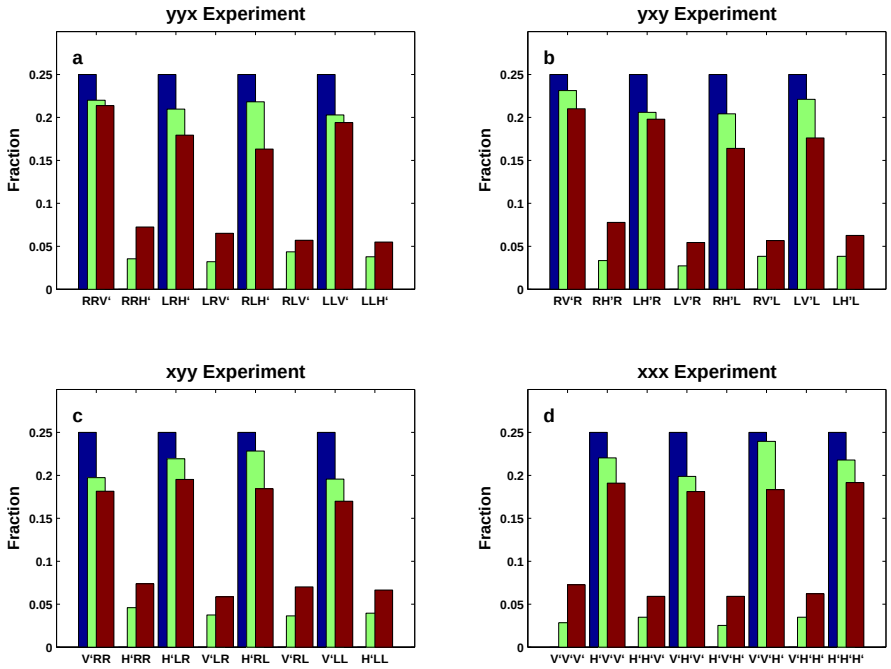

Figure A.4: All outcomes for the yyx, yxy, xyy and xxx experiments. The blue bars represent the quantum mechanical predictions, the green bars are the experimental results measured by Pan *et al.* and the red bars are the fractions from simulations with the EOLMDI model. The number of generated photons (150000) was adjusted such that for each quantum mechanically undesired (desired) state around 44 (132) fourfold coincidences were registered.

crystal is employed as photon source. Using this fact, we can assume that the correct value HV^i_{norm} for the BBO source in the EOLMDI model is $HV^i_{norm} = 0.4$ instead of $HV^i_{norm} = 0.5$. The simulations with the modified EOLMDI model result in distributions for the four experiments yyx, yxy, xyy and xxx that predict for the quantum mechanically undesired states a total fraction of 0.11 ± 0.02 and for the quantum mechanically desired states a total fraction of 0.89 ± 0.02 (Figure A.5).

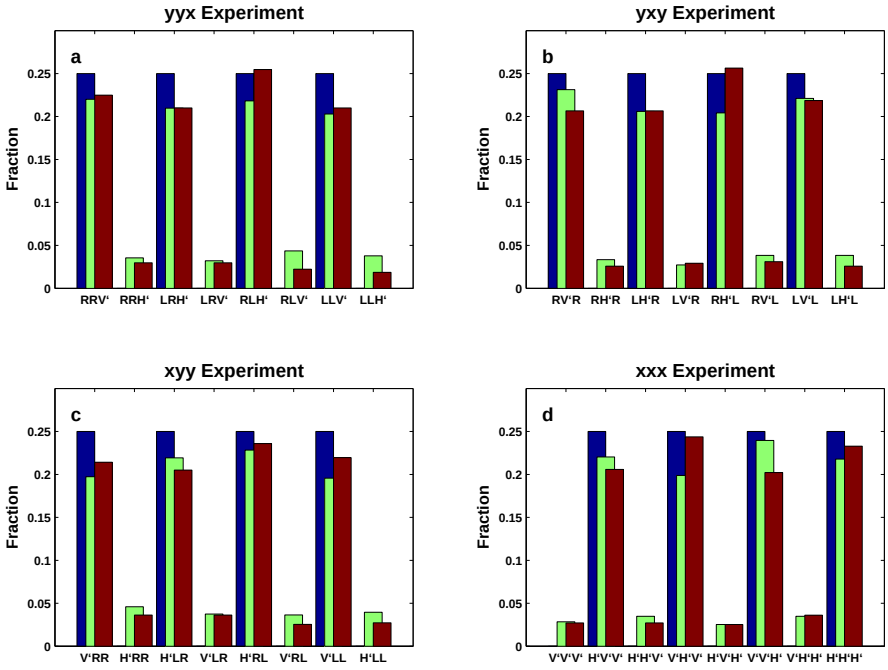

Figure A.5: All outcomes for the yyx, yxy, xyy and xxx experiments. The blue bars represent the quantum mechanical predictions, the green bars reproduce the experimental results measured by Pan *et al.* and the red bars are the fractions from a simulation with EOLMDI ($HV^i_{norm} = 0.4$). The number of generated photons (900000) was adjusted such that for each quantum mechanically undesired (desired) state around 17 (125) fourfold coincidences were counted.

In conclusion, it was shown that EOLMDI is able to explain the measured results reported in [1].
To check the model, two additional simulations were carried out. Figure A.6 shows the simulation results of the four experiments yxx, xyx, xxy and yyy not reported by Pan *et al.*. It can be seen in Figure A.6 that the EOLMDI model predicts on

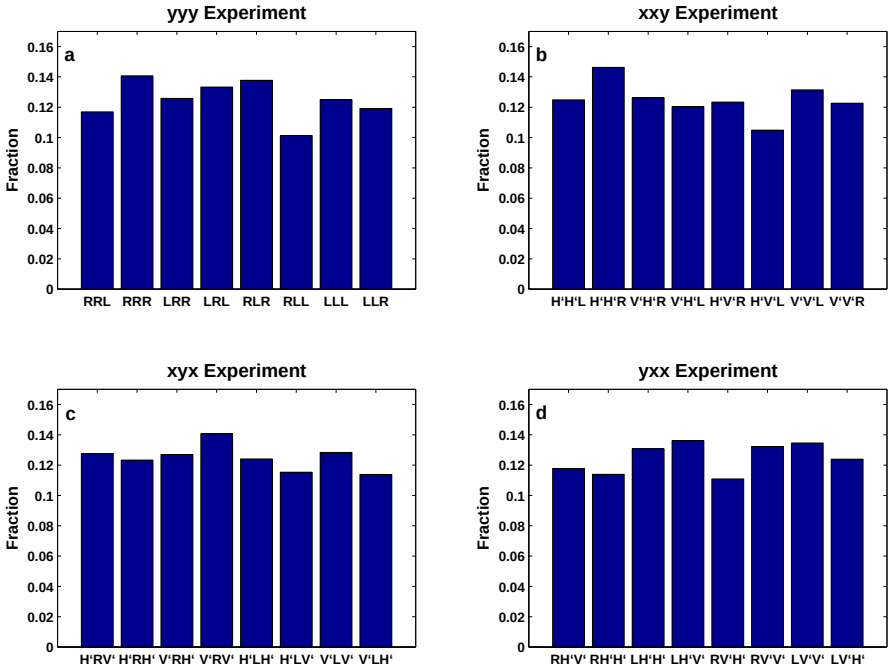

Figure A.6: All outcomes for the yyy, xxy, xyx and yxx experiments. On average 85 fourfold coincidences were registered for each setting. A longer simulation confirmed that the EOLMDI model predicts for all outcomes a fraction of exactly $\frac{1}{8}$.

average a fraction of around $\frac{1}{8}$ for all eight possible setting combinations of each experiment[14]. This prediction is in agreement with the predictions of the quantum mechanical model of Pan *et al.* that is based on the entangled three-photon GHZ state

$$|\psi\rangle = \frac{1}{\sqrt{2}} \left(|H\rangle_1 |H\rangle_2 |H\rangle_3 + |V\rangle_1 |V\rangle_2 |V\rangle_3 \right) \tag{A.30}$$

and the transformations (2.36-2.39).
Finally, the simulation of the fourfold coincidences in the H-V basis (Figure A.7) confirmed the plausibility of the EOLMDI model. It is shown in Figure A.7 that EOLMDI predicts the experimentally observed entangled three-photon GHZ state[33] correctly.

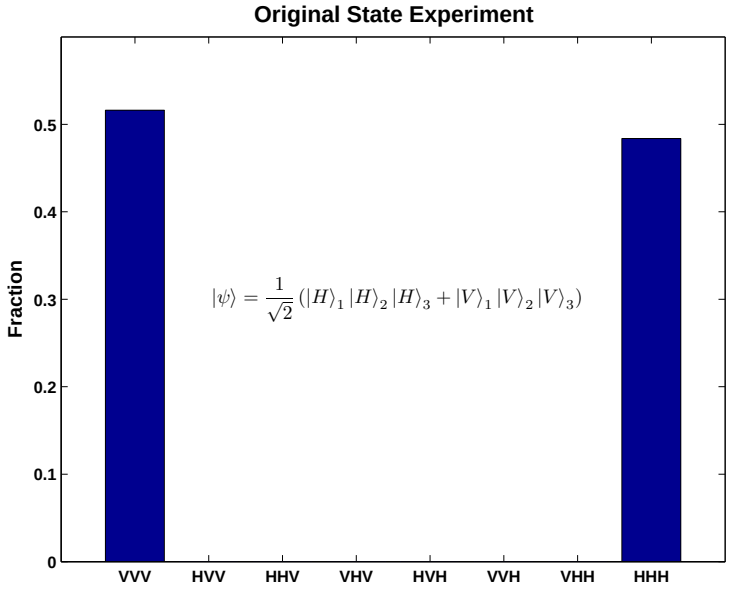

Figure A.7: All outcomes for the $x_o x_o x_o$ experiment measured in the H-V basis.

A closer look at the EOLMDI model shows that two model components are vital to explain the experimental results presented by Pan *et al.*.

Hidden Parameter Vector: In the EOLMDI model, it is assumed that photons do not only have a polarization, frequency or phase but also a hidden parameter associated with them. It is also assumed that different photons can interact with

[14]In other words, within a given time period, equally many fourfold coincidences are counted for all eight possible settings of one experiment.

each other. Of course we are aware that photons do not interact in free space. Therefore, in the EOLMDI model it is assumed that the photons influence the values of the hidden parameter vector of each other with the help of optical elements such as polarizing beam splitters or beam splitters. The exact physical process that is responsible for the suggested hidden parameter averaging in the PBS or BS is not known. But such an interaction seems to be plausible. Especially because it is known that quantities such as the polarization or the phase of a photon can be influenced by optical elements.

Additionally, the idea of information exchange between spatially close photons does not contradict the measured dependence of the fourfold coincidences on the delay between photon 1 and 2 at the final polarizing beam splitter (Figure 4.6). It can be seen that at a large delay of more than $60\mu m$ no entanglement is observed. This result is normally interpreted as an experimental evidence, that at a delay larger than $60\mu m$, the two photons are no more coherent. It is interesting that the $60\mu m$ are equal to the spacial length of the pump pulse ($200fs * 3 \cdot 10^8 \frac{m}{s} = 60\mu m$). Using EOLMDI to interpret this observation, it means that the amount of exchanged information is proportional to the spacial overlap of the involved photons in the PBS/BS. Only when the photons overlap in the PBS/BS and exchange information, entanglement can be observed.

Detection Inefficiency Loophole: The second important model component is the detection inefficiency loophole. The plausibility of this loophole was already discussed in section 3.2.3.

It is realized that the EOLMDI model is a highly simplified description of the complex processes that go on in nature. Nevertheless, EOLMDI does not contradict the known behavior of the optical elements and has therefore to be considered as a plausible model.

Although most scientists working in the area of quantum nonlocality consider the detection inefficiency loophole as insignificant it is noteworthy that despite of many improved experiments it has not yet been possible to close this loophole. It is also interesting to realize that within the last decades no significant improvement in the detection efficiency was achieved [30]. The failure of improving the detection efficiency in optical experiments might be based on physical restrictions on the detection efficiency imposed by hidden parameters.

Appendix B

Entropy Calculations for Objective Local Models

In section 5.4, the generalized entropic Bell test is explained. To check this test, several entropies for three objective local models for the Pan *et al.* realization of the GHZ Gedankenexperiment are used. In the following the detailed entropy calculations for these three models are carried out.

Local EoR model with $A = B = C = D = -1$: This model is the local realistic model based on elements of reality introduced in section 4.2 and denoted as POLT. Each photon i has two elements of reality X_i for the linear polarization in the $H' - V'$ basis and Y_i for the circular polarization in the $R - L$ (right-handed - left handed) assigned. In POLT, it is assumed that the following eight combinations of source parameters are possible:

$$\begin{aligned} \Lambda = X_1Y_1X_2Y_2X_3Y_3 \quad \in \quad & \{H'_1R_1H'_2R_2V'_3L_3, H'_1R_1V'_2L_2H'_3R_3, \\ & H'_1L_1H'_2L_2V'_3R_3, H'_1L_1V'_2R_2H'_3L_3, \\ & V'_1R_1H'_2L_2H'_3L_3, V'_1R_1V'_2R_2V'_3R_3, \\ & V'_1L_1H'_2R_2H'_3R_3, V'_1L_1V'_2L_2V'_3L_3\}. \end{aligned} \tag{B.1}$$

Each of the four random variables A, B, C and D represent one of the four experiments measured by Pan *et al.* (5.33-5.36). From the definition of the four random variables and the source parameter Λ it is clear that the four random variables are not independent of each other. In the following, the entropies listed in Table 5.3 are calculated for POLT. Because for each of the four random variables A, B, C and D four different realizations (i.e. $A \in$

$\{R_1R_2V_3', L_1R_2H_3', R_1L_2H_3', L_1L_2V_3'\}$) with equal probability $\frac{1}{4}$ are possible, the entropy for the individual random variables are

$$H(A) = H(B) = H(C) = H(D) = -4 \cdot \frac{1}{4} log_2 \left(\frac{1}{4}\right) = 2. \tag{B.2}$$

For the calculation of the joint entropy of two experiments, the following relation (Theorem 1.4.4 in [39])

$$H(A, B) = H(A|B) + H(B) \tag{B.3}$$

is used. The knowledge of one experimental result (i.e. $A = R_1R_2V_3'$, reduces the freedom of choice for the second experiment to two possible outcomes (i.e. $B \in \{R_1H_2'L_3, R_1V_2'R_3\}$) [1]. Therefore $H(B|A) = 1$ and $H(A, B) = 3$. Because of symmetry, $H(A, C) = H(A, D) = H(B, C) = H(B, D) = H(C, D) = 3$. Similar calculations are used to obtain $H(A, B, C) = H(A, B, D) = H(B, C, D) = H(A, B, C, D) = 3$. For the calculation of the remaining entropies listed in Table 5.3, equations (5.37-5.42) are used.

Local EoR model with $A = B = C = -1, D = +1$: This model is based on the same source (B.1) as the previously discussed POLT model. The only difference to the above analysis concerns the allowed outcomes for the xxx experiment represented by the random variable D. Instead of the local realistic predictions for the xxx experiment, only the quantum mechanically predicted results $H_1'H_2'H_3'$, $H_1'V_2'V_3'$, $V_1'H_2'V_3'$ and $V_1'V_2'H_3'$ are allowed. But because the elements of reality defined by the source parameter (B.1) and the quantum mechanical predictions are mutually exclusive, the event D=+1 is impossible. Thus we know with certainty[2] that for the experiment D and any joint distributions of the four experiments which include D, has only the outcome of the impossible event. Therefore

$$\begin{aligned} H(D) = H(A, D) = H(B, D) = H(C, D) = H(A, B, D) \\ = H(A, C, D) = H(B, C, D) = H(A, B, C, D) = 0. \end{aligned} \tag{B.4}$$

Individual and joint distributions not including the random variable D are the same as for the previously discussed POLT model. This is because the source and also the allowed outcomes $A = B = C = -1$ are the same in both models. All the other entropies shown in Table 5.3 are calculated with the relations of

[1] It is assumed that the measurement is performed on the same source parameter λ.

[2] With probability equal to unity.

equations (5.37-5.42). It can be seen that $H(D|A,B) = -3$ contradicts the monotonicity of Shannon entropies, which implies that conditional entropies such as $H(D|A,B)$ are non-negative. Under the condition that the given joint entropies are correct[3] and the fact that the conditional entropy $H(C|A,B) = 0$, we can conclude that experiment D can not be defined on the same probability space as the other three experiments.

LIS: The local instruction-set model based on elements of reality is explained in section 4.2. The source can produce 32 different combinations (Table 4.1) of the six elements of reality X_i and Y_i $(i = 1, 2, 3)$. As can be seen in Figure 4.4 the LIS model predicts the quantum mechanically desired states and the undesired states in a ration of 3:1 for all four experiments A, B, C and D. Therefore, the entropies for the individual experiments are

$$\begin{aligned} H(A) &= H(B) = H(C) = H(D) \\ &= -4\left(\frac{1}{16}\cdot log_2\left(\frac{1}{16}\right) + \frac{3}{16}\cdot log_2\left(\frac{3}{16}\right)\right) = 2.26. \end{aligned} \tag{B.5}$$

The joint entropy of two experiments that are performed on the same source parameter λ are best calculated by using the joint probability distribution of the joint ensemble of the two investigated experiments (i.e. AB)[4]. With Table 4.1 it can easily be checked that the joint ensemble of two experiments can have 24 different outcomes (i.e. AB with $A = R_1R_2V_3'$ and $B = R_1H_2'L_3$). 16 of these outcomes can occur with a probability of $\frac{1}{32}$ and the remaining eight with a probability of $\frac{1}{16}$. Therefore the joint entropies of two experiments are

$$\begin{aligned} H(A,B) &= H(A,C) = H(A,D) = H(B,C) = H(B,D) = H(C,D) \\ &= -16\cdot\frac{1}{32}\cdot log_2\left(\frac{1}{32}\right) - 8\cdot\frac{1}{16}\cdot log_2\left(\frac{1}{16}\right) = 4.5. \end{aligned} \tag{B.6}$$

The joint entropies of the joint ensembles for the three and four joint experiment ensembles ABC, ABD, BCD and $ABCD$ are calculated with the same method. Finally, for the calculation of the remaining entropies seen in Table 5.3 the relations (5.37-5.42) are applied.

[3] The definition (B.4) for joint entropies including the random variable D is considered to be the most intuitive. It seems to be a simple and reasonable approach to perform the generalized entropic Bell test. Because the relations (5.37-5.42) are only valid under the condition that all random variables can be defined on one common probability space unintuitive entropies might occur when the condition is not valid.

[4] Because of symmetry, each of the possible joint ensembles AB, AC, AD, BC, BD and CD have the same joint probability distribution.

Appendix C

List of Abbreviations

BS	Beam Splitter
CHSH	Clauser-Horne-Shimony-Holt
EOLMDI	Extended OLMDI
EPR	Einstein-Podolsky-Rosen
GHSZ	Greenberger-Horne-Shimony-Zeilinger
GHZ	Greenberger-Horne-Zeilinger
HWP	Half-Wave Plate
LIS	Local Instruction-Set
NBF	Narrow Bandwidth Filter
OLMDI	Objective Local Model based on Detection Inefficiency
PBS	Polarizing Beam Splitter
QWP	Quarter-Wave Plate
TCME	Time Coordinated Measuring Equipments

Bibliography

[1] M. Daniell H. Weinfurter J.-W. Pan, D. Bouwmeester and A. Zeilinger. Experimental test of quantum nonlocality in three-photon greenberger-horne-zeilinger entanglement. *Nature*, 403:515 – 519, February 2000.

[2] P. Grangier A. Aspect and G. Roger. Experimental realization of einstein-podolsky-rosen-bohm gedankenexperiment: A new violation of bell's inequalities. *Physical Review Letters*, 49(2):91–94, July 1982.

[3] J. Dalibard A. Aspect and G. Roger. Experimental test of bell's inequalities using time-varying analyzers. *Physical Review Letters*, 49(25):1804–1807, December 1982.

[4] P. Grangier A. Aspect and G. Roger. Experimental tests of realistic local theories via bell's theorem. *Physical Review Letters*, 47(7):460–463, 1981.

[5] B. Podolsky A. Einstein and N. Rosen. Can quantum-mechanical description of physical reality be considered complete? *Physical Review*, 47:777–780, May 1935.

[6] N. Bohr. Can quantum-mechanical description of physical reality be considered complete? *Physical Review*, 48:696–702, July 1935.

[7] J.S. Bell. On the einstein-podolsky-rosen paradox. *Physics 1*, pages 195–200, 1964.

[8] J.S. Bell. *Speakable and Unspeakable in Quantum Mechanics*. Cambridge University Press, 1993.

[9] A. Shimony J.F. Clauser, M.A. Horne and R.A. Holt. Proposed experiment to test local hidden-variable theories. *Physical Review Letters*, 23(15):880–884, October 1969.

[10] N.D. Mermin. What's wrong with these elements of reality? *Physics Today*, June 1990.

[11] M. Horne D.M. Greenberger and A. Zeilinger. Going beyond bell's theorem. In M. Kafatos, editor, *Bell's Theorem, Quantum Theory, and Conceptions of the Universe*, pages 73–76. Kluwer Academic, 1989.

[12] C. E. Shannon. A mathematical theory of communication. *Bell Syst. Tech. J.*, 27:379–423,623–656, 1948.

[13] C. E. Shannon. Coding theorems for a discrete source with a fidelity criterion. *IRE National Convention Record*, 4:142–163, 1959.

[14] W. Weaver C. E. Shannon. *The mathematical theory of communication.* University of Illinois Press, 1963.

[15] http://www.aip.org/history/heisenberg/p09.htm.

[16] A. Fine. *The Shaky Game Einstein Realism and the Quantum Theory.* The University of Chicago Press, 1986.

[17] http://panda.unm.edu/Courses/Fields/Phys491/notes/ComplementarityPrinciple.pdf.

[18] J. von Neumann. *Mathematische Grundlagen der Quanten-mechanik.* Julius-Springer Verlag, Berlin, 1932.

[19] C.A. Kocher and E.D. Commins. Polarization correlation of photons emitted in an atomic cascade. *Physical Review Letters*, 18:575–577, 1967.

[20] D. M. Greenberger et al. Bell's theorem without inequalities. *American Journal of Physics*, 58(12):1131–1143, 1990.

[21] K. Hess and W. Philipp. Breakdown of bell's theorem for certain objective local parameters spaces. *PNAS*, 101(7):1799–1805, February 2004.

[22] K. Hess and W. Philipp. Bell's theorem: Critique of proofs with and without inequalities. *Quantum Physics*, October 2004.

[23] J. Bass. Sur la compatibilit´e des fonctions de r´epartition. *C.R. Acad. Sci.*, 240:839–841, 1955.

[24] N.N. Vorobev. Consistent families of measures and their extensions. *Theory of Probability and its Applications*, 1962.

[25] C.H. Thompson. Subtraction of "accidentals" and the validity of bell tests. *quant-ph*, (9903066), July 2004.

[26] E. Hecht and A. Zajac. *Optics*. Number ISBN: 0-201-02835-2. Addison-Wesley Publishing Company, 1974.

[27] F. Rieke and D.A. Baylor. Single-photon detection by rod cells of the retina. *Reviews of Modern Physics*, 70(3):1027–1036, July 1998.

[28] P. Pearle. Hidden-variable example based upon data rejection. *Physical Review D*, 2(8):1418–1425, October 1970.

[29] G. Badurek M. Baron Y. Hasegawa, R. Loidl and H. Rauch. Violation of a bell-like inequality in single-neutron interferometry. *Nature*, 425:45–47, September 2003.

[30] P. G. Kwiat et al. Ultrabright source of polarization-entangled photons. *Physical Review A*, 60(2):773–776, August 1999.

[31] G. Weihs et al. Violation of bell's inequality under strict einstein locality conditions. *Physical Review Letters*, 81(23):5039–5043, December 1998.

[32] R. Ursin G. Weihs A. Zeilinger J.-W. Pan, S. Gasparoni. Experimental entanglement purification of arbitrary unknown states. *Nature*, 423:417–422, May 2003.

[33] M. Daniell H. Weinfurter D. Bouwmeester, J.-W. Pan and A. Zeilinger. Observation of three-photon greenberger-horne-zeilinger entanglement. *Physical Review Letters*, 82(7):1345–1349, February 1999.

[34] K. Hess and W. Philipp. The bell theorem as a special case of a theorem of bass. 2005.

[35] N. J. Cerf and C. Adami. Negative entropy and information in quantum mechanics. *Physical Review Letters*, 79(26):5194–5197, December 1997.

[36] B. Schumacher. Quantum coding. *Physical Review A*, 51(4):2738–2747, April 1995.

[37] M.A. Nielsen and I.L. Chuang. *Quantum Computation and Quantum Information*. Cambridge University Press, 2000.

[38] D. J.C. MacKay. *Information Theory, Inference, and Learning Algorithms*. Cambridge University Press, 2003.

[39] R. Ash. *Information Theory*. Interscience Publishers, 1965.

[40] N. J. Cerf and C. Adami. Quantum mechanics of measurement. In M. Biafore T. Toffoli and J. Leao, editors, *Proceedings of the 4th Workshop on Physics and Computation*.

[41] N. J. Cerf and C. Adami. Entropic bell inequalities. *Physical Review A*, 55(5):3371–3374, May 1997.

[42] R. W. Yeung. On entropy, information inequalities, and groups.

[43] A. Wehrl. General properties of entropy. *Reviews of Modern Physics*, 50(2):221–260, April 1978.

[44] S. Barraza-Lopez K. Hess W. Philipp, G. Adenier. Local computer model emulating the results of the pan et al. experiment. *arXiv quant-ph/0412209*.

[45] X. Liu Y. Han, Q. Li and B. Zhou. rchitecture of high-order all-fiber birefringent filters by the use of the sagnac interferometer. *IEEE Photonics Technology Letter*, 1999.

[46] P. G. Kwiat et al. New high-intensity source of polarization-entangled photon pairs. *Physical Review Letters*, 75(24), December 1995.

[47] Matthew Daniell. *Multi-photon Entanglements*. PhD thesis, University of Vienna, September 2000.